6-30-2016

Enabling Studies to Optimize Biomaterials for the Treatment of Myocardial Infarction

Eva Adriana Romito
University of South Carolina

Enabling Studies to Optimize Biomaterials for the Treatment of Myocardial Infarction

by

Eva Adriana Romito

Bachelor of Science
University of South Carolina, 2012

Submitted in Partial Fulfillment of the Requirements

For the Degree of Doctor of Philosophy in

Biomedical Engineering

College of Engineering and Computing

University of South Carolina

2016

Accepted by:

Francis Spinale, Major Professor

Tarek Shazly, Major Professor

Edie Goldsmith, Committee Member

Michael Sutton, Committee Member

Jason Burdick, Committee Member

Lacy Ford, Senior Vice Provost and Dean of Graduate Studies

DEDICATION

To my husband who has borne all of my stress, frustrations, stubbornness, and overwhelming joys with impressive exuberance for all the years we've been together.

To my family that fiendishly encouraged inquiry, and developed my argumentative nature with great affection.

To my friends always responsive to moments of insanity with creative sources of sanity in conversation, and adventure.

ACKNOWLEDGEMENTS

My sincere acknowledgment and gratitude go to my advisors Drs. Francis Spinale and Tarek Shazly. I have received invaluable assistance, advice and innumerable suggestions that have furthered my knowledge base as well as impacted my individual growth as a researcher. They have both devoted an enormous amount of time into fostering my scientific capabilities in thought as well as writing and presentation. I would like to thank my dissertation committee members Dr. Jason Burdick, Dr. Edie Goldsmith and Dr. Michael Sutton for their guidance and support. I express my sincere thanks to all my lab-mates, colleagues, and friends who are always with me for support and assistance. Lastly, and with utmost importance I would like to thank my family, my husband and my friends for their unconditional love, understanding and unfaltering support of my endeavors throughout my life.

ABSTRACT

The canonical mechanism of wound healing is disrupted following a myocardial infarction (MI), manifesting as an unregulated response that negatively impacts left ventricular (LV) function. This mechanism, termed post-MI remodeling, culminates in an outcome that favors progression to a systolic heart failure state and death for the patient. Therapeutic approaches following the occurrence of a MI are designed to modulate the natural remodeling process and mitigate the loss of cardiac function. The mechanics and structure of the healing infarct have been the focus of numerous pre-clinical and clinical investigations, leading to the impending clinical introduction of material injections as a means to favorably alter remodeling outcomes. However, to date there is no body of work that provides a coherent framework for evaluation of targeted material therapies. To form a basis for optimization of material-based MI treatments, we have integrated measurements of MI regional mechanics, the morphology of the local extracellular matrix, and the biophysical impact of material injections into the MI region in a porcine model of MI. The combined findings of this study have enhanced a mechanistic understanding of material-based post-MI interventions, elucidated the relationship between MI regional mechanics and LV function throughout the natural and attenuated history of LV remodeling, and has developed mechanical metrics of value to move forth towards future developments of a generalizable computational tools for screening and evaluation of new strategies for MI injections.

TABLE OF CONTENTS

LIST OF TABLES

LIST OF FIGURES

LIST OF ABBREVIATIONS

CVD ..... Cardiovascular Disease

ECM ..... Extra cellular matrix

EF ..... Ejection Fraction

HF ..... Heart Failure

LG-MRI ..... Late Gadolinium Enhanced

LV ..... Left Ventricle

LS-STE ..... Layer Specific Speckle Tracking Echocardiography

LVEDP ..... Left Ventricular End Diastolic Pressure

LVEDV ..... Left Ventricular End Diastolic Volume

MI ..... Myocardial Infarction

MRI ..... Magnetic Resonance Imaging

SPAMM ..... Spatial Modulation Magnetization

STE ..... Speckle Tracking Echocardiography

CHAPTER 1

INTRODUCTION

1.1 Overview

Clinical Motivation and Natural History of MI

The prevalence of heart disease across the United States and the western world presents an ever-increasing problem that has severe health implications with regards to longevity and quality of life. Currently, cardiovascular disease (CVD) accounts for the largest mortality rate in the U.S. every year [61]. In its broadest definition, CVD refers to many different etiologies affecting the circulatory system, with its central component being the heart muscle [61,62]. Acute coronary events directly affect the heart and ultimately compromise cardiac function to an extent beyond repair with current clinical practice [111,154]. Every year three-quarters of a million of Americans suffer a new coronary event [62]. One such event is that of a myocardial infarction (MI) in the left ventricle (LV). A MI is an ischemic event, meaning there is a lack of oxygen delivered to a specific portion of the myocardium. Once the oxygen supply is lost the tissue in the affected region quickly looses viability (Figure 1.1).

As the contractile units of the myocardium (cardiomyocytes) die, the portion of affected tissue becomes necrotic and loses functionality [33,111,117]. Survival of a MI is possible, but patient quality of life is invariably compromised. The reduction of life expectancy from an MI has been addressed by multiple studies and has been recognized

as a major contributor to the development of systolic heart failure [33,71,111]. Once a patient enters a state of HF the rate of survival to a normal life expectancy decreases for both sexes. A study carried out over a decade in Scotland comprehensively observed patients of both sexes that were suffering from common cancers (ovarian, lung, stomach, prostate, breast) as well as MI and HF with regards to their survival rates [161]. The resulting data demonstrated markedly low survival rates for patients suffering from HF with a trend that was significantly lower than most cancers affecting both sexes (with the exception of stomach cancer) [161]. Such a threatening trend gave verisimilitude to an extreme conclusion from the authors of the study; as they deemed HF to perhaps be "more malignant than cancer". Although MI showed high probability of survival in this study, the likelihood of transgressing to HF after the initial acute occurrence presents patients and healthcare professionals with a delicate situation for treatment in patients. A primary and decisive factor in the pathway to HF from MI is the effect of the structural remodeling that takes place post-MI [9,33,111]. Since MI and post-MI remodeling are major contributors to the etiology of the HF state, it is imperative to rapidly curtail the otherwise progressive loss of cardiac function.

In a normal setting, the most common treatment of MI involves reperfusion therapy, but it is only achievable for a short period of time after its onset, where a supply of oxygenated blood can be reestablished at the affected site [33,111,117].Studies have shown there is a notable benefit from reperfusion therapy on cardiac function and post remodeling markers [33]. It is the remodeling aspect post-MI that becomes the largest driving force in the decline of cardiac function [33,111,133]. Affecting the progression of remodeling is the ideal target for a therapeutically relevant outcome.

Post-MI remodeling is a multifactorial process that overtakes the canonical wound healing response that would occur after injury. Following the ischemic event, a series of pathways are triggered by the natural inflammatory response to injury. Various biochemical cascades contribute to the readsorption of necrotic tissue post-MI, as the proliferation of fibroblasts and fibrillar collagen deposition within the affected region fundamentally change the material composition of the extra cellular matrix (ECM) at the site of injury [51,111,145,154]. Drastic changes in geometry and structure combine to create adverse effects on cardiac function and the likely inception of HF. The chief attributes of remodeling include changes in LV geometry evidenced by the thinning of the infarct region (MI thinning) and hypertrophy of the remote/opposing myocardium. The thinning of the MI region is in part due to the scarification that occurs as necrotic tissue is removed, and a proliferative phase of fibroblasts takes place. During this infiltration there is a marked increase in the collagen content in the ischemic region as the non-viable injured myocardium is transformed into scar tissue [111,145]. This MI scar becomes thin and expands the LV in volume (Figure 1.2 top) such that the difference in geometry has deep mechanical repercussions.

The dispersion of mechanical loads across the LV through the cardiac cycle is severely affected when there is a geometric change. The peak wall stresses and strains experienced by the LV wall are a function of material characteristics and geometry. The behavior of the material (viable myocardium and MI scar) is vastly changed after injury. The scar lacks the contractile forces required to adequately contribute to the main pumping action of the LV and eject blood during the systolic part of the cardiac cycle. In application of the law of LaPlace (eq. 1) the tension in the wall must increase to achieve

functional stroke volumes and reduce insufficiencies. Such an increase in tension exerts a higher mechanical demand on viable tissue [49,154,193]. The structural integrity of the MI scar is so changed from the normal myocardium that its inherent stiffness is notably reduced and therefore cannot adequately generate the contractile force required for ejection [72,73,117]. The dense network of collagen that forms the scar is more susceptible to deformation induced by changes in pressure (mechanical load) [49,72,73,154]. The change in geometry from expansion of the thinned MI region and hypertrophy of the remote region also impinges on the mechanical dispersion of loads across the wall. The peak stresses and deformation observed in the MI region only serve to contribute to the forward-feeding mechanism of remodeling, where expansion begets more expansion [133]. In the presence of an aberrant mechanical environment the remodeling is unbridled and will continue until catastrophic failure occurs. Although an initially compensatory and adaptive process, the changes in tissue architecture that occur as a result of remodeling also create an unsuitable environment to retain LV function.

Among the most important determinants of cardiac function that are indicative of increased risk towards HF are those dealing with volume, pressure and pumping efficiency. The clinical parameters that directly describe these functions are: ejection fraction (EF %), left ventricular end diastolic volume and pressure (LVEDV and LVEDP, respectively), heart rate, cardiac output and other associated pressures (dP/dt, Ao pressures). As the consequences of remodeling become more pronounced the behavior of the LV is deeply affected, which in turn will worsen cardiac function.

Increasing the understanding of the mechanical behavior and composition of the developing scar will aid the targeted approach towards curtailing negative aspects of

remodeling. Forward strides have been made in the hopes of reaching a more comprehensive solution; among these steps are classic mechanical studies and interventional approaches utilizing biocompatible materials delivered directly to the MI region.

State of the art investigations on Post-MI mechanics

Classical studies of normal myocardium are well established, and utilize a range of *in vitro* and *in silico* techniques. However, understanding the totality of change induced by remodeling requires a combination of not only these techniques, but also complementary animal models to identify key remodeling outcomes of high clinical significance [72,92,155].

The bulk of investigations on the mechanics of scar tissue formed following MI have taken place under *ex vivo* conditions with hearts isolated from their respective animal models, arrested then passively inflated for study [49,68,73,145,173]. Canonical studies on the mechanics of scar tissue include those done by Fomosky, Holmes and Covell. Their investigations centered on the mechanics of the developing scar post-MI in porcine, and rat models, but have limitations in their respective testing parameters and experimental set up. There are three major limitations to the study of myocardial scar mechanics: the employed animal model, discernment of passive vs. active mechanics, and maintaining the integrity of the tissue. A clear focus on the impact of collagen deposition has dominated these studies. Collagen architecture is thought to be the largest contributor to scar mechanics throughout the healing process and is therefore of main concern in understanding the regional mechanics. It is important to note that different animal models

have shown opposing outcomes in the organization of collagen in the developing scar [51]. In considering a rat model, studies have found scar tissue to be highly disorganized in collagen structure and mechanically isotropic [49]. In ovine, canine and porcine models however, it has been found that collagen fibers can be highly organized and can even display a preferred alignment through their thickness when compared to the surrounding viable tissue [73,133,181]. Though creation of MI in various animal models is well established, the mechanical testing of the heart itself is often flawed in the basic simulation of the *in vivo* environment and has been deprived of the contractile forces that control the major function of the muscle—rendering mechanics to be of a passive nature alone. The lack of an active component in mechanical testing deprives the full description and understanding of the underlying regional mechanics of the scar. Scar tissue from the myocardium has also been subjected to mechanical testing with biaxial experiments, but has suffered from the limitations and introduction of artifact associated with such. Planar biaxial testing is appropriate for specifying constitutive relations of mechanically orthotropic tissues (seen in MI scar of large animal models), but cutting the tissue to necessary dimensions to facilitate testing often is difficult and compromises the specimen integrity[55,87,115].

Studies that provide a direct study of mechanics of the heart in an *in vivo* state commonly utilize tools such as MRI imaging, and more directly sonomicrometry array localization.

Sonomicrometry Array Localization

The use of highly specialized sonomicrometry crystals has garnered a lot of interest in studying mechanics and function of the heart. Sonomicrometry crystals transmit and receive sound energy. Each crystal is a digital sonomicrometer that takes some electrical signal (voltage) to emit an ultra-sound burst that can ping multiple receiving crystals. The voltages are converted into sound energy through the tissue medium the crystals are placed in. The frequencies that transmitting crystals output are in the 1 MHz range. This allows for a calculation of distance between crystals as the information gathered from transmission-reception time lapse is recorded in Herz (number of cycles/second) and the known speed of sound through biological materials is 1540 meters/ second [34,38,181]. The size of the crystals can be modified for implantation directly on the epicardial and endocardial surfaces of the heart or embedded within the myocardial wall.

The capabilities of these crystals to transmit information as well as their size provide an advantageous tool with which to study mechanics in an *in vivo* context. Investigations of MI scar mechanics have utilized this tool in a limited capacity with its primary focus being a means to measure global LV function or strain alone instead of a comprehensive regional mechanical characterization of scar behavior during the cardiac cycle (scar evolution, extension of border zone, local mechanical characterization, etc.) [38,49,51,73,193].

State of the art biomaterial therapies

In the pursuit of viable therapies to impede negative remodeling effects, polymeric targeted approaches have shown rising interest and success. Investigations in

the relationship between regional mechanics and their impact on collagen deposition have demonstrated a correlation between the two in a rat model [51,54,102,155,175]. Such studies present the foundation for the idea of impacting the regional scar mechanics via interventional therapies to modulate collagen architecture and altering the natural remodeling process.

Approaches to modify the mechanics of the scar include the use of passive restraints, biomaterial injectates and cellularized versions of each [92,102,114,155]. Further categorizing these approaches is the distinction of synthetics vs. natural materials. In the passive restraints avenue of treatment cardiac patches and meshes have been widely studied. The idea behind mesh strategies is to impede the outward dilation of the infarct region by physically restraining it in the area of coverage [45,89,90,121,155]. Materials that have been investigated include a wide range of synthetic and natural polymers such as polypropelene (merselene, synthetic) and fibrin based (natural) options [121]. The range of coverage has also been tested with meshes that cover the infarct alone to cardiac support devices that cover both ventricles of the heart with positive outcomes for both [45]. Aside from acting as purely passive mechanical supports, meshes and patches have also incorporated cellular and bioactive deliverables with some successful impact on remodeling outcomes [28,89,114,171]. The largest detractor from these solutions in a clinical setting is the invasive nature of applying the devices to the epicardial surface of the heart and the associated risks with such a procedure in patients that have already incurred increased health risks from acute coronary events.

The promise of biomaterial polymeric injectates provides a possible, thought eventual, alternative to largely invasive procedures [29]. Biomaterial therapies provide a

targeted approach that has the potential to translate into a catheter style delivery for injectable hydrogels [22,54,56,70,77,114]. Polymers that are synthetic or natural in origin can be tailored for specific material characteristics including: mechanical stiffness, degradation mechanics, bioactive delivery kinetics and biocompatibility. Principal studies in the field of biomaterial injections have shown similar promise in altering remodeling outcomes post-MI in various animal models [77,102,171] with a multitude of material choices [155]. Naturally derived materials such as fibrin, collagen, alginates and hyaluronic acid derivatives are attractive options due to their tuneability for specific mechanics as well as biocompatibility of their cross-linked forms and degradation byproducts [29,54,155].

1.2 Project Scope

Studies in the mechanics of myocardial scar have explored experimental avenues that have severe limitations in representing the physiological environment and bypassing active components of mechanical behavior of the MI scar. The direct use of sonomicrometry crystals to obtain measures of regional scar mechanics outside of global LV responses demonstrates a gap in the basic understanding and knowledge in the field. Various combinations of experimental techniques have been used in assessing plausible therapeutic approaches, yet no single comprehensive model exists to directly correlate parameters of material characteristics to regional remodeling outcomes. The creation of such a predictive framework could further the optimization of material parameters and define the regional dependence necessary to optimize material delivery strategies. To this effect a comprehensive understanding of biomaterial-tissue interactions needs to be carried out and therefore we pose the following questions:

1. Can we characterize the regional behavior of the developing MI scar in terms of classical mechanistic variables of stress, strain, material stiffness and compliance via a sonomicrometry approach?
2. Can we parameterize material characteristics and their imparted effects on the MI tissue in terms of global and regional mechanics and LV geometric outcomes?
3. Can we characterize mechanical effects of the HA treatment in a regional manner to aid the creation of a predictive computational framework relating mechanical characteristics of the initial MI region, biomaterial-MI tissue hybrid and remodeling outcomes for optimization of injectable therapies?

1.3 Specific Aims

The specific aims of this dissertation are focused on further investigation MI regional mechanics as well as developing a comprehensive strategy for optimization of a hyaluronic acid based hydrogel injectate. The goals of this work are divided into three primary specific aims:

Specific Aim 1: Characterize the mechanics of the MI region throughout early post-MI remodeling following injection of an HA gel primarily via sonomicrometry in a pig model and supported by echocardiography and ex-vivo mechanical testing of a MI-HA gel hybrid.

Specific Aim 2: Generate in-vitro metrics of HA gel degradation, erosion, and mechanical stiffness and seek correlation to in-vivo metrics of remodeling outcomes following HA gel injection into the MI region.

Specific Aim 3: Generate a robust data set of mechanical metrics with a regional focus in the LV that incorporates measurements of MI region geometry and material mechanics (with and without HA gel injection) to better characterize the effects of an HA gel injectate at a relevant time point post-MI with methods applicable to other possible therapeutics as a framework for understanding the mechanical effects of material injection throughout LV remodeling.

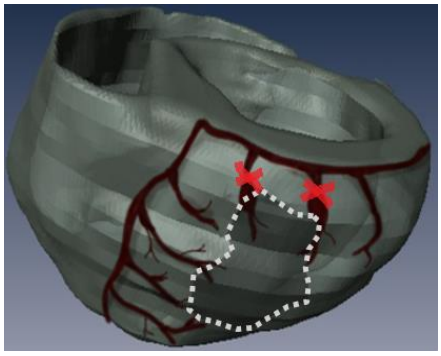

Figure 1.1 3-D rendering of LV with MI. Three-dimensional rendering of porcine heart depicting an acute coronary event. Marked region demonstrates a blockage in oxygenated blood delivery causing an ischemic region to form (within dotted line).

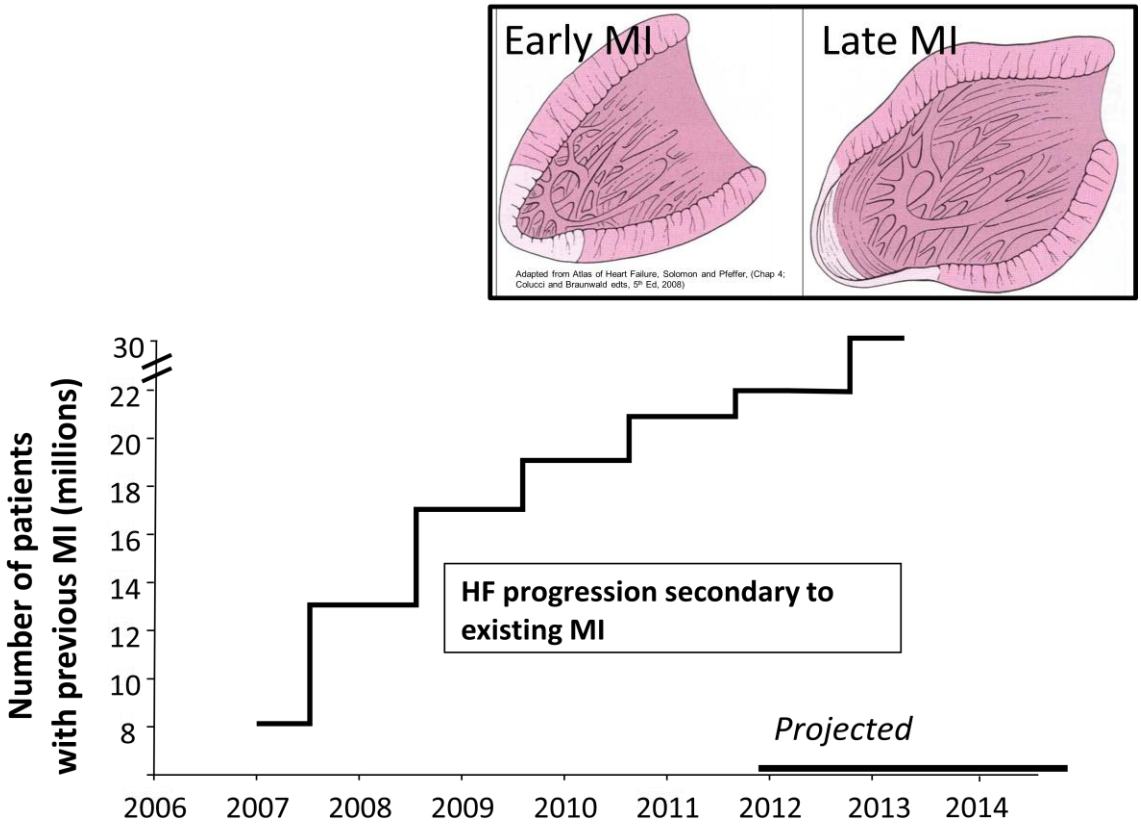

Figure 1.2 Representative MI and incidence. Representative figure of the left ventricle post-MI (top). Incidence of MI and trend of progression to heart failure by year.

CHAPTER 2

ASSESSMENT OF IN-VIVO POST-MYOCARDIAL INFARCTION; A FOCUS ON REGIONAL MECHANICS AND THE ROAD AHEAD[1]

[1] Romito, E, Shazly T, and Spinale, F.G. Submitted to Journal Of Applied Physiology 02/5/2016

2.1 Abstract

Cardiovascular disease, particularly the occurrence of myocardial infarction (MI), remains a leading cause of morbidity and mortality.[61,62] There is growing recognition that a key factor for post-MI outcomes is adverse remodeling and changes in the regional structure, composition, and mechanical properties of the MI region itself. However, in-vivo assessment of regional mechanics post-MI can be confounded by the species, temporal aspects of MI healing, as well as size, location, and extent of infarction across myocardial wall of the MI. Moreover, MI regional mechanics have been assessed over varying phases of the cardiac cycle and thus uniform conclusions regarding the material properties of the MI region can be difficult. This review assesses past studies that have performed in-vivo measures of MI mechanics and attempts to provide coalescence on key points from these studies as well as put forth potential recommendations for unifying approaches in terms of regional post-MI mechanics. A uniform approach to biophysical measures of import will allow comparisons across studies as well as provide a basis for potential therapeutic markers.

2.2 Introduction

Despite improvements in reperfusion therapy, prolonged periods of ischemia often culminate in permanent injury to the myocardial parenchyma, otherwise known as myocardial infarction (MI).[20,61,62,118,129,134,150,161,170] The resultant MI can lead to left ventricular (LV) pump dysfunction due to both a direct loss of contractile units and by placing the viable myocardium at a mechanical disadvantage.[133,164] The MI region itself is not static but rather undergoes significant changes in composition and structure over time. The elapsed time post-MI can be related to the phases of the normal wound

healing response: post-acute/inflammation, proliferation, and maturation. [31,32,39,40,46,52,53,142,163,177] However, the complete resolution of the wound into a fully formed and contracted scar, which is the end result of a prototypical wound healing response, does not occur in this context. Instead, the MI region undergoes continuous remodeling due to persistent proliferation of fibroblasts and turnover of newly formed extracellular matrix, and as a consequence, is structurally unstable.[50,120,130,163] This deviation from prototypical wound healing can be partially attributed to the continuous cyclical loading of the myocardium with resultant stresses and strains governing the activity of resident fibroblast cells. [23,25,100] Thus, while the remodeling process is certainly complex and multifactorial, it is likely that local alterations in stress and strain patterns that occur within the MI region contribute significantly to structural instability, thinning of the MI region, and increased MI area as a function of time.[85,113,179,180] Moreover, the continuous changes in the material properties of the MI coupled with abnormalities in stress and strain result in a "feed forward" mechanism for progressive MI expansion, LV dilation, and ultimately LV failure - termed adverse post-MI remodeling.[33,164] Therefore, the continued development of therapeutic strategies to interrupt/attenuate adverse post-MI remodeling requires consideration of the mechanical properties and behavior of the MI region itself. [29,69,77,90,179] For example, mechanical restraint devices that surround part or all of the LV have shown potential to limit MI region dilation up to 8 weeks post-MI. [90] Accordingly, the overall goal of this review is to evaluate past studies that have examined biophysical properties of the MI region and to coalesce these findings into unifying concepts regarding the relation of these properties to the post-MI remodeling process.

Past studies have utilized different post-MI models, measurement systems, and time points to quantify MI region mechanics, all of which must be taken into consideration for meaningful interpretation of reported results. To that end, this review places past studies in temporal context to the post-MI phases of remodeling identified as post-acute (3-7 days), intermediate (7-14 day), and late remodeling (>14 days). While these temporal phases are rather arbitrary and overlapping, they serve to demark relevant cellular/extracellular changes that likely impact biophysical properties of the MI region.[133,140] However, it is important to note that for clinical observations, some exceptions have been made for inclusion within the post-acute phase, as most studies approximate the onset of MI and only report the elapsed time since reperfusion. In this review, the acute phase of ischemia will not be considered, because biophysical measurements in this time period are confounded by the effects of reperfusion, differences in myocardial viability and stunning, and significant variances in overall tissue viability. In general, these events have dissipated by ~72 hours following the index event.[19,41,48,89,164] A number of landmark studies have been performed, whereby the myocardial mechanical properties have been examined from excised specimens taken from normal and infarcted LV regions.[66,88,116,117,120,123,187] These studies have provided critical insight into the development of models that characterize key aspects of cardiac muscle biophysical behavior. However, the translation of these in-vitro studies to the intact cardiac preparation, specifically in terms of the mechanical properties of the MI region, is much less clear. Accordingly, this review will focus upon studies that have examined the mechanical properties of the MI region only under in-vivo conditions.

2.3 Post-Acute Time Phase (3-7 Days)

Significant cardiac myocyte cell loss via necrosis/apoptosis occurs in the post-acute phase, which is accompanied by the elaboration of cytokines and an egress of inflammatory cells, such as neutrophils and macrophages.[40,52,53,145,166] These biological/cellular events are accompanied by an increased release of a number of proteases that degrade cellular and extracellular components and thus contribute to structural remodeling of the MI region.[40,52,145,162] Notable physiological results of these cellular and extracellular events are increased vascular permeability and changes in interstitial oncotic pressure, which in turn promote localized edema within the MI region.[4,50] Together, these changes in composition, structure, and turgor pressure will significantly affect mechanics within the MI region.

While the generalized inflammatory pathways and cell types can be similar across species in this post-acute phase, there are temporal differences in the pattern of inflammation between small and large mammals post-MI.[39] For example, a robust increase in the cytokine tumor necrosis factor alpha is observed early in rodent MI models with a tendency to plateau and resolve by one week post-MI.[40,52,162] In contrast, a more progressive and sustained increase in tumor necrosis factor alpha within the MI region is reported in large animal models.[39,40,52] The temporal cytokine profile observed in large animal models in this post-MI period is similar to the cytokine profile observed in plasma samples obtained in humans.[18,33,46,52,53,85] Similarly, temporal differences in the release of matrix proteases and development of local tissue edema have been observed between small and large animal models post-MI. A summary of the temporal changes in some of these post-MI processes is presented in Figure 2.1. Perhaps the most striking

outcome of interspecies differences is the occurrence of myocardial rupture. Specifically, myocardial rupture is a rare event clinically post-MI and exceedingly uncommon in large animal models.[17,108,119] In contrast, rodent models of MI, particularly those of mice, have reported rupture rates between 29-53%.[26,162,166] These observations would suggest significant differences in the cellular and extracellular architecture and composition within the MI region of rodents as opposed to large mammals, which in turn would directly influence regional mechanical properties. Accordingly, the type of animal model used will have significant implications for measurements of MI region mechanics in the post-acute phase.

Imaging studies

A large number of studies have utilized various imaging modalities to study the function and mechanics of the LV and specifically the MI region. The most common techniques include magnetic resonance imaging (MRI) as well as ultrasound in both humans and animals. [2,6,57,59,128,143,172,176,186] The primary goal of most studies has been to identify correlations among MI size, mechanics, and functional measures. Imaging techniques present an attractive opportunity for less invasive and clinically translatable approaches. [30,64]

Ultrasound

Traditional 2-D ultrasound measurements have been utilized extensively to examine LV volumetric and pump function in the post-MI period. For the purposes of focus, studies that have utilized ultrasound to examine aspects of myocardial strain, and in particular strain during the filling phase of the cardiac cycle, will be examined to quantify cavity dimensions and extract mechanical measures of the LV post-MI. Tissue

Doppler Imaging (TDI), a form of ultrasound, is a noninvasive method by which regional indices of myocardial function, such as contraction (from endocardial and epicardial velocities) and wall motion, may be assessed. [8,60,172,182] Strain rate imaging (SRI) can be acquired and has proven to be an effective tool in the evaluation of both MI and viable surrounding myocardium (Figure 2.2).[43,60,168,189] While the precise post-MI period was not specified, Edvardsen *et al* reported that following the acute post-MI period in patients, abnormal deformation patterns exist in the post-MI LV with longitudinal stretching in the MI region compared to shortening (in the same direction) in the remote myocardium. [43] Moreover, radial cycle dependent strains within the MI region were indicative of localized thinning rather than thickening (Figure 2.2A [43,78,189]). The study by Zhang *et al* used strain rate imaging to assess various markers of LV function relevant to the mechanics of the region, which included early diastolic strain rate and peak systolic strain rate (reference length at end diastole) in patients with varying extents of infarction across myocardial wall at 2-6 days post-MI. [189] This study determined that the peak systolic strain rate and early diastolic strain rate decreased most markedly in patients where a completely transmural MI was present (Figure 2.2B [43,78,189]). In those patients with a transmural MI, the greatest decline in both peak systolic strain rate and early diastolic strain rates occurred. From the results of this study, the influence of infarction across myocardial wall as a factor affecting the mechanics of the MI region can be gleaned.

Magnetic Resonance Imaging

MRI has long been heralded as the gold standard technique for assessment of LV mechanics due to its high spatial resolution and non-invasive nature. [3,58,149] A common use of MRI involves the tagging of the LV and MI region with a set of horizontal and vertical lines (by saturation) to track points or segments during multiple cardiac cycles, termed spatial modulation of magnetization (SPAMM, or MR tagging). In general, MR tagging strain measurements are derived from radiofrequency pulses that produce magnetic saturation, enabling the tracking of segment or line lengths that can be analyzed over cardiac cycles.[3,30] Measurements of tracked points/segments through the cardiac cycle can then be converted to linear dimensions, hence an index of mechanical strain. Using this approach, it has been identified, for example, that a reduction (from referent control values) in peak systolic strain (absolute values) within the MI region is related to the reduction in LV pump performance, whether strain is measured along a longitudinal, circumferential, or radial direction.[174] With consideration of the relatively accelerated remodeling process in rodents, Ross *et al* utilized MRI to assess the extent of wall thickening (among other regional functional measures) at 1 day post-MI.[143] The authors noted that the percentage of wall thickening (presented as % of end diastolic wall thickness) showed an approximate 60% decline from baseline to roughly 10% after only 1 day post-MI. While wall thickening clearly declined, radial strain at different times post-MI varied significantly, with differences attributed to edema-related changes in the end diastolic wall thickness. This study also reported the disappearance of such edema at day seven post-MI, which was accompanied by a further decrease in wall thickening. This change in wall thickening in the MI region could potentially be interpreted as

change in strain, likely in the radial direction (here seemingly affected by edema). These changes in MI thickness and motion over a 3-7 day time period are consistent with the inflammatory timeline for rodents (Figure 2.1 [39,40,46,52,53,79,80,86,98,183]). Young *et al* reported circumferential and longitudinal cycle dependent strains in a rodent MI model to exhibit spatial variation throughout the LV, although there is a persistent decrease in magnitude (compared to referent normal strains) at all locations.[188] Since there is a relatively collapsed time window for the acute post-MI period and the spatial resolution of MRI in rodents can be limited, this technique is primarily relegated to large animal models to examine regional mechanics post-MI. Using a pig model, Saeed *et al* found similar decreases in longitudinal and circumferential cycle dependent strains at 3 days post-MI (compared to remote myocardium) and also reported significantly decreased peak systolic strain in all directions (radial, circumferential, longitudinal) in the analyzed segments contained within the MI region.[149] Another study in pigs quantified the differences in peak circumferential cycle-dependent strain between the MI region and peri-infarct zone. [152] This study used late-gadolinium enhancement-cardiac MR to quantify regional strains, finding the 3 day time point to show a significant decrease in both MI region and peri-infarct zone strain. Such findings of variances in strain in the different regions (MI region, peri-infarct zone, remote, etc) underscore that variations in strain occur non-uniformly over time.

Various studies have been carried out in a clinical setting with MRI techniques as a basis for the study of the post-MI myocardium. Using MR tagging in patients, Bogaert *et al* found that normal and shear strains in the MI region decreased significantly by 5 days post-MI.[16] This study noted a slight increase in edema contributing to MI wall

thickness, which has previously been shown to modulate wall stress and strain patterns and lead to an increase in structural stiffness.[4] Garot *et al* used tagged MRI coupled with harmonic phase imaging (HARP).[57] This dual approach isolates segmental motion of tagged myocardium (MRI tagging), which is then analyzed using a HARP algorithm that produces phase images (based on the spectral peaks in the Fourier domain). In these images, the motion of points can then be tracked along with the accompanying direction of movement.[126] In this past clinical study, MRI using HARP was performed approximately 3 days post-MI while arguably, prior to the time points of interest in this review, holding relevance in terms of regional mechanics within both normally perfused and MI segments. Specifically, this study identified that regional systolic strain pattern changes in both perfused and non-perfused segments occurred at this early post-MI time point. Gerber *et al* also utilized tagged MRI in conjunction with contrast enhanced MRI at 4 days post-MI in patients to analyze the peak circumferential shortening strain (fractional change of length between end diastole and end systole) recorded at end systole. The authors found that circumferential strain significantly decreased in segments that displayed early hypo-enhancement (lower retention of contrast indicative of viable tissue) as well as delayed hyper-enhancement (increased retention of contrast indicative of MI) when compared to remote segments. These findings demonstrate that in addition to quantifying the extent of an infarction, hypo- and hyper-enhancement can be used to develop MRI-based indices of myocardial function. In this study, the dysfunctional segments contained within the MI region demonstrated a significant relationship of circumferential shortening improvement (increased contractility) dependent on

hyper/hypo-enhancement that represented the extent of infarction across myocardial wall of the MI. [58]

Mechanical implications

The post-acute phase is temporally offset across animal models with rodents exhibiting collagen deposition and scar maturation twice as fast as large mammals. In all animal models, the strain in the MI region decreases as compared to controls, albeit to different extents. It is important to note that the remote myocardial region in treatment groups serves as a referent control in some studies. Although this is a common study design, it is well-known that the remote region geometry and properties change throughout the remodeling process.[16] Therefore, sham animals should be used for control groups when possible. The MI region nominally exhibits a high degree of mechanical anisotropy with most studies reporting changes in the absolute values of strain that differ along the principal directions (where coordinate directions correspond to zero shear) and over time. The local decrease in strain is often interpreted as a change in the material properties of the MI region and has been described in terms of dyskinetic wall motion with respect to the remote myocardium.[165] Studies that utilized various imaging modalities have identified progressive wall thinning and decreased curvature in the LV, both of which contribute to an observed increase in global wall stress. Some studies have focused on the mechanics of the regions adjacent to the MI and likewise found a decrease in recorded strain magnitudes. Post-MI remodeling results in changes to both material and structural properties. The material properties of the MI region are impacted by the

local change in myocardial composition (increased collagen content, presence of edema, etc) and can only be identified based on stress-strain relations. Post-MI changes in structural properties of the LV depend on the evolution of both material properties and geometry and can be quantified from pressure-volume relations obtained at the chamber level (i.e. chamber stiffness). Measurements of both material and structural properties are affected by the loss of contractile units in the MI region and the forces applied on this region by the surrounding viable myocardium. As a result, quantification of MI region material properties are better assessed during diastole, with the myocardium considered as a passively deforming material. Moreover, structural properties of the LV should always be reported along with a corresponding point in the cardiac cycle. Together, studies suggest that changes in regional strain and stress do correlate with concurrent changes in functional indices.

2.4 Intermediate Time Phase (7-14 Days)

This post-MI phase is associated with increased expression of anti-inflammatory cytokines and pro-fibrotic molecules, where one of the most notable is transforming growth factor beta. [21,37,44,99,106,158] Studies involving a range of animal models consistently report increased fibroblast proliferation within the MI region in concurrence with changes in intra- and intercellular protein expression profiles.[39,40,46,69] Fibrillar collagen content within the MI region is elevated in comparison to the border or remote regions, and changes in LV geometry consistent with the MI expansion process occur. [178–180] Since this post-MI phase is accompanied by significant transitions in inflammation, signaling molecules, and matrix formation, very dynamic changes also occur in biophysical response variables within the MI region, such as strain, strain rate, and stress (quantity

that must be calculated). As stated previously, the temporal changes in biochemical/cellular events that occur in this post-MI phase are also species dependent (Figure 2.1a [39,40,46,52,53,79,80,86,98,183]), whereby temporal events in inflammation and matrix formation/maturation are shifted to the left (as per the figure) with respect to small and large animals. For example, in mouse MI models, a relatively mature MI scar (defined as a thinned, collagen rich region) has been reported to occur within two weeks post-MI.[31,32] Conversely, the MI region in larger animal models remains highly cellular and structurally dynamic throughout this phase and up through the late phase (28 days post-MI and beyond). Biomechanical response variables (which include stress and strain) are directly affected by the loss of contractile forces in the MI and active viable surrounding myocardium (affecting calculated stress) with architectural changes also impacting strain. [11,31,49,109,110,125,130,138] Thus, the temporal difference in scar maturation within the MI region with respect to different animal species constitutes an important consideration when evaluating stiffness in this post-MI time period.

Ultrasound

Modifications and expanded use of ultrasound, such as speckle tracking echocardiography (STE), layer-specific STE (LS-STE), and Tissue Doppler Imaging (TDI), have been used to examine changes in the length of segments and direction of strain within the MI, often at time points beyond this intermediate period. More specifically, these methods allow for computations of strain and strain rates of targeted chords within the MI region based on tracking the relative positions of individual speckles, a defined acoustic marker or pattern that can be tracked over time.[64] This

section will focus upon the admittedly few studies that have examined relative strain values within the MI region using these techniques in this time frame.

While the use of high resolution/frequency transducers (ultrasound probes) has improved spatial resolution and thus applications in rodent post-MI models, the majority of studies (primarily at acute or later time points) have been performed in large animals and humans. However, a study utilizing LS-STE in a rodent model at two weeks post-MI reported a depth-dependent decrease in the peak circumferential strain compared to baseline values. In transmural infarcts, a significant decrease in peak circumferential strain was found only in the layers spanning the endocardium and midwall. Conversely, non-transmural infarcts exhibited an increase in peak circumferential strain in the endocardial layer. These findings highlight the dependence of strain on extent of infarct across the myocardial wall, a model-specific factor which therefore should be considered and reported along with mechanical measurements of the MI region. (Figure 2.3 [10])

Using a dog model, Park *et al* reported a decrease in radial and longitudinal strain rate at both early and late diastole in concurrence with a reduction (from control values) in strain magnitudes. [127] The authors reported stiffness indices in the MI region (derived from wall thickness and hemodynamic pressure measurements) to increase in correlation with a decrease in diastolic strain rate and changes in composition. The end diastolic stress in the circumferential direction of the MI region was also noted to have a more drastic decrement compared to longitudinal direction. Here, the authors conclude with the suggestion that diastolic deformation indexes and functional measurements (rather than systolic) of the MI region could be significant metrics of study in future clinical applications.

In patients, it has been established that the extent of infarction across the myocardial wall affects the magnitude of strain changes post-MI.[12,189] To this effect, studies in patient populations using STE and 2D-echocardiography at a time point described as early, but beyond acute occurrence of MI, are here categorized as falling in the intermediate phase. In these studies, the segments with a completely transmural MI resulted in decreased peak systolic strains in both circumferential and radial directions at both short and long axis. A significant decrease compared to referent normal values in strain rates (systolic, same directions) was also associated with extent of infarction across the myocardial wall.[12,27]

Magnetic Resonance Imaging (MRI)

MRI studies using rat and mouse models in the intermediate time frame have shown a continued decrease in strain (in all directions) compared to the acute time period. This decrease is consistent with the progress toward maturation of the MI (Figure 2.1 [39,40,46,52,53,79,80,86,98,183]). In rats, Young *et al* utilized MRI tagging and late gadolinium enhancement-MRI (LGE-MRI) techniques with a finite element model (FE) to map LV wall strain. The results at the 7 day time point found the longitudinal, circumferential, and 3D principal strains to be most affected (compared to the control) in the apical region and midventricular regions.[188] Here, the 3D principal strain was defined as the maximal contraction at a given point in a direction not usually aligned with a traditional image plane, highlighting regional differences of strain post-MI.

In a dog model, SPAMM tagged MRI in conjunction with a finite element (FE) model showed significant decreases in strain in all directions at 10 days post-MI, with

circumferential strain at the apex of the LV most affected.[97] Studies on pig MI models have sought to define regional strains and regional mechanical dyssynchrony using cardiac MRI and LGE-MRI, with results that are in general agreement with previous findings in large mammals (decreased strain in all directions).[1] Similarly, a pig model studied at 11 days post-MI with LGE-MRI in conjunction with HARP analysis showed MI region strains that were significantly less than baseline healthy segments. The circumferential strain displayed the greatest reduction in the MI region, although adjacent regions also exhibited significant alteration of principal strains. Here, principal strains are defined along coordinate directions that correspond to zero shear. It is interesting to note that this study eliminated segments that were not completely transmural, thus anticipating and accounting for the possibility of mechanical heterogeneity in the radial direction.[159]

Physical Approaches: Sonomicrometry and Markers

Sonomicrometry arrays are formed with ultrasonic crystals that each emit and receive high-frequency pulse waves, enabling the measure of relative distances between crystal pairs when implanted within the myocardium.[186] Tissue-embedded arrays can provide high spatial resolution of local deformation fields with some freedom in the creation of a reference coordinate system. A study carried out in a rat model by Fomovsky *et al* used seven sonomicrometry crystals to study MI region mechanics from 1-6 weeks post-MI. The authors found the circumferential and longitudinal strains were significantly decreased from referent normal values at both 1 week and 2 week time points. Critically, no collagen fiber alignment was seen in the MI region of the rats and thus it was considered a mechanically isotropic material. While appropriate here, the

categorization of MI region mechanical properties as isotropic may not be suitable for larger animal models that exhibit a high degree of fiber alignment. [49]

In larger animal models, such as sheep, the implantation of 9 sonomicrometry crystals along the MI region showed significant regional differences in strain with a two week time point. In this study, remodeling strain was defined as the change in end diastolic dimensions from baseline configuration of the crystals on the LV free wall to a deformed configuration at a specific time post-MI. In essence, this remodeling strain is representative of transient changes in geometry rather than cycle dependent ones. A significant increase in remodeling strain was observed at the 14 day time point, with a concomitant reduction in MI region end-systolic cyclical strain also promoting akinesis. The authors also found a correlation between markers of apoptosis and measures of remodeling strain and concluded that this is a promising mechanics-based target for interruption of post-MI remodeling.[93] Jackson *et al* tracked the areas of the MI region, border zone, and remote regions from baseline to 8 weeks post-MI and reported nearly 40% expansion (increase in total area) within the MI region after two weeks compared to the baseline. At the same time point, the border zone experienced a 10% expansion, and the remote showed <5% expansion. (Figure 2.2C [43,78,189]) Interestingly, the authors note that the rate of expansion immediately following the onset of infarction was similar in all regions.[78] Although not reported in this study, a measure of remodeling strain (change from baseline length) would have likely shown an increase as the expansion of the MI region took place.

A combinatorial approach entails implantation of physical markers within the MI region, such as titanium or gold beads, and subsequent utilization of an imaging

technique to track their relative positions. Using a sheep model, Gorman *et al* used MRI tagging and titanium markers along the border zone of the MI region. Obtained results show that systolic border zone radial strain had significantly decreased by one week post-MI and would continue to decline over the next 12 weeks, while the MI region area gradually increased in size. [15] Another study by Holmes *et al* used gold beads implanted in the LV free wall of pigs and biplane cineradiography to track deformations at 1 and 3 weeks post-MI. This study used a plexiglass phantom with embedded beads to calibrate a coordinated system for calculation of principal and remodeling strains. Reference lengths for strain calculations were obtained at end diastole in a control animal. At one week, the authors report a marked circumferential LV expansion, an increase in remodeling strains, and a decrease in cycle-dependent radial and in-plane strains, with the plane of interest defined by the longitudinal and circumferential directions (tangent to the epicardium). [74]

Mechanical implications

Post-MI healing throughout the intermediate phase significantly differs among animal models, with rodents entering a period of scar maturation while larger mammals continue to exhibit fibroblast proliferation and collagen deposition. Numerous factors impact recorded strain patterns, including the presence of edema, the MI size, the extent of infarction across myocardial wall, and its location with respect to the anatomical long axis of the LV. Consistent mechanical observations include a decrease in MI region cyclic strain and an increase in remodeling strain. Direct comparisons among studies show quantitatively different strain magnitudes due to the use of different reference lengths, cardiac axis definition, extent of MI, location, and cardiac points of reference (systolic versus diastolic), although general trends in strains and strain rates persist. These

trends coupled with related qualitative descriptors of wall motion facilitate comparison among studies, although a comprehensive structure-function relationship of in-vivo mechanics of the MI region has not yet been reached. Increased remodeling strains were noted to be most prominent in the circumferential direction, with segment lengths changing as the MI region dilates post-MI. Along with changing strain, reports indicate that wall stress is generally increased, with the most significant changes observed in the diastolic pressure range.

2.5 Late Time Phase (14 days and beyond)

The late remodeling phase is characterized by lowered or absent cellular inflammatory infiltrate in the MI region.[39,40,46,52] The scar maturation process is underway across species in the MI region, whereby an index of MI/matrix maturation includes increased expression of lysyl oxidase, interleukin-10, and TIMP-1.[40,50,163] While total collagen content is uniformly elevated within the MI region, the relative stability and maturation of the matrix is species dependent as described previously and summarized in Figure 2.1. Moreover, the increased proliferation of fibroblasts, particularly fibroblasts with a secretive phenotype, occurs in this phase of post-MI remodeling. Thus, this phase can be associated with continued/persistent release of matrix proteases, which in turn will affect collagen maturation and turnover within the MI region. As a result, species dependent as well as fibroblast/protease dependent processes will directly affect the structural composition and integrity of the MI region, and in turn, measurements of strain/stiffness within this region.

Ultrasound

Benejam *et al* used a rat model and STE to characterize segmental dysfunction throughout the LV at a time point of 4-10 weeks post-MI. Their results demonstrated lowered absolute values for midwall circumferential and radial strains and strain rates. The authors also report a marked difference in strain amongst segments, with highly fibrotic segments displaying the lowest strain in the MI region. Peak systolic and early diastolic circumferential and radial strains showed lowered absolute values and strain variations in the MI region.[13] Liao *et al* used 2D strain echocardiography at this same time point and animal model in order to assess the development of the MI region. The authors determined strain and strain rate were decreased at different magnitudes dependent on location within the MI region, which was divided into anteroseptal, anterior, and anterolateral sections.[105] The results of these studies are generally consistent in rat models at the 4 week time point.[13,14,105]

A variation of STE was used in a dog model by Wong *et al*, where speckle tracking displacement estimates in the mid-wall were combined with shape tracking using compactly supported radial basis functions to improve quantitative deformation analyses. At a six week post-MI time point, acquired radial strain maps were consistent with previous reports of reduced MI region strains.[182]

Sakamoto *et al* utilized 2-D echocardiography and a sheep model to compare reperfused versus non-reperfused MIs at 8 weeks post-MI. The authors extend their measurements of remodeling strain (defined as the ratio of a baseline reference length to a deformed length post-MI) and wall motion to qualitatively assess the extent to which

reperfusion impacted MI region stiffness. The authors found that although thinning still occurred, the animals in the reperfusion group had MI regions that trended toward akinesis, signifying greater stiffening in contrast to the quantified dyskenesis in the non-reperfused group. [150] Comparably, a previously mentioned study in a dog model by Park *et al* at a similar time point reported the radial diastolic strain rates significantly decreased (by more than half in the case of radial late diastolic strain) compared to baseline values.[127] The decrease in strain rate prompted the authors to suggest an increase in MI region stiffness in the presented sheep study, although it is important to note contractility also inherently plays a role in the calculated strain rate.

In clinical observations, Thorstensen *et al* used 3-D echocardiography to compare global function in patients with small and large MI volume fractions (large >12% infarct volume fraction). They report decreased 3D global strain rate values in all directions (longitudinal, circumferential, and radial) that were significant in patients with large MI as compared to healthy controls.[169] Helle-valle *et al* used STE at 6 months post-MI to analyze strain, rotation, and wall motion in the segments within the MI region, border zone, and remote myocardium. [68] This study found that the center of the MI region displayed the greatest dyskenesis with a concomitant reduction (from referent normal values) in strain, i.e. abnormal motion is most extreme at the center of the infarct with a tendency to normal motion toward the edges. The authors noted an interesting pattern in rotation, with the counter-clockwise border (assuming a clockface orientation) zone showing hyper-rotation shifting to intermediate rotation towards the center of the MI region and trending towards hypo-rotation at the clockwise MI border. The authors suggest that systolic strain is reflective of regional contractile function and focus on this

portion of the cardiac phase. Experimental findings from this study were combined with a finite element model to resolve the apparent inconsistencies between regional apical rotation and strain. The authors conclude from simulation results that an imbalance in active contractile forces from the interaction of the MI region and surrounding viable myocardium is the cause for the oppositely directed rotations at the two MI border regions and low strain in the center of the MI region.[68]

Magnetic Resonance Imaging

A mouse model study by Ross *et al* used MRI and reported that the percent wall thickness (interpreted as increased remodeling radial strain) at 4 weeks post-MI was negative in the MI region, indicative of local thinning. This study also reported systolic wall bulging, which is representative of dyskinetic motion in the MI region.[143] Liu *et al* found post-MI heterogeneous changes in strain (presented as maximal stretch and maximal shortening independent of any coordinate system) in rats at a 4 week time point. This study utilized SPAMM tagging along with HARP analysis and found a reduction (compared to control values) in strain at the apex, while the strain at the LV base increased (Figure 2.4C-D [107,191]). These results suggest regionally dependent changes in strain occur in this late time period, as the apex and base of the LV were noted to have opposing changes post-MI in a model with an anteroapical infarct. [107] Espe *et al* studied the LV motion in a rat model at 6-weeks post-MI by using phase contrast-MRI (PC-MRI).[47] This study calculated regional circumferential strain from the acquired PC-MRI velocity data and found the peak circumferential strain to decrease both globally and in the MI region with significant heterogeneity throughout the LV. This study focused its measurements in the systolic portion of the cardiac phase, thus obtaining peak strain for

both global and regional measurements. From these rodent studies, it can be concluded that mechanical changes (strains and other mechanical descriptors) post-MI in the late remodeling period occur in a heterogeneous manner through the MI region and the LV as a whole. These changes are expressed in structural, functional (loss of contractility), and compositional variation that effectively reduces strain (with implications of an increase in stiffness) and concomitantly affects motion in the MI region.

Larger animal models, such as pigs used in a study by Saeed *et al*, indicated a reduction in MI region strain in all directions, which peaked at the 5 week point, and interestingly, slightly recovered (compared to control values) in the circumferential and longitudinal directions by 10 weeks.[149] Similarly, Schuleri et al found that circumferential strain decreased in the MI region of pigs and demonstrated lowest values at 30 days post-MI (instead of 5 weeks) with a similar trend in the peri-infarct zone. The assertion that changes in the cycle-dependent strain are different between the MI and the peri-infarct region (border zone around MI) was the prime conclusion of that study. The authors go on to suggest that the differences in peak circumferential strain at the border of the peri-infarct zone and the MI ultimately contributes to continued remodeling.[152] In a pig model, elevated dyssynchrony and a significant reduction in global peak circumferential strain were observed from 7 to 33 days post-MI in the infarct and border regions.[1] Dyssynchrony refers to the abnormal activation of tissue elements in the myocardium during a normal cardiac cycle. This study showed this index of motion at an early time point (1 week post-MI) to be a potential indicator of the extent to which MI affects mechanical synchrony at longer periods post-MI and other mechanical

descriptors, such as strain. Further, the authors suggest this finding could affect therapeutic options (such as cardiac resynchronization therapy). [1]

In sheep, Walker *et al* used tagged MRI to build and validate an FE model at 22 weeks post-MI. The model was populated with material properties acquired from biaxial mechanical testing of excised myocardium and was validated by comparison of predicted and measured (via MRI) wall stress. The results of the simulation were found to be in agreement with stress calculated from MRI data and included a dramatic increase in midwall systolic stress in the fiber and cross-fiber directions in the border zone. Using this methodology, the authors demonstrated model accuracy in terms of predicted circumferential strains in the MI, border zone and remote regions, as well as systolic stress in the MI region. [174]

Ventriculography

Clinical observations by groups such as Mitchell *et al* used ventriculography to study the LV geometry, contractility, and effects of treatment at 3 weeks and one year post-MI. Digitized silhouettes of the LV were used to quantify wall motion via tracking of demarcated chords, ultimately showing that contractile segment length (defined as the length spanning the LV wall) increased after one year. Such an increase is consistent with larger end diastolic volumes. The authors speculate that the global increase in sphericity coupled with MI region flattening together redistribute wall tension in a manner that compensates for the less compliant MI region.[118] Hayashida *et al* also compared digitized silhouettes of the LV over multiple cardiac cycles, and further related measured deformation to chamber pressure to generate a regional stiffness coefficient. The stiffness

coefficient at one year significantly increased from baseline in the MI region (apex) but slightly decreased at the base of the LV.[67]

Physical Approaches: Sonomicrometry and Markers

Fomovsky *et al* integrated sonomicrometry with imaging and biochemical analysis in a rat MI model. The authors report that at six weeks post-MI, the circumferential and longitudinal strains decrease compared to normal values. However, in contrast to aforementioned findings in pigs, the MI region exhibited mechanical isotropy. The authors note that the typical shape of the MI region is different than seen in larger animal models and suggest a causal relationship to the differential rates of cellular infiltration and inflammation between species.[49] In sheep, Yankey *et al* used sonomicrometry crystals from 2-8 weeks post-MI to assess MI and surrounding region deformations.[184] Metrics of end systolic strain and remodeling strain were calculated from the sonomicrometry data. At two weeks post-MI, fractional contraction of the MI region significantly decreased while remodeling strain increased. Using a dog model, Theroux *et al* found that at four weeks post-MI the percent shortening of segments (determined by crystal pair lengths) was dramatically reduced in the MI region compared to normal myocardium.[167]

Using a pig model, Holmes *et al* combined gold bead implantation, biplane cineradiography, and a finite element modeling to study the mechanical outcomes of remodeling 3 weeks post-MI. Their results demonstrated a significant change in strain in all directions, reflective of the remodeling changes noted in the circumferential bulging (reflective of dilation) and a significant decrease in wall thinning.[73] Zimmerman *et al*

used a similar model and technique with a bead set and a phantom to establish fiber and fiber-sheet reference coordinate systems. These reference systems allowed for calculation of remodeling strains (in principal normal directions) of the area adjacent to the MI region (Figure 2.4A-B [107,191]). The remodeling strains were calculated from the difference between the control and 3 weeks post-MI diastolic bead configurations. Findings report differences in all directions (circumferential, radial, and longitudinal) between the outer and inner halves of the LV wall. The radial remodeling strain of the inner half was most affected, and the transmural remodeling strains showed differences depending on the depth of the myocardial wall. In the fiber coordinate system, the average transmural fiber remodeling strain was most different near the endocardium, while in the fiber sheet coordinate system, there was minor sheet reduction at the endocardium.[191]

Mechanical Implications

The late remodeling phase is characterized by a highly fibrous and mature scar across all animal models and clinical studies. The mechanical response of the MI region continues to be modulated by its size, location, extent of infarction across myocardial wall, collagen content, organization, and edema. Wall motion analyses at time points beyond 2 weeks and up to a year have shown the MI to be dyskinetic with respect to adjacent or referent normal myocardium, including abnormalities in both expansion and rotation. Global strain and strain rate are consistently decreased, most notably in conjunction with large MI regions. Regional strain measurements using both physical and image-based measurements indicate mechanical anisotropy and heterogeneity within the MI region in small and large mammals, as well as a reduced strain response in the adjacent and remote myocardium. Consistent among studies is the reported increase in

end-diastolic wall stress within the MI region. Bulging in the MI region was noted to decrease at the one year time point, indicative of structural stiffening.

2.6 Summary

Due to temporal differences across animal models, MI region size and location, presence of edema, extent of infarction across myocardial wall, and measurement approaches, unifying concepts relating geometrical and compositional changes within the MI region to stiffness and other mechanical metrics have not been forthcoming. By focusing on species- and time-dependent differences, this review underscores both the complexity and inherent need to develop standard mechanics-based metrics.

The majority of past studies focused upon systolic strain/stiffness measurements in the post-MI period, which reflect the loss of contractile units or have examined strain in the post-MI period without a focus upon the timing of the cardiac cycle or region (Table 1). In this review, the main focus was on how continuum mechanical descriptors, such as stress and resulting strains, are affected during the cardiac cycle (impacted by contractility) post-MI and how this is associated with changes in composition. Using these factors as guiding principles, we put forth the following recommendations to be considered in order to improve the standardization and interpretation of post-MI remodeling (Figure 2.5 [184]).

Recommendations for future studies

Recommendation One: Remodeling Strain.

The reporting of strain as a primary metric of value has been a constant among the presented literature. The Lagrangian strain is (in the literature contained herein) often

calculated with a reference length taken at a specific point in the cardiac cycle and time post-MI, representing a cyclic strain. Largely, the trends in cyclic strain post-MI show regionally and directionally dependent decreases while remodeling strain (where reported) shows an opposing trend (increasing with time) (Figure 2.5 [184]). Remodeling strain is reflective of the changing geometry (dilation post-MI) and perhaps better characterizes the underlying transitions of the damaged myocardium. In light of this, we make our first recommendation on the consistent reporting of remodeling strain in experimental studies. Although not a new concept, only a handful of *in-vivo* studies report this metric where the reference length is defined at baseline and used thereafter for calculations.[74,78,93]

Recommendation Two: Operative Diastolic Pressure.

Our second recommendation pertaining to the diastolic pressure range for strain data is applicable to both experimental and clinical studies. Depending upon the extent of infarction across the myocardial wall of the MI as well as the influence of adjacent viable myocardium, systolic strain as an index of contractility/ejection performance is often measured. However, reporting strain during the systolic portion of the cardiac cycle alone could be misleading, as forces exerted from surrounding viable myocardium could mask important differences in the MI region in terms of intrinsic material properties. In recommending the diastolic pressure range as a principal point in the cardiac cycle to gather data, we contend that this is an important indicator of regional mechanical differences that exist in the LV. Further, the in-vivo study of this pressure range can elucidate passive material properties without the limitations in tissue integrity of ex-vivo preparations. We must note that fundamental chamber and material properties such as

stiffness, dyskinesis, and impaired myocyte relaxation can affect diastolic strain behavior making ex-vivo studies that can fully isolate passive material properties an important part of comprehensive study of MI scar tissue. It has previously been noted in rodent ex-vivo studies that the strain behavior at a low pressure range (Figure 2.6A [104,132,139]) is significantly affected compared to its higher counterparts (diastole vs. systole) with respect to time post-MI. Often, ex-vivo studies are used to isolate variables of interest (such as stiffness) and to perhaps amplify the observable effects by means of control over applied loads. Canonical examples of ex-vivo experiments with intact heart preparations include those represented in Figure 2.6.[24,104,125,132] These few examples of ex-vivo intact preparation studies on rodent models support the important factors derived from in-vivo findings with the compiled results corroborating the potential effects of important variables, such as time, species, size, composition, and loading conditions (here, pressure range). The net effect of the MI region transitions includes a visible and measurable difference in strain at a low pressure range and a local reduction (from a control value) in peak strain over the cardiac cycle, despite the dilation known to occur in the remodeling process (the latter addressed by our first recommendation).

Recommendation Three: Data Repository and Modeling

The final recommendation to be made is the establishment of an appropriate database for data from ex-vivo and in-vivo studies. This would be an important asset to ease comparisons and perhaps validate emerging techniques for the purposes of computational/mathematical modeling. More recently, data from ex-vivo experiments of both intact preparations and tensile testing are being incorporated into predictive computational models, wherein acquired mechanical measurements are used to develop

and validate simulations of MI region behavior. [34,75,76,176] Already, findings from studies using FE models have shown predictive value when results were compared to those from imaging approaches.[63,146,174,188] Other in silico studies have used in-vivo parameters for their geometric basis and for comparison as well as for using material parameters from biaxial tensile experiments.[92,94,175] In order to successfully integrate data from experimental and clinical studies, fastidious cataloging must take place, while paying close attention to the factors identified throughout this review. In doing so, a scaling factor between species stemming from the differences in healing timetables can perhaps be standardized. The fundamental advantage of these models is the possibility to examine in isolation the effect of key variables in the complex remodeling process. [146,174] Thus, invaluable insight can be gained that would otherwise be costly (due to requisite study size) or be unattainable in animal studies/clinical observation, emphasizing the need for a readily available database from which mechanical properties of the post-MI myocardium of different species, size, location, and maturity can be obtained. Ultimately, these models could aid in the design and evaluation of therapeutic strategies intended to alter LV mechanics in a post-MI context.

Acknowledgements.

This work was supported by the National Institute of Health grants HL11090, HL089944, HL43617, HL67922, and Merit Award from the Veterans' Affairs Health Administration. The authors wish to express their sincere appreciation to Ashley Sapp for her editorial assistance.

Table 2.1 Summary of Techniques.

Abbreviation	Technique and description
MRI	**Magnetic resonance imaging** - imaging technique utilizing a magnetic field and radio frequency pulse waves with high spatial resolution of soft tissues.
SPAMM/MR tagging	**Spatial modulation of magnetization** -saturation bands (in a grid) are created by radio frequency pulses, enabling the tracking of segment or line lengths that can be analyzed over cardiac cycles.
HARP	**Harmonic phase analysis** - spectral peaks of tagged MRI (in the fourier domain) are used to calculate phase images of the inverse fourier transforms. Motion of points in the resulting images can then be tracked.
LG-MRI	**Late-gadolinium enhancement MRI** - a gadolinium contrast is utilized for enhanced visualization of scar tissue post-MI.
SRI	**Strain rate imaging** - echocardiography technique that tracks deformation of myocardium.
TDI	**Tissue Doppler imaging** - echocardiography technique that describes myocardial motion.
Biplane cineradiography	Imaging technique utilizing an x-ray field to create a three-dimensional coordinate system by use of radio-opaque markers to calculate interpoint distances and deformation.
Ventriculography	Imaging technique used in the determination of function of the left ventricle, utilizing catheterization and injection of contrast for definition in x-ray images.

Table 2.2 Tabulated studies. *Studies are grouped by species, time frame, mechanical variables of note along with techniques used for quick reference from the text.*

Animal Model	Study	Time Frame Post-MI	Post-MI mechanical variables	Technique
Mouse	104	Early - Late	↓ E_R	MRI
Rat	135	Early - Late	↓Global E	MRI/SPAMM
Rat	7	Early - Intermediate	↓ Global E_C, E_R, E_L	LS-STE
Rat	10	Late	↓ EC dependent on fibrosis	STE
Rat	78	Early - Late	↓ End Diastolic E_R, E_C, SR_C, SR_R	2D SE
Rat	11	Early - Late	↓ Global and Regional ER, SR	STE
Rat	80	Early - Late	↓ E_1, E_2	MRI/SPAMM
Rat	37	Late	↓ Global Peak E_C	PC-MR
Rat	39	Intermediate - Late	↓ E_C, E_L	Sonomicrometry
Dog	93	Intermediate - Late	↓ Diastolic SR_R, SR_L	Doppler
Dog	73	Intermediate	↓E_1 apical region	MRI/ SPAMM
Dog	130	Late	↓ E_R	4DSE/MRI
Sheep	71	Late	↓ Peak E	Sonomicrometry
Sheep	60	Intermediate	↓ E_S	Sonomicrometry
Sheep	12	Early - Late	↓ Systolic E_R	MRI
Sheep	108	Early - Late	↓ Stretch	2D SE
Sheep	132	Late	↑ RE in MI and border zone	Sonomicrometry
Pig	107	Early - Late	↓ Peak E_R, E_L, E_C	MRI
Pig	109	Late	↓ Peak E_C	MRI

Pig	111	Intermediate - Late	↓ E_C. E_R, E_L	MRI/ SPAMM
Pig	56	Early - Late	↓ E_C, E_R, E_L	Biplane Cineradiography
Pig	1	Early - Late	↓Global and regional Peak E_C	CMR
Pig	138	Late	↑ RE_C, RE_R	Biplane Cineradiography
Human	34	Early	↓ E_L , E_C	TDI,SDE,MRI
Human	136	Early	↓ SR_S, SR_D, SR_A	TDI, SRI, Ce-MRI,
Human	13	Early	↓ E_R, E_C, E_L in MI and borderzone	MRI
Human	43	Early	↓ E_C	MRI
Human	44	Early	↓ E_C in segments with early hypo/delayed hyper enhancement.	Ce-MRI
Human	9	Intermediate	↓ Peak E_C, E_R, SR_C, SR_R	2DSE/Ce-MRI
Human	119	Late	↓ End systolic Global E_L, E_C, E_R	STE
Human	53	Late	↓ End systolic regional E	TDI
Human	52	Late	↑ Regional Wall Stress	Left Ventriculography

All strains reported are cycle dependent strains unless otherwise noted, and time periods are defined in the manuscript
Legend for mechanical variables is as follows :
Circumferential strain (E_C), Radial strain (E_R), Longitudinal strain (E_L)
Remodeling strain (ER), remodeling circumferential strain (REc), remodeling radial strain (RE_R)
Circumferential strain rate (SR_C), Radial strain rate (SR_R), Longitudinal strain rate (SR_L)
Principal strains are defined within the text and denoted as E_1, E_2

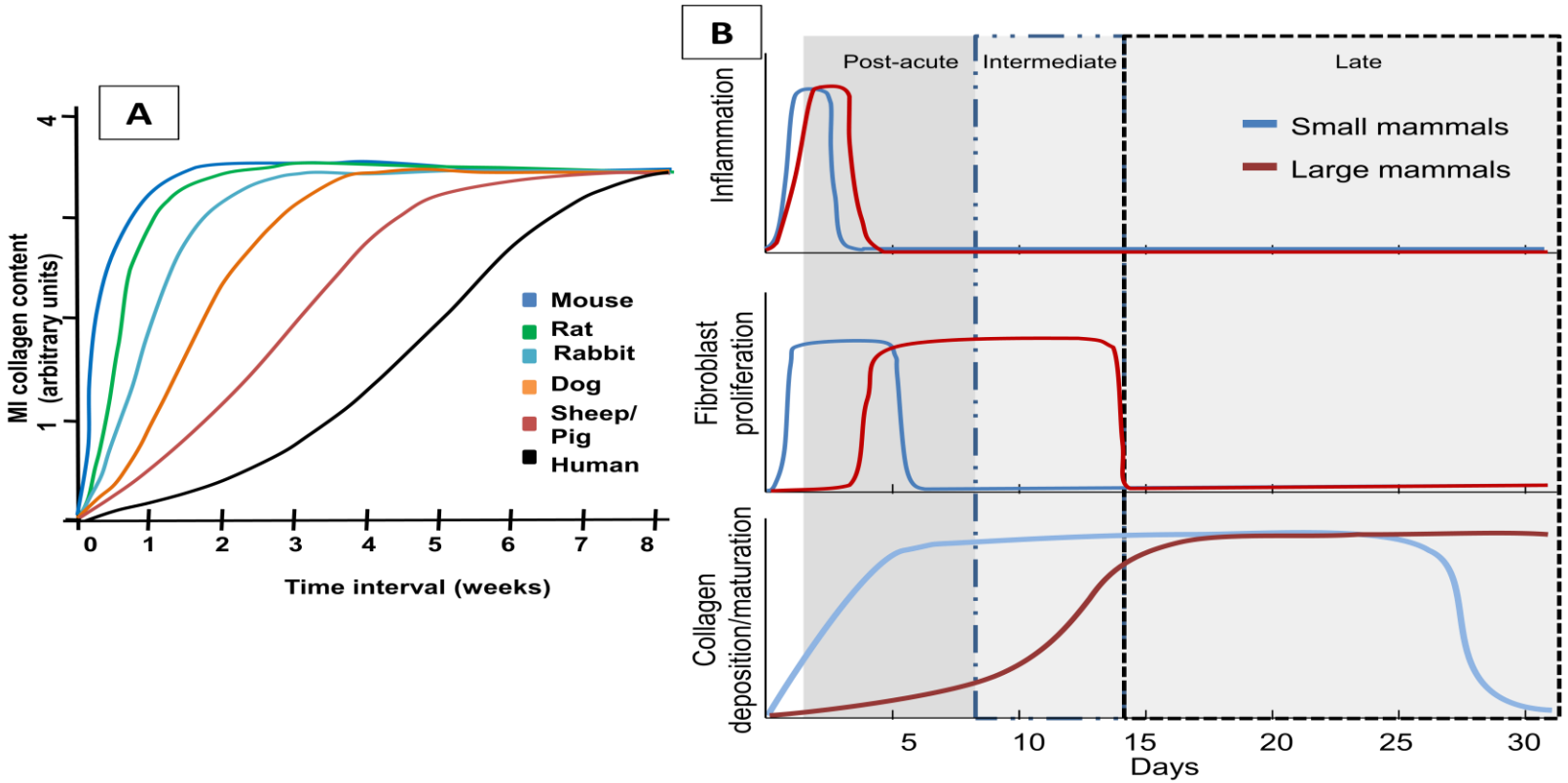

Figure 2.1 Species differences. Temporal representation of biological events post-MI in rodents and large mammals which can affect physical properties of the MI region. **(A)** Summary time plot of the rate of collagen accumulation as a function of time post-MI in different species. Figure adapted from Jugdutt et al [83] with original research from [48,86,91,140]. **(B)** Relative to large mammals, rodents exhibit accelerated resolution of the inflammatory phase **(Top)**, an earlier and abbreviated fibroblast proliferation phase **(Middle)**, and rapid collagen deposition and maturation **(Bottom)**. Figure compiled from data reported in Frangiogianis et al, Ertl et al, etc. [39,40,46,52,53,79,80,86,98,183]

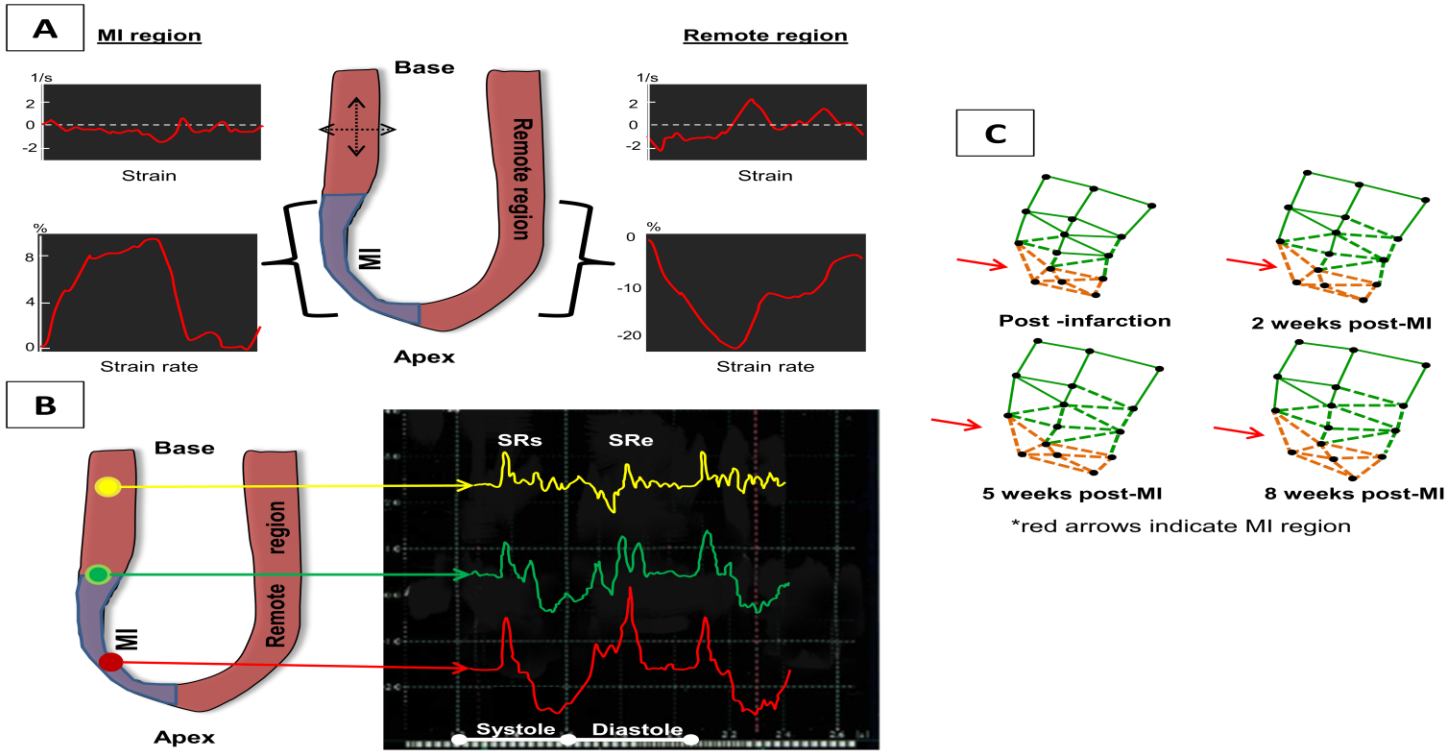

Figure 2.2 Strain heterogeneity. (A) The regional heterogeneity of LV strain following MI in patients (early post-MI period) was examined using tissue Doppler. Both cyclic longitudinal strain and strain rate exhibited significant variation between the MI and remote regions. Figure adapted from Edvardsen et al. [43] **(B)** Representative strain rate (SR) calculations using tissue Doppler in patients during the early post-MI period (2-6 days post index event), including both peak systolic strain rate (SRs) and early diastolic strain rate (SRe) Trace location is demarcated by line color: yellow= basal, green =mid-, red=apical segments. Adapted from Zhang et al.[189] **(C)** Representative chord reconstructions of a partial LV in adult sheep, whereby sonomicrometry crystals span the MI, border and remote regions. Occlusion of the distal segment of the left anterior descending coronary artery yielded an MI within the apical LV region (orange chords). Over time, a significant increase in these all chord lengths was observed. Figure adapted from Jackson et al.[78]

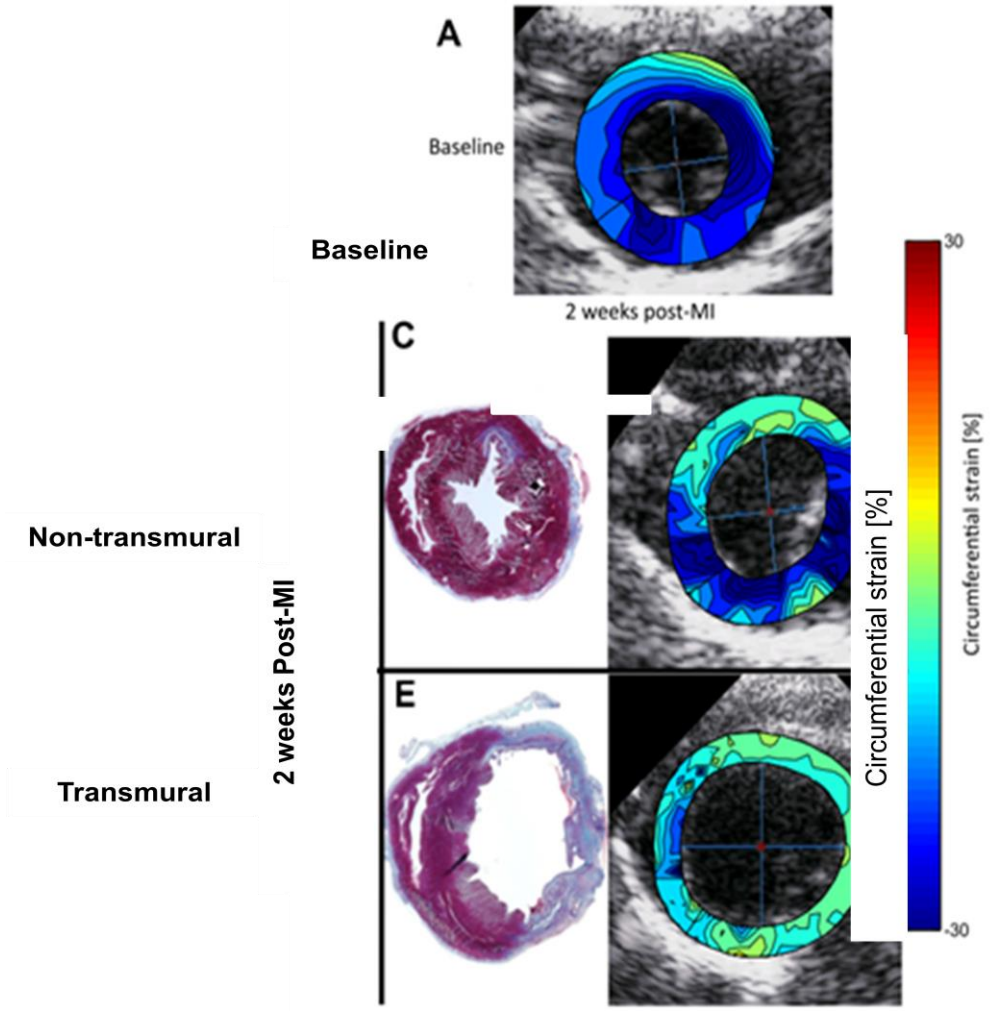

Figure 2.3 Extent of infarction across myocardial wall. Layer-specific speckle-tracking echocardiography depicting peak strain in a rat MI model with varying degrees of infarction across the myocardial wall(**Top**) Baseline cyclic strain at systole is nearly homogeneous and compressive. LV strain maps at 2 weeks post-MI of a non-transmural **(Middle)** and completely transmural **(Bottom)** MI depict a reduction in compressive strain magnitudes and uniformity, which is magnified by the depth of infarction across the myocardial wall. Figure adapted from Bachner-Hinenson et al.[10]

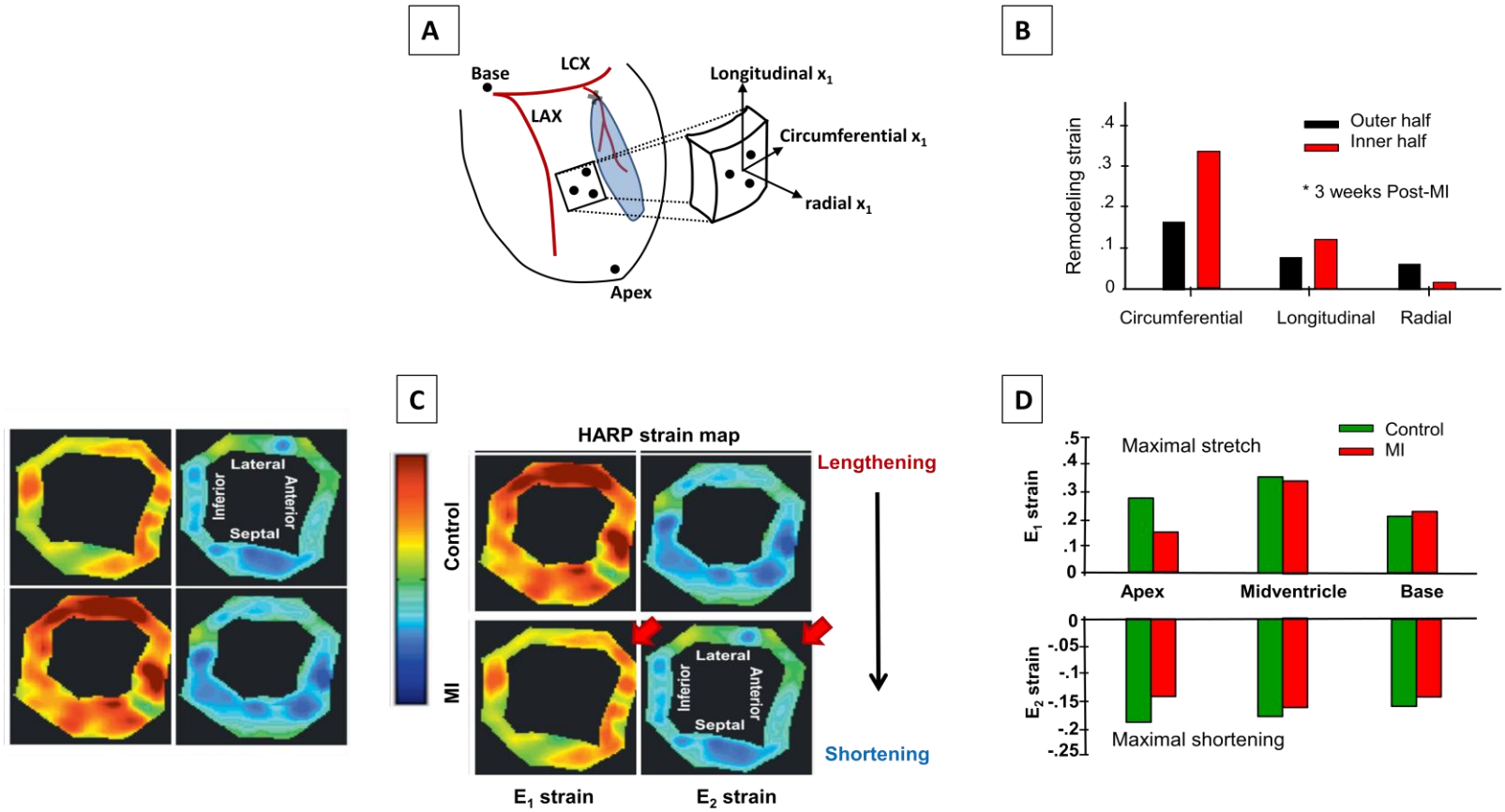

Figure 2.4 Directional dependence. (A) A schematic of an experimental MI model in pigs, whereby radio-opaque markers (●) were implanted to allow for directional measurements of strain using bi-plane cineradiography. **(B)** Remodeling strain depends on direction and depth across the LV wall. Figure adapted from Zimmerman 2004 et al. [191] **(C)** Magnetic resonance imaging (MRI) coupled with harmonic phase analysis (HARP) yields strain maps of a rat LV immediately following induction of an MI, with MI location denoted by the red arrows. **(D)** Calculated maximal stretch **(Top)** and maximal shortening **(Bottom)** by HARP analysis at distinct anatomical locations (base to apex) E_1 and E_2 represent principal stresses independent of coordinate system. Figures adapted from Liu et al. [107]

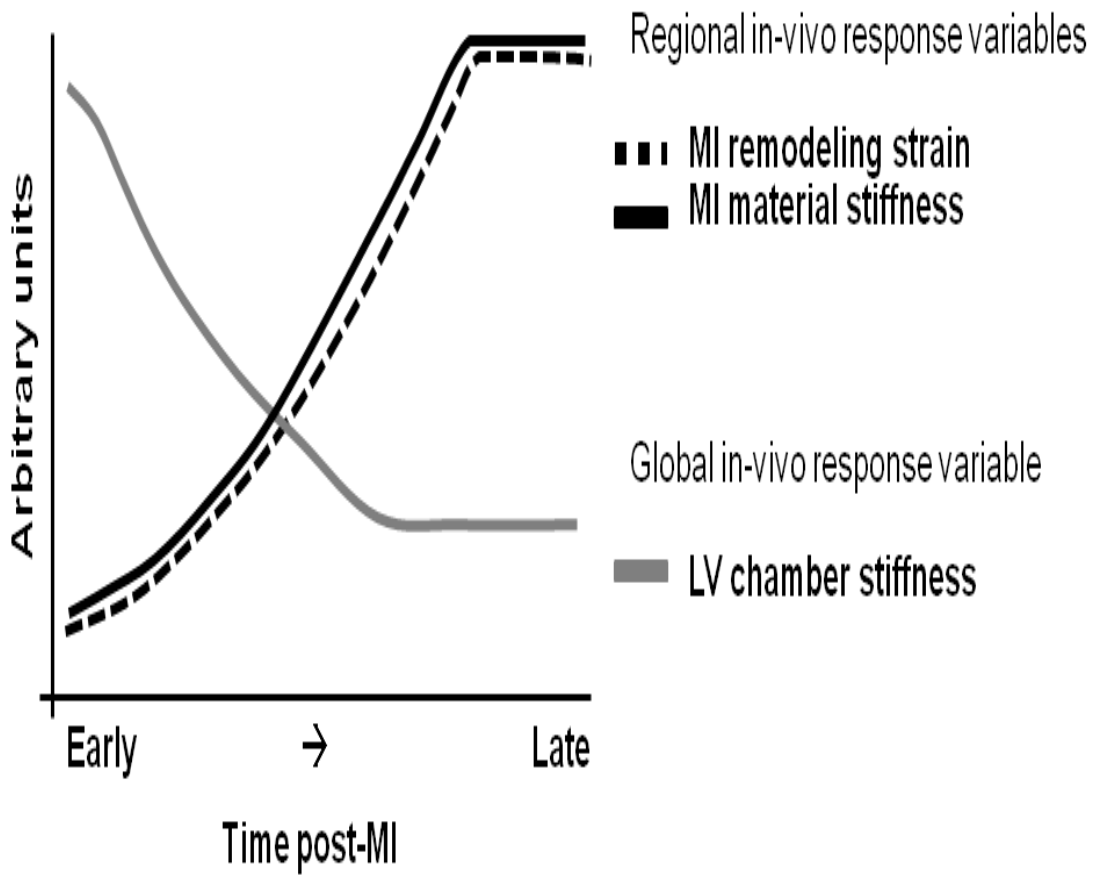

Figure 2.5 Summary recommendations. Regional and global measurements recommended for inclusion in future experimental studies. From the data contained in this review, this figure underscores the inverse trends in post-MI changes in local material properties/behavior (MI remodeling strain and stiffness) and global mechanical behavior post-MI (LV chamber stiffness). While the specific time-course of these changes is animal model-dependent, the trends represented by this figure are universal.

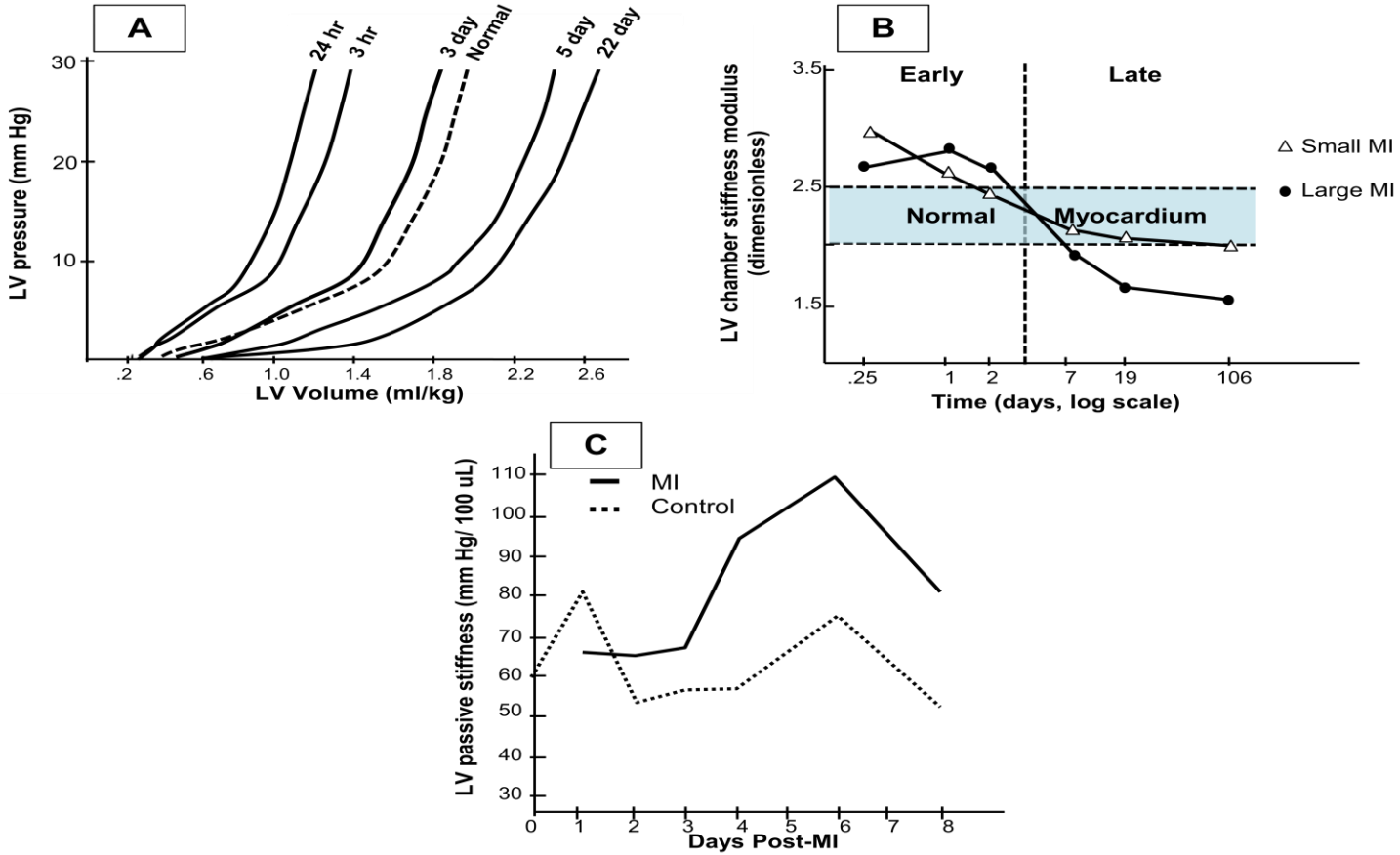

Figure 2.6 In-vivo chamber stiffness. Summary of reported LV pressure-volume relationships with passive filling and derived calculations of chamber stiffness following MI. (**A)** In a rat MI model, the passive pressure-volume curves initially shifted to the left (day 0-3) and later to the right (day 5-22) with respect to the referent normal response. Adapted from Raya et al. [139] (**B)** Temporal variation in LV chamber stiffness was reported in a rat MI model and found to depend on the absolute MI size. Adapted from Pfeffer at al. [132] **(C)** Passive stiffness in a rabbit MI model exhibits non-monotonic variation post-MI, but was consistently elevated with respect to referent normal at later times (3-8 days post-MI). Adapted from Lerman et al.(77)

CHAPTER 3

SONOMICROMETRY-BASED ANALYSIS OF POST-MYOCARDIAL INFARCTION REGIONAL MECHANICS[2]

[2] Romito E, Doviak H, Logdon C, Freels P, Shazly T, Spinale FG. Submitted to *Annals of Biomedical Engineering. 12/16/2015*

3.1 Abstract

Immediately following myocardial infarction (MI), adverse changes to the geometry, composition, and mechanical properties of the left ventricle (LV) are initiated in a process generally termed adverse post-MI remodeling. Cumulatively, these changes lead to a loss of LV function and are deterministic factors in the progression to heart failure. Proposed therapeutic strategies to target aberrant LV mechanics post-MI have shown potential to stabilize LV functional indices throughout the remodeling process. The *in-vivo* quantification of LV mechanics, particularly within the MI region, is therefore essential to the continued development and evaluation of strategies to interrupt the post-MI remodeling process. The present study utilizes a porcine model and *in-vivo* sonomicrometry to characterize MI region stiffness at 14 days post-MI and demonstrates a significant dependence of mechanical properties on location and direction within the MI region, as well as cardiac phase. Efforts to comprehensively characterize transient changes of regional post-MI mechanics still need be improved; however, this work is put forth to provide insight into the complexities within the finite MI region itself.

3.2 Introduction

Despite significant improvements in achieving early reperfusion with an acute coronary syndrome, myocardial injury still commonly occurs, ultimately leading to myocardial infarction (MI) and progressive left ventricle (LV) remodeling. [33,124,141,170,178,179] This process, generally termed adverse post-MI remodeling, is a major contributory factor to the development and progression of heart failure (HF). [81,113,133,164] Due to increased survival rates following the initial coronary event, the number of patients that carry the post-MI burden has been steadily rising over the past three

decades. [61,62] Currently, post-MI standard of care is largely relegated to symptomatic management, leaving patients vulnerable to the deleterious consequences of the post-MI remodeling process. As such, significant research efforts spanning academia and industry have been devoted to the development of effective strategies to curtail post-MI remodeling and the progression to HF in this growing patient population. [82,90,101,103,121,134,156,185]

Post-MI remodeling is a multi-factorial process, causing progressive changes in the geometry (MI region thinning, remote wall thickening, and LV dilation) and mechanical properties (MI region stiffness) of the myocardium. [24,32,40,41,94,122,163] Therefore, proposed strategies to interrupt post-MI remodeling are largely focused on restoring or stabilizing the mechanical behavior of the MI region. To date, various attempts to directly (via physical restraint or localized biomaterial injections) or indirectly (via local delivery of stem cells or bioactive compound/cells) modulate the mechanical behavior of the MI region have shown promising results in terms of *in-vivo* indices of LV function. [42,54,82,121,137] To facilitate the continued advancement and clinical translation of these and other emergent strategies to attenuate the remodeling process, there is a clear need for high fidelity, *in-vivo* measurements of LV wall mechanics that can characterize behavior throughout the cardiac cycle, within specific regions, and in defined directions.

Previous studies of post-MI mechanics have utilized quantitative approaches, including imaging modalities (ultrasound, MRI, etc.), physical techniques (implantable markers, tensile testing, sonomicrometry), or a combination of both, to evaluate changes in LV wall stress, strain, and stiffness. [35,96,97,144,153,186,187,194] A majority of past studies

have characterized myocardial mechanics at the chamber level and thus provide global measures of LV properties, response, and function (i.e. chamber stiffness, segmental shortening, and wall strain rate). [14,71,112,127,136,144,153,165,189,190] Continued advancements in both image-based and physical techniques have enabled increasingly precise quantification of regional mechanical behavior and thus distinction of normal and infarcted myocardial mechanics. Among the techniques for regional mechanical assessment, sonomicrometry has emerged as a leading approach due to the ability to obtain segmental lengths in specified directions while maintaining high spatial and temporal resolution. [5,49,65,95,167,186]

Comparison among past studies utilizing sonomicrometry and other techniques demonstrate that experimental variables including the employed animal model and MI location, size, and transmurality significantly impact mechanical measurements. [51,84,86,135,168] While it is now well-accepted that post-MI remodeling induces time-dependent changes in mechanical behavior throughout the LV and most notably in the MI region, the precise dependence of these changes on experimental variables remains only partially understood. To better understand the natural progression of adverse post-MI remodeling and evaluate emergent approaches for its interruption, there is a clear need for large animal and pre-clinical MI models that enable high fidelity mechanical measurements within a well-defined and experimentally repeatable MI region.

The present study utilizes a porcine MI model, whereby a repeatable MI region with regards to size, location, and transmurality is surgically created via coronary artery ligation. A six-crystal sonomicrometry array is acutely implanted within the myocardium at 14 days post-MI with an array location and structure that facilitate quantification of MI

region mechanical anisotropy and heterogeneity. The 14 day post-MI time point is selected for mechanical analyses to ensure that significant changes in MI region composition and geometry have emerged as a result of the remodeling process. [86] Sonomicrometry measurements are obtained under loads corresponding to the systolic and diastolic cardiac phases, allowing distinction between MI-induced changes in extracellular matrix properties (passive myocardial response) and the regional loss of contractile units (active response). Obtained sonomicrometry chord length data are processed to develop stress-strain relationships and measures of myocardial stiffness. Our findings demonstrate that mechanical heterogeneity and anisotropy are differentially altered by post-MI remodeling and underscore the need to specify cardiac phase in the quantification of MI region mechanical behavior.

3.3 Materials and Methods

Overview

All animals were treated and cared for in accordance with the National Institutes of Health Guide for the Care and Use of Laboratory Animals, and all protocols were approved by the University of South Carolina's Institutional Animal Care and Use Committee. We utilized an adult pig model of MI induced through permanent coronary artery ligation, which was previously shown to yield a reproducible MI size and consistent progression of post-MI remodeling as indicated by classical functional indices. [42,137] In this porcine MI model, wound healing completed by two weeks post-MI is characterized by a relative reduction in inflammation and a significant accumulation of collagen - i.e. fibrosis within the MI region. [32] Accordingly, this time point was chosen for assessment of MI region mechanical properties, which was compared to identical measurements performed in the same region of the LV in referent non-MI controls. Using

2-dimensional targeted echocardiography followed by placement of a sonomicrometry array and LV microtransducers within the region of interest, [38,65,78] steady-state and pressure-dependent measurements of functional indices and chord length data were recorded. To generate adequate sonomicrometry data for chord stiffness calculations, LV preload was altered by transient caval occlusion. Acquired data were aggregated and processed to compute stress-strain relationships and mechanical stiffness for each chord under systolic and diastolic pressure ranges.

Animal Model

A total of 11 mature male Yorkshire pigs (25 kg, Palmetto research swine, Reeseville, SC) were randomized into two different groups, a referent control (N=6) and an MI group (N=5). The MI group was anesthetized with isoflurane (2%) and underwent a left thoracotomy to induce the MI, reproducing a previously established MI model. [122] Briefly, once access to the heart was achieved, the pericardium was opened to expose the targeted obtuse marginal arteries (OM1, OM2). These arteries were then ligated near their origin from the circumflex artery to create a reproducible infarct geometry (Figure 3.1A). The infarct was confirmed initially by changes in ST segment elevation in the electrocardiogram signal as well as visible blanching of the myocardium in the target MI region. Animals in the MI group were carefully monitored for the following 14 days leading to the endpoint echocardiography and sonomicrometry studies (as described below).

Ultrasound

The animals were sedated at the terminal time point with 200mg of diazepam administered orally prior to the procedure. Two dimensional and M-mode echocardiographic studies were then conducted from a right parasternal approach using a GE vivid 7 dimension with an M4S transducer. [42,137] Obtained measurements were processed to yield LV dimensions and functional indices.

Sonomicrometry

A custom array of six sonomicrometric crystals was implanted to monitor regional LV mechanics in both the referent control and MI groups (Sonometrics, London, Ontario, Canada). As the terminal procedure, a median sternotomy was performed and the crystal array was implanted into the LV wall at the 14 day post-MI time point for both study groups (Figure 3.1A). The target placement of this array is contained within the MI region or analogous location in the control group. The array layout consists of four crystals on the epicardial surface of the LV and two crystals placed subendocardially, thus producing a set of chord lengths in orthogonal directions, described as longitudinal (from base to apex), radial (from epicardium to endocardium), and circumferential. Output from the crystal array was matched to a left ventricular pressure trace from a catheter inserted directly into the LV (Millar Instruments, Houston, TX). Changes in pressure were achieved through partial occlusion of the inferior vena cava in order to provide an effective loading range in both referent normal and MI groups (Figure 3.1B). Data analysis was done on a beat-by-beat basis during steady state and occlusion runs, thus enabling quantification of pressure-chord length relationships for each chord (Ponemah software version 5.0, Data Sciences International, St. Paul, MN).

Data analysis

Segmental shortening Chord length data gathered at end diastole and end systole were used to calculate segmental shortening. This quantity is traditionally reported as a single measure to reflect the chamber deformation along the short-axis. In the present study, this measure was calculated as a percent change in all chord lengths from end diastole (EDL) to end systole (ESL), i.e. [(EDL-ESL)/EDL]*100, thus quantifying segmental shortening at the short-axis chamber level and in orthogonal directions within the MI region.

Stress-stretch relationships Pressure-length curves were generated for each chord, with pressure recorded by a catheter placed directly in the LV (Millar Instruments, Houston, TX), and chord length via sonomicrometry. Chord length data were further processed to yield a stretch ratio, where a theoretical initial chord length (L_0) was derived from a regression of the recorded pressure-length relationships. At a given loading state, the average wall stress σ was calculated as

$$\sigma\left(\frac{g}{cm^2}\right) = \left[\frac{PD}{4h\,(1+\frac{h}{D})}\right] \times 1.36$$

where P is the chamber pressure [mmHg], D is the minor axis length [cm], h is the posterior wall thickness [cm], and 1.36 is a conversion coefficient for gcm^{-2}. [160] The pressure ranges used to calculate stress were consistent across the data sets of both study groups with a range of 40-95 mmHg for systole and 2-10 mmHg for diastole.

Stiffness Incremental chord stiffness was calculated based on a linearization of the resultant stress-stretch relations for each chord over the mid-range portion of pressure in systole (60-70 mmHg) and diastole (4-7 mmHg).

Relative anisotropy and relative heterogeneity The relative anisotropy (RA) of mechanical stiffness within the MI region was determined using chords originating from a common crystal but oriented in each coordinate direction (circumferential, longitudinal, and transverse). The RA was calculated by the equation below, where the stiffness of chords C1, L3, and T1 are represented by $X_{i,}$ and μ represents the mean stiffness among the three chords.

$$RA = \frac{1}{\mu}\sqrt{\frac{\sum_{i=1}^{3}(X_i - \mu)^2}{3}}$$

The relative heterogeneity (RH) in stiffness within the MI region was determined by an analogous equation, with the three relevant chords now oriented in the same direction (circumferential) but differentially located within the MI region (chords: C1, C2, C3). The structure of the implanted crystal array was such that only the circumferential direction could be used to compute a measure of mechanical heterogeneity.

Statistical Analysis

All reported results, aside from the percent change in relative anisotropy/relative heterogeneity, were analyzed using non-parametric statistical tests due to the non-normal distribution of data. The stiffness data was analyzed using Mann-Whitney tests for

significance between groups and Wilcoxon rank tests for pair-wise comparisons within groups.

3.4 Results

Hemodynamics All of the animals successfully completed the protocol, and the summary hemodynamics and global/regional indices of LV function are provided in Table 1. In the post-MI group, LV developed pressure and posterior wall thickness, while ejection fraction decreased from respective control values. Pulmonary capillary wedge pressure (an index of LV diastolic filling) was increased as was LV end-diastolic volume in the post-MI group. Thus, two weeks following coronary occlusion, systemic hemodynamics and LV function were consistent with the MI phenotype, which has been well reported previously. [42,137] LV regional function, as measured by segmental shortening, was reduced in the post-MI group with respect to the LV short axis and circumferentially oriented chords. Longitudinal and transverse chords exhibited no significant change in segmental shortening post-MI.

Chord Stiffness Chord stiffness significantly changed between groups at both systolic and diastolic pressure ranges. The stiffness of the chords at diastolic pressure demonstrated a significant difference between the circumferential and longitudinal chords of the control and MI (Figure 3.2B, chords C1-L2). All chord stiffness in both control and MI groups were an order of magnitude greater in the systolic pressure range than the diastolic, with trends reflecting a general increase in myocardial stiffness post-MI (Figure 3.2A).

Relative Anisotropy The relative anisotropy did not significantly differ between control and MI groups in either systole or diastole. However, the MI group RA percent change from control was significant at the systolic pressure range (Figure 3.3A).

Relative Heterogeneity The relative heterogeneity did not significantly differ between control and MI groups in either systole or diastole. However, the MI group RH percent change from control was significant at the diastolic pressure range (Figure 3.3B).

3.5 Discussion

An active area of basic science as well as clinical research is to understand the basis and prevention of adverse changes in myocardial structure and function that occur following a myocardial infarction (MI), i.e. adverse post-MI remodeling. Post-MI remodeling is comprised of both regional and global changes in left ventricular (LV) geometry and composition. Together, these changes impact LV mechanics and motivate the quantification of evolving myocardial mechanical properties as a means to understand the time course and implications of heart disease progression. In particular, *in-vivo* measurements of the mechanical properties of the MI region, such as stiffness, have emerged as promising targets in the development of increasingly refined therapeutic strategies to attenuate adverse post-MI remodeling. [82,89,103,147,157] In an effort to provide a comprehensive description of MI region mechanics at a critical post-MI time point, the present work utilized 2-D echocardiography and an acutely implanted sonomicrometry array to quantify MI region mechanical stiffness at 14 days post-MI in a porcine model. The sonomicrometry array structure and the inherent spatial and temporal resolution of this technique allowed for assessment of mechanical anisotropy and heterogeneity within the MI region at distinct loading conditions physiologically relevant to the systolic and

diastolic phases of the cardiac cycle. Our findings underscore the complexity of post-MI mechanics, here manifested as directional and spatial variations in stiffness within the MI region and significant dependence on cardiac phase.

The use of a six crystal sonomicrometry array allowed for the computation of seven chord stretch ratios within the MI region, which when combined with mean wall stress calculated via echocardiography, enabled estimation of chord stiffness.[36] Here, the stiffness in systole was found to be less affected post-MI than its diastolic counterpart, with only one chord showing significant changes with respect to referent normal controls. The stiffness of all chords under systolic pressures was significantly higher than diastolic pressures, confirming the nonlinear mechanical behavior of myocardium (even in the post-MI state). The loss of contractile units within the MI region would suggest a decreasing systolic stiffness post-MI; however, no significant change was observed with respect to the controls. This seemingly counterintuitive result can be attributed to the effect of the viable myocardium surrounding the MI, as the generated contractile forces confound explicit measurement of MI region mechanical properties. Conversely, diastolic chord stiffness was generally increased post-MI, although there was notable chord-to-chord variation in the magnitude and statistical significance of this change (Figure 3.2). The observed increase in circumferential chord stiffness is in agreement with a previous study by Holmes *et al*, where strain was found to decrease the circumferential direction indicating a concomitant increase in stiffness. [73] Taken together, these results support the notion of restoring referent normal biomechanical behavior with focus on the diastolic cardiac phase as a promising post-MI therapeutic target.

The relative anisotropy (RA) in chord stiffness indicates the directional dependence of material properties under physiologic loading (Figure 3.4, right). Normal myocardium has a heavily ordered fiber architecture and as a result is mechanically anisotropic, which like many soft tissues is an evolved characteristic that promotes its biomechanical function. [36,131,148,187] Mechanical anisotropy of the normal and infarcted myocardium has been previously reported in terms of strain, but here uniquely presented as a function of mechanical stiffness in three coordinate directions defined by the implanted sonomicrometry crystal array (circumferential, longitudinal, and transverse). The significant increase in systolic RA post-MI reflects the cumulative effects of altered material properties and geometry of the MI region as well as the active contractile forces transmitted to the MI region. Conversely, MI-induced changes in diastolic RA were not significant at the 14 day post-MI time point. This finding suggests that despite the occurrence of significant adverse remodeling as indicated by hemodynamic indices, the normal extracellular matrix architecture is at least partially preserved at this post-MI time point. This finding is in qualitative agreement with previous work by Zimmerman *et al*, where it was reported that the native microstructure of the myocardial extra cellular matrix is retained within the MI region and serves as a scaffold that guides new collagen deposition. [192]

The relative heterogeneity (RH) provides a description of the spatial variation in chord stiffness within the MI region, with our crystal array structure facilitating comparison among three circumferentially oriented chords (Figure 3.4, left). A significant increase in diastolic RH post-MI suggests that the degree of collagen synthesis and deposition differ throughout the MI region. Although the diastolic RA results

discussed above suggest some retention of normal collagen architecture post-MI, the non-uniform geometry of the MI region would give rise to wall stress field heterogeneity and in turn differential rates of mechanically-mediated collagen synthesis/deposition. [7,24,39,141,151]

3.6 Conclusion The use of in-vivo sonomicrometry to characterize post-MI LV mechanics reveals a complex dependence of mechanical stiffness on the location and direction of measurements within a well-defined MI region, as well as significant variation with respect to the cardiac phase. We demonstrate that at the 14 day post-MI time point in a porcine model, the degree of mechanical heterogeneity in diastole and mechanical anisotropy in systole are significantly elevated as compared to normal myocardium. Efforts to comprehensively characterize transient changes of regional post-MI mechanics still need be improved; however, this work is put forth to provide insight into the complexities within the finite MI region itself.

3.7 Limitations Several study limitations must be considered for careful interpretation of the obtained results. Firstly, a *global* mean wall stress was used to develop chord stress-stain relationships and ultimately calculate chord stiffness, although *local* stress elevations, particularly along the border of the MI region, are likely present. A second study limitation is that post-MI mechanics were assessed at only one select post-MI time point. Although this is an acceptable time point to evaluate the effects of remodeling following significant collagen deposition in a porcine model, [84] it does not allow for full characterization of the transient mechanical changes during post-MI remodeling. Finally, some animal-specific variation in the size and thinning of the MI

region occur in all MI models, which inevitably affects the placement of the crystal array and potentially changes the sensitivity and error of obtained measurements.

Acknowledgements

Figure 3.1 was generated by Dr. Adam Hartstone-Rose, in the department of Cell Biology and Anatomy at the University of South Carolina School of Medicine. This work was supported by the National Institute of Health grants HL11090, HL089944, HL43617, HL67922, and Merit Award from the Veterans' Affairs Health Administration. The authors wish to express their sincere appreciation to Ashley Sapp for her editorial assistance.

Table 3.1 Left Ventricular Global and Regional Function in Referent Control and Post-Myocardial Infarction. †

		Control (n=5)	MI (n=5)
Heart Rate (beats/min)		99 ± 4	95 ± 11
Aortic Pressure (Mean; mmHg)		66.6 ± 2.6	64.8 ± 4.4
End Systolic Pressure (mmHg)		86.8 ± 3.4	81.1 ± 4.1
dP/dt max (at 40 mm Hg; mmHg/s)		1528 ± 170	1030 ± 68*
Pulmonary Capillary Wedge Pressure (mmHg)		4.0 ± 0.1	9.1 ± 0.7*
Cardiac Output (L/min)		2.7 ± 0.3	1.7 ± 0.2*
End Diastolic Volume (mL)		50 ± 1	73 ± 3*
Diastolic Posterior Wall Thickness (cm)		0.81 ± 0.1	0.57 ± 0.1*
Ejection Fraction (%)		60 ± 1	43 ± 3*
LV Sonomicrometry			
Segmental Shortening (%)			
Circumferential	C1	12.7 ± 5.9	4.8 ± 0.7
	C2	14.3 ± 2.2	5.5 ± 1.3 *
	C3	7.1 ± 1.7	4.3 ± 1.6
Longitudinal	L1	9.6 ± 1.6	5.9 ± 1.6 *
	L2	10.5 ± 2.4	9.3 ± 1.6
	L3	7.6 ± 1.5	10.9 ± 1.9
Transverse	T1‡	4.8 ± 0.8	3.05 ± 0.9
LV chamber short-axis		32.5 ± 5.2	13.6 ± 2.7 *

Data is presented as the mean ± SEM; * p<.05 vs. referent control

† Post-MI: 14 days following coronary ligation

‡ Presented as wall thickening rather than segmental shortening.

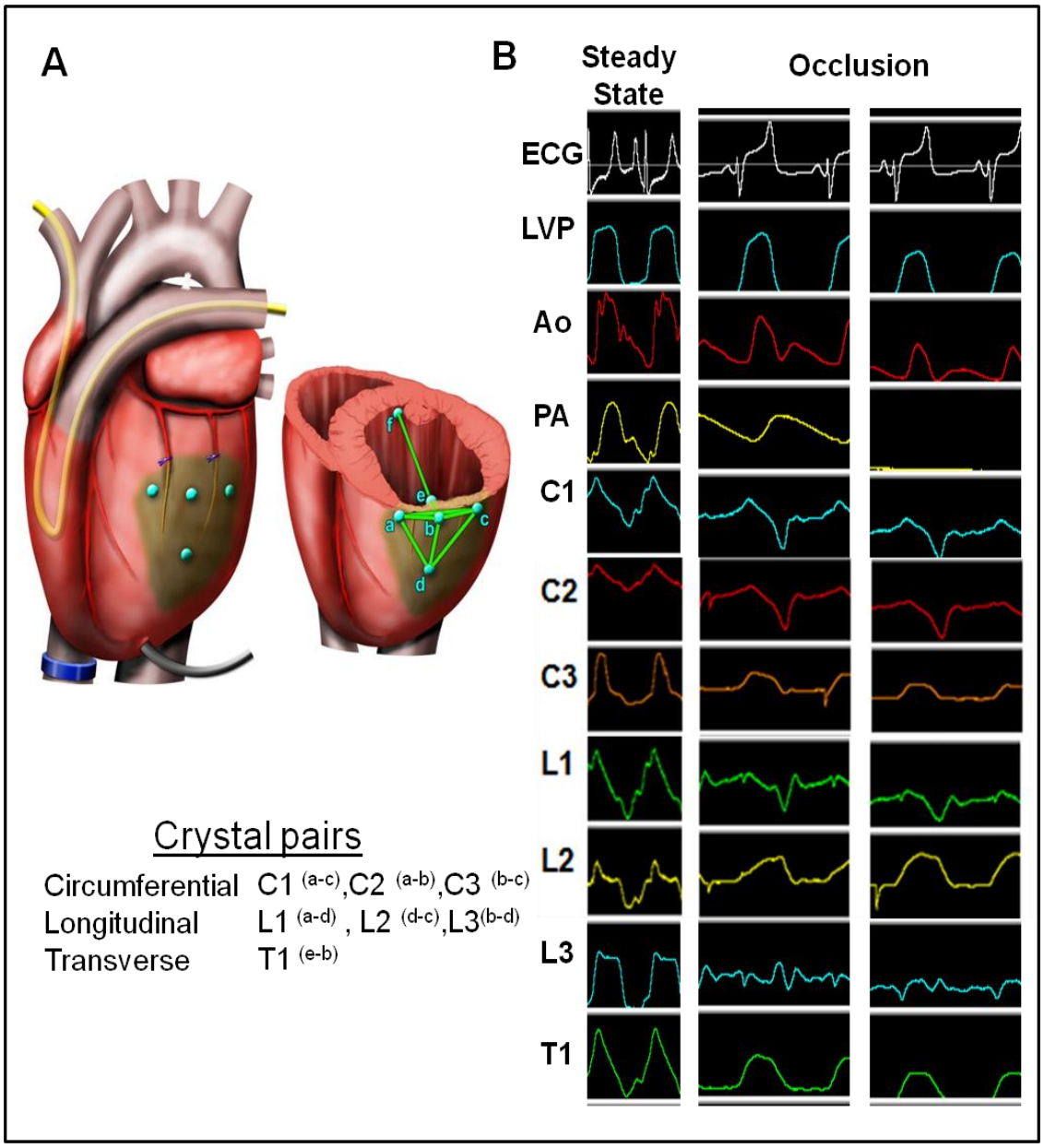

Figure 3.1. Sonomicrometry Array. **(A)** The sonomicrometry crystal array is presented in schematic form to identify the location of the crystals and the chords that were measured. The LV cross-sectional view demonstrates the location and relation of catheters and endocardial/epicardial crystals, whereby the small case letters identify the specific chord lengths measured. **(B)** Representative hemodynamic and LV myocardial chord lengths under steady state conditions and with transient reduction in LV pre-load by caval occlusion. The LV pressure fell in a predictable manner with transient reduction in LV pre-load and hence allowed for the construction of a family of isochronal LV pressure-chord values, which were then used to compute regional stiffness moduli. (LVP- LV pressure, Ao- Aortic pressure, PA pulmonary artery pressure).

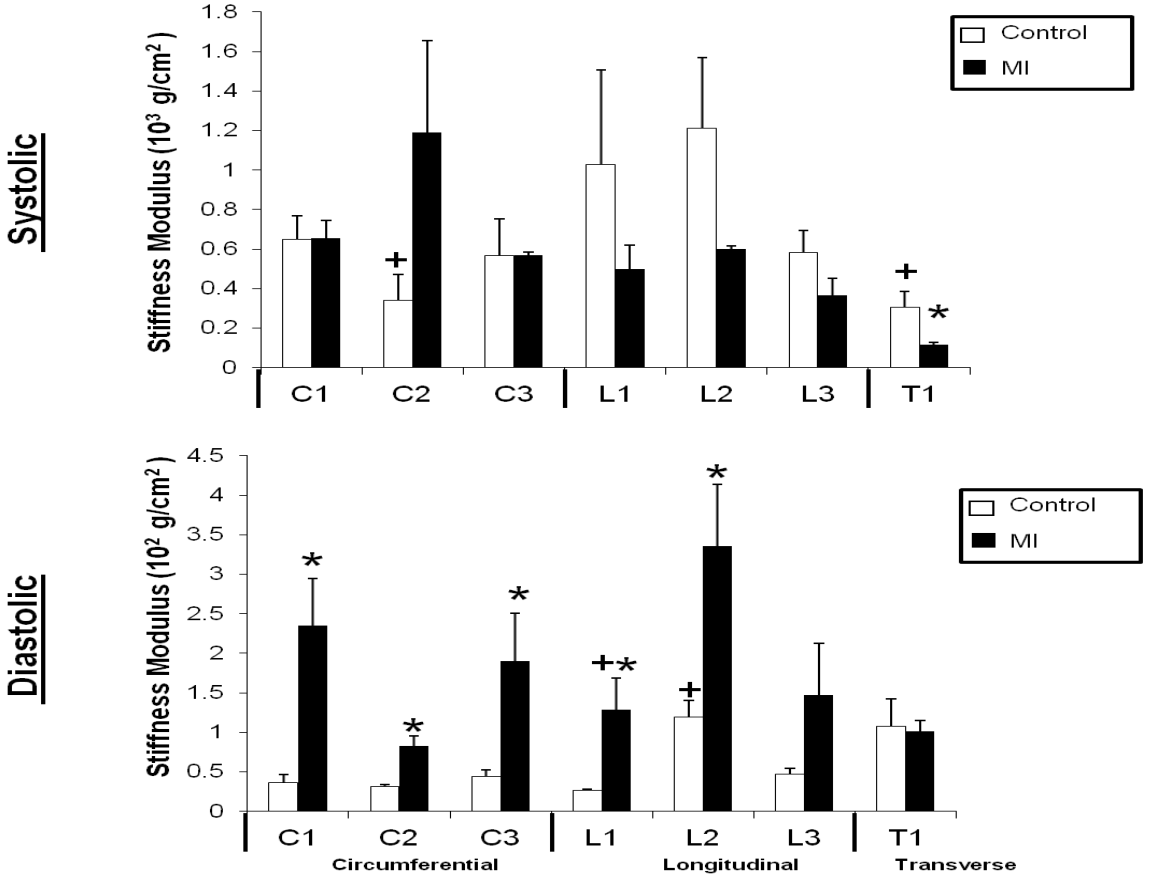

Figure 3.2 Regional stiffness. The regional stiffness modulus was computed for both the systolic and diastolic phase of the cardiac cycle by utilizing isochronal values of LV pressure and chord lengths obtained by variously loaded beats within each of these cardiac phases. (**A**) Systolic regional stiffness shows little statistical difference between groups, where active forces potentially overcome any effects of the material alone in such a pressure range. (**B**) Diastolic pressure range clearly demonstrates differences in stiffness between groups, with changes observed within differently oriented regions within the crystal array. Data shown as mean ± SEM; *p<.05 vs. respective control values, +p<.05 vs. respective C1 chord (note scale difference in systolic and diastolic modulus values).

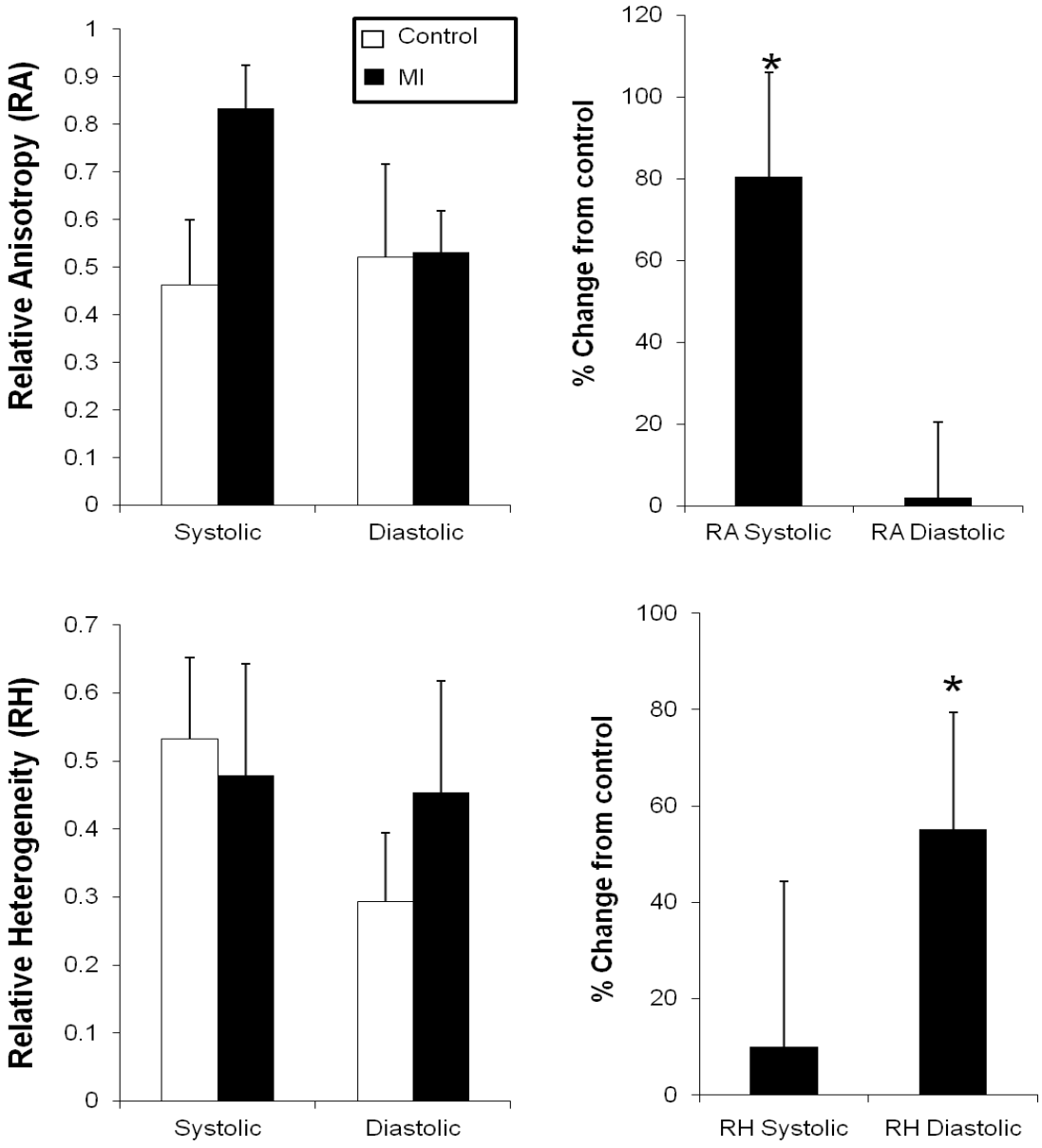

Figure 3.3 Relative anisotropy and heterogeneity. (**A**) The calculated relative anisotropy (RA) based on the three principal directions defined within the crystal array (circumferential, longitudinal, transverse), percent change from control RA presented adjacent. (**B**) Relative heterogeneity (RH) calculated from three circumferentially oriented chords in the MI region (C1, C2, C3), percent change RH presented adjacent. Data shown as mean ± SEM; *p<.05 vs. respective control values.

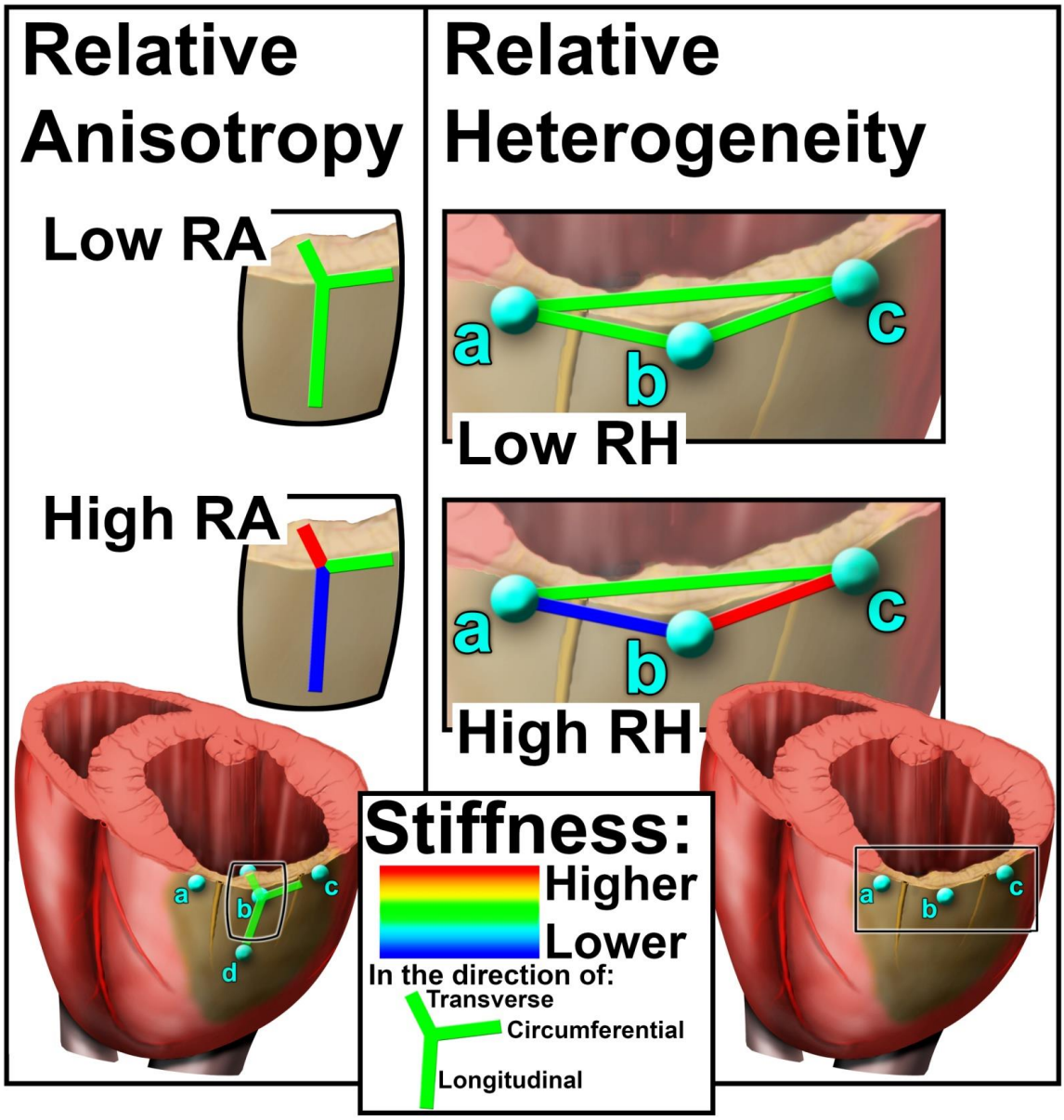

Figure 3.4 Stylized relative anisotropy and heterogeneity. The relative anisotropy serves as a descriptor of directional mechanical dependence of a material at a finite point, here calculated at the intersection of the defined directions (circumferential, longitudinal, transverse) within the crystal array (**A**). Relative heterogeneity (RH) describes the spatial disorder within a material. In the present study, the circumferential direction is defined within the crystal array for assessment of RH (**B**).

CHAPTER 4

BIOPHYSICAL EFFECTS OF A HYALURONIC ACID BASED HYDROGEL ON AVERAGE PEAK WALL STRESS OF THE LEFT VENTRICULAR WALL POST-MYOCARDIAL INFARCTION[3]

[3]Juarez Perez E, Purcell B. P, Loeb D, Logdon C. B, Doviak H, Schuman J, Novak C, Zellars K. N, Pettaway S, Gorman J H III, Gorman R. C, Burdick J. A, Shazly T, Spinale F.G. 2013. *American Heart Association, Scientific Sessions*. Reprinted here with permission of publisher.

4.1 Introduction

Following myocardial infarction (MI) the consequent changes that occur due to left ventricular (LV) remodeling is a primary therapeutic target to prevent progression into a state of heart failure (HF). Key outcomes of remodeling are characterized by mural wall thinning of the MI region and LV dilation, resulting in increased peak wall stress. Past studies have demonstrated that targeted injection of biomaterials within the MI region, such as hydrogels (gels), can alter this process. However, the temporal relationship between these LV remodeling events to gel biophysical effects remained unknown, and therefore formed the purpose of this study.

4.2 Materials and Methods

MI Model and Echocardiography

MI was induced in male Yorkshire pigs (25 kg) by coronary ligation of OM1 and OM2. Two distinct groups were created and randomized to targeted injections immediately post-MI of a hyaluronic acid (HA) based hydrogel (n=3) or saline injections (control, n=3) in a grid pattern (total of nine, 100uL injections seen in Figure 4.1). The HA has been modified with the addition of hydroxyethyl methacrylate groups to allow for hydrolytic degradation of its backbone to a degree of 15% methylation of groups along the HA backbone. The formulation utilized for the study was of a 4 wt % polymer content and was crosslinked through a redox reaction utilizing TEMED and APS as activators as previously described by Tous *et al* [22,77,92]. The study was carried out for a period of 14-days post-MI at which point samples from the MI region were excised for mechanical testing. Echocardiographic measurements (Figure 4.2) were taken at baseline, three, seven and fourteen day time points to gather data of the developing infarct characteristics including: wall thickness of the MI region, septal wall thickness, end-diastolic left ventricular volume and diameter.

Average Peak Wall Stress Calculations

The average peak wall stress was calculated using measurements gathered via echocardiography of LV inner diameter, wall thickness (septal and MI) at end diastole, as well as pressure readings from catheterization. These parameters were then applied to equations 1-3 to calculate the average peak wall stress for the animals at the three, five, seven, and fourteen day time points. This wall stress was assumed to be equal in all directions, one of the limitations of this study.

$$\Sigma(EDD + PWtd + SWtd) = D \qquad \textbf{(Eq. 1)}$$

$$\left(\frac{D}{2}\right) - PWtd = r \qquad \textbf{(Eq. 2)}$$

$$\frac{P \times R}{PWtd} \times 1.36 = Wall\ stress\ (g/cm^2) \quad \textbf{(Eq.3)}$$

***In vitro* HA Compression Testing**

The HA based gels were injected into an in-vitro mold simulating the in-vivo injection, to create suitable shape for unconfined uniaxial compression testing (Bose Enduratec 3200) as has been previously published by Burdick *et al* [77,171]. The samples were immersed in saline (37°), to allow for swelling and bulk erosion that mimics physiological conditions (Figures 4.3, 4.4, 4.7, 4.8). Each of the samples (n=5) were then tested under compression (30% compression) at time points identical to the echocardiography measurements of the control and MI group animals. The resulting data was analyzed in a stress-strain context and the compressive modulus determined in the

linear range of the material behavior [22,77,171]. The resulting modulus from each time point was then compared to changes in peak wall stress during the course of the study.

4.3 Results

MI thinning and average peak wall stress

The changes in MI thinning were found to be significant between the two treatment groups as early as three days post-MI (Figure 4.5). This supports the use of our chosen HA gel treatment as a method by which the thickness of the wall may be retained. Concerning average peak wall stress, it is clear that it increased as a function of time post-MI in both groups, but was significantly attenuated in the MI/gel group post-MI (Figure 4.6). The changes in average peak wall stress post-MI became significant in the MI/gel treatment group only after a significant loss in modulus was observed in the in-vitro mechanical testing of the gels at matched time points. The cross over point between gel mechanical strength and peak stress in the treatment group supports the plausibility of matching material properties tested in-vitro to in-vivo remodeling outcomes as a means to maximize therapeutic gain.

4.4 Limitations

This study has some clear limitations in the creation of an in-vitro environment that closely mimics the physiological conditions the HA gel is exposed to after injection. The volume of the gels required for testing was larger than the individual injections (100 uL) that were utilized in the animal model. The geometry of the gel once injected is also limiting in this experiment as the geometry and overall surface area that is exposed to an

aqueous environment has an impact on the bulk erosion that occurs in the gel post-injection. Refreshing of the saline solution during the incubation of the gels in the in-vitro experiment should suffice to lessen the impact of this particular limitation.

4.5 Conclusions

Retaining the thickness of the wall in the MI region has previously shown to be beneficial in the distribution of mechanical loads as well as mitigating the loss of overall cardiac function, and positively impinging on the remodeling outcomes [33].This study presents a clear example of the biophysical impact an HA gel injectate can have on key remodeling hallmarks of mechanics and geometric outcomes. These findings suggest that matched in-vivo and in-vitro biophysical measurements can be utilized to optimize hydrogel formulations which alter the post-MI remodeling process, and thus hold therapeutic relevance.

4.6 Proposed next steps

To successfully complete each of the proposed specific aims more sophisticated experiments to asses remodeling outcomes as a result of hydrogel interventions will be undertaken. The following chapter continued this work with a sophisticated cardiac MRI study that incorporates a HARP analysis technique to quantitatively assess changes in strain as a result of HA material interventions. The collective data from the studies included in this dissertation will serve to improve the understanding of biomaterial mechanical impact post-MI and influence future similar studies, fulfilling the overarching goal of this dissertation.

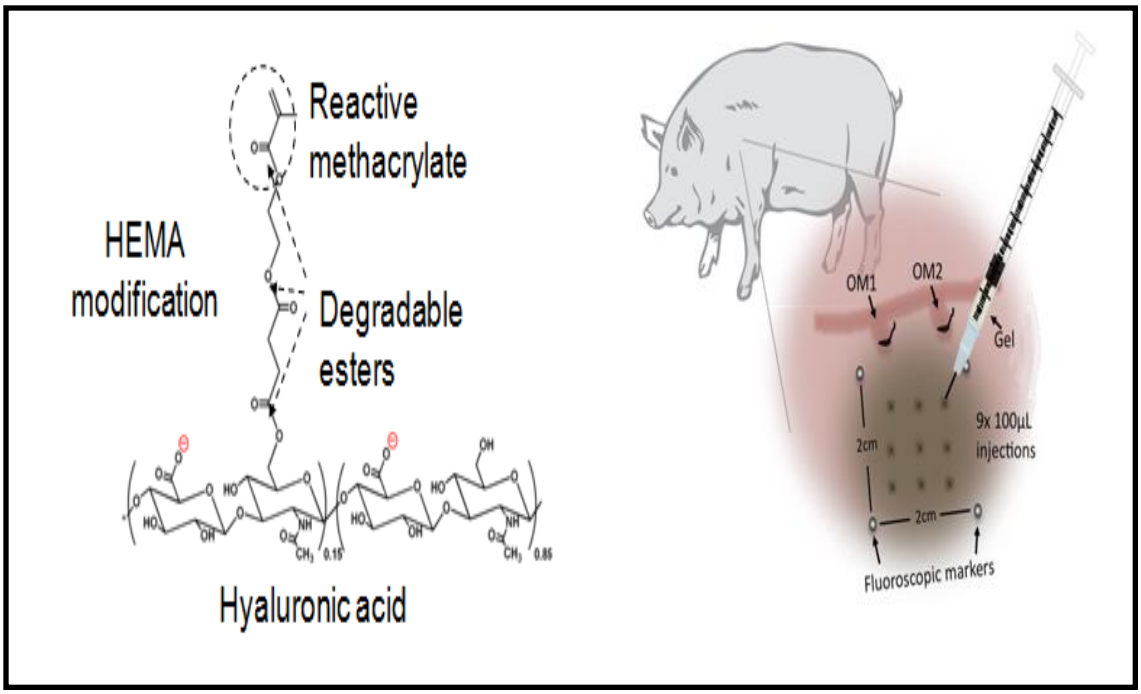

Figure 4.1 HA structure and injection pattern. HA gel chemical composition and experimental injection schematic.

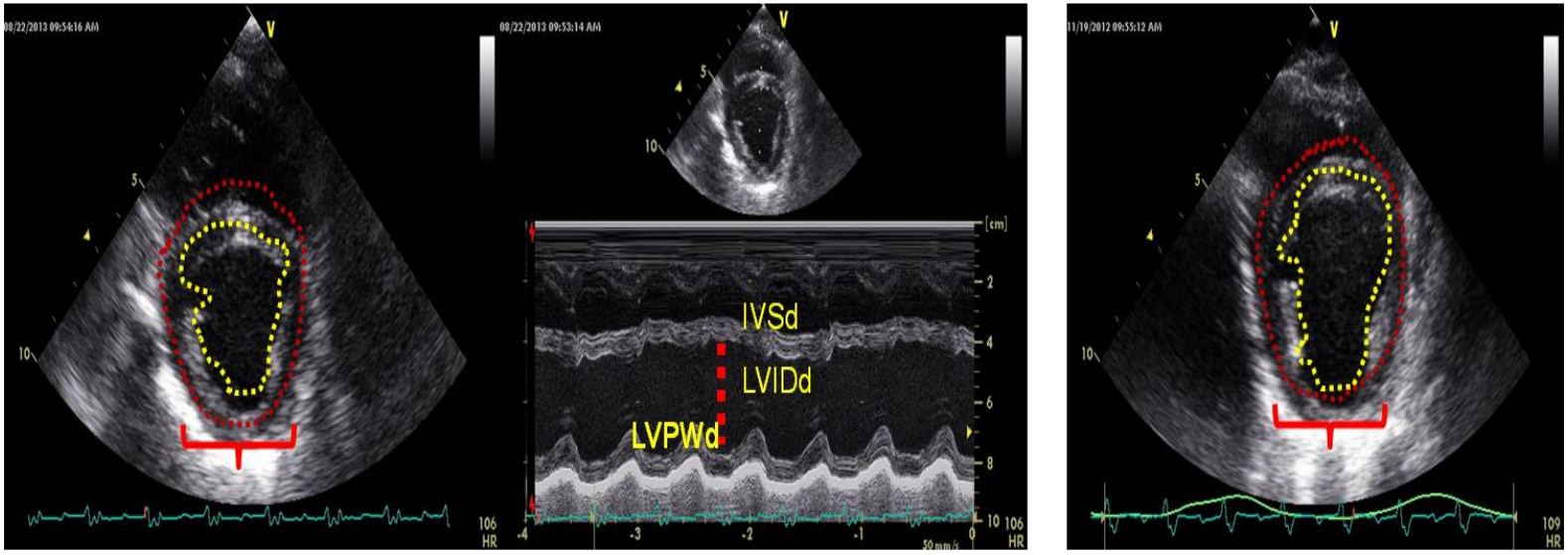

Figure 4.2 Echocardiography. of left ventricle, control group left and MI on right. Inner diameter is marked by yellow outline and outer diameter by red. M-mode is shown in middle panel to describe left ventricular inner systolic diameter (LVISd) and left ventricular inner diastolic diameter (LVIDd).

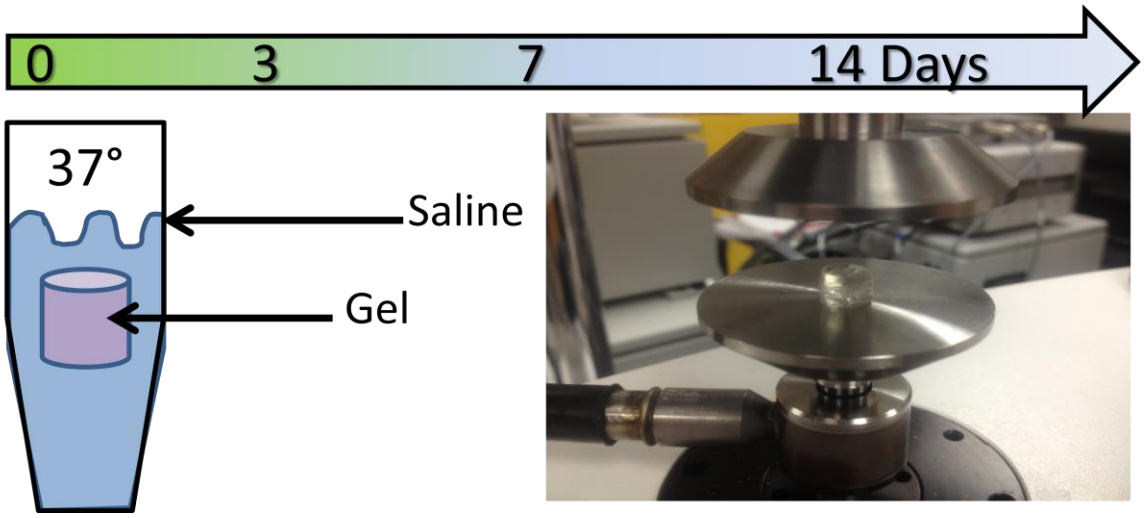

Figure 4.3 Schematic of gel time line. Experimental protocol for compression testing at various degradation states within the fourteen day study. .

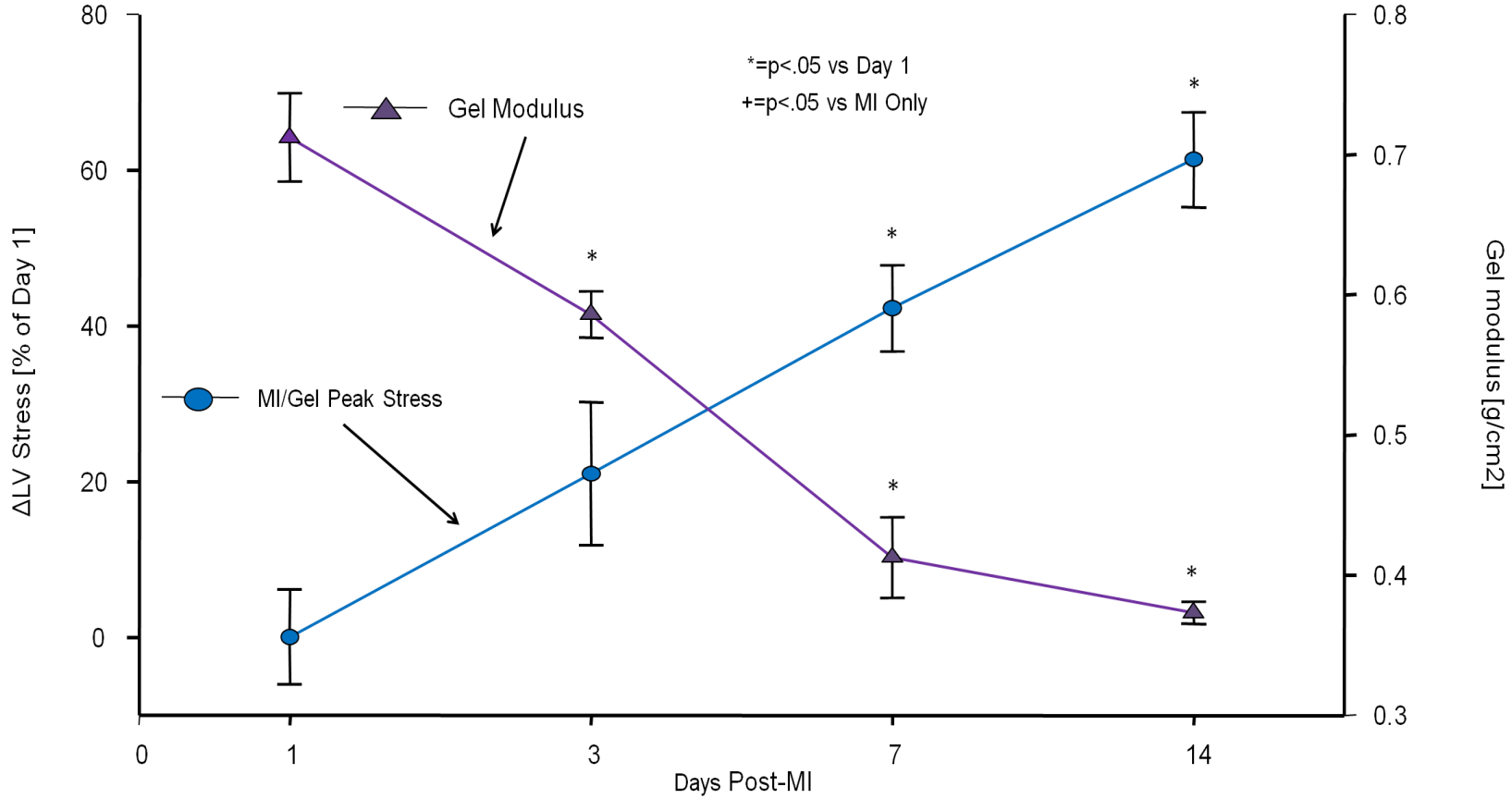

Figure 4.4 Isochronal plot of LV Stress and gel modulus. Change in LV Walls stress and HA gel modulus * denotes significance of p<.05 between values compared to day 1 of their respective groups, correlation coefficient between data sets was of r= -.90

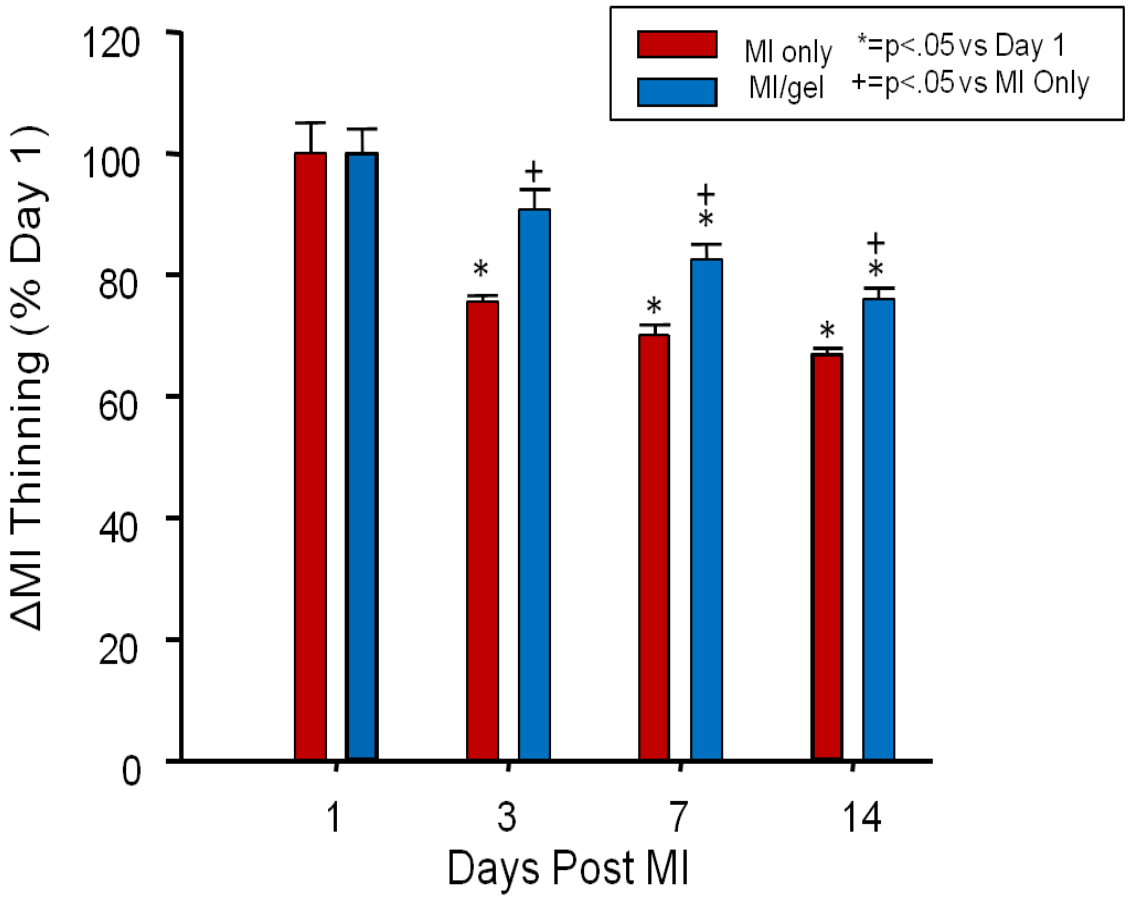

Figure 4.5 Change in MI thinning. MI thinning presented as a percent change from day 1 values. A* denotes a significance of p<.05 between values within the same group, and + denotes a significance of p<.05 between values of the MI only and MI/gel groups.

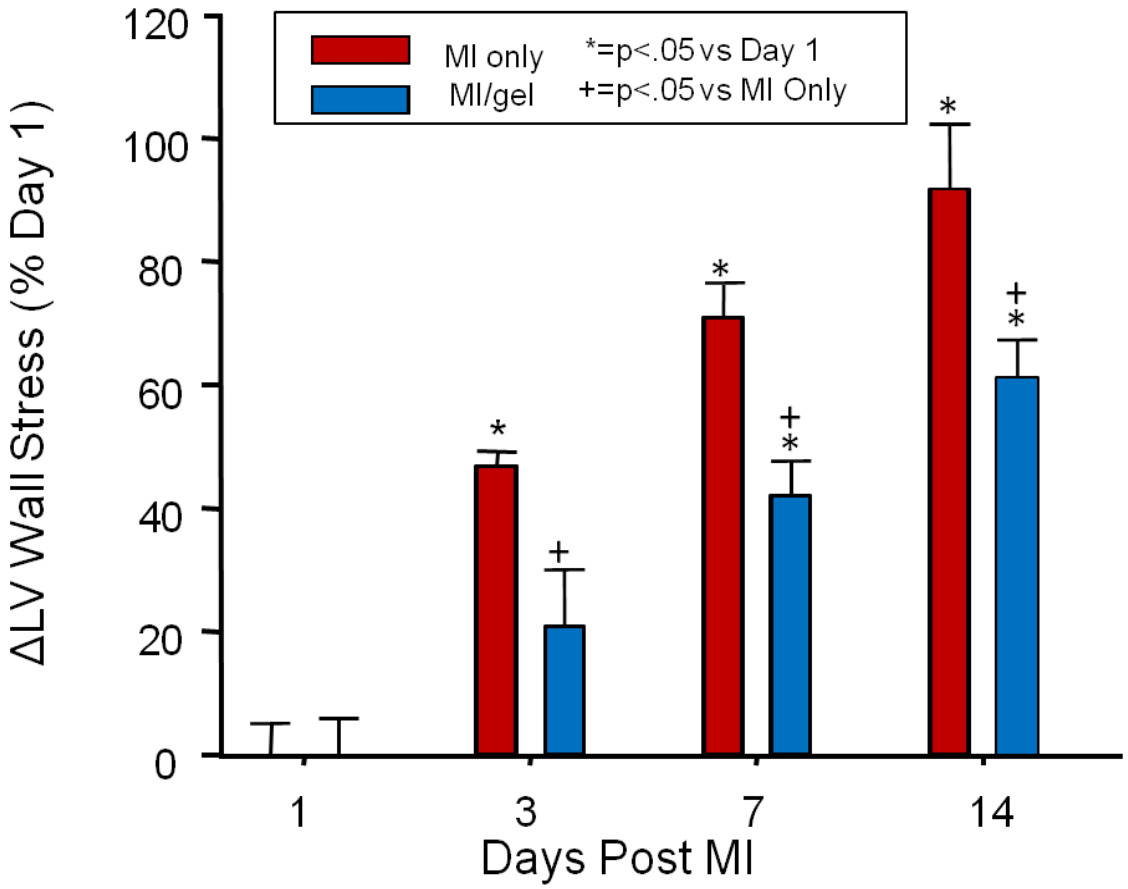

Figure 4.6 Change in LV stress. Average peak wall stress (right) presented as percent change from day 1 values. A * denotes a significance of p<.05 between values within the same group, and + denotes a significance of p<.05 between values of the MI only and MI/gel groups.

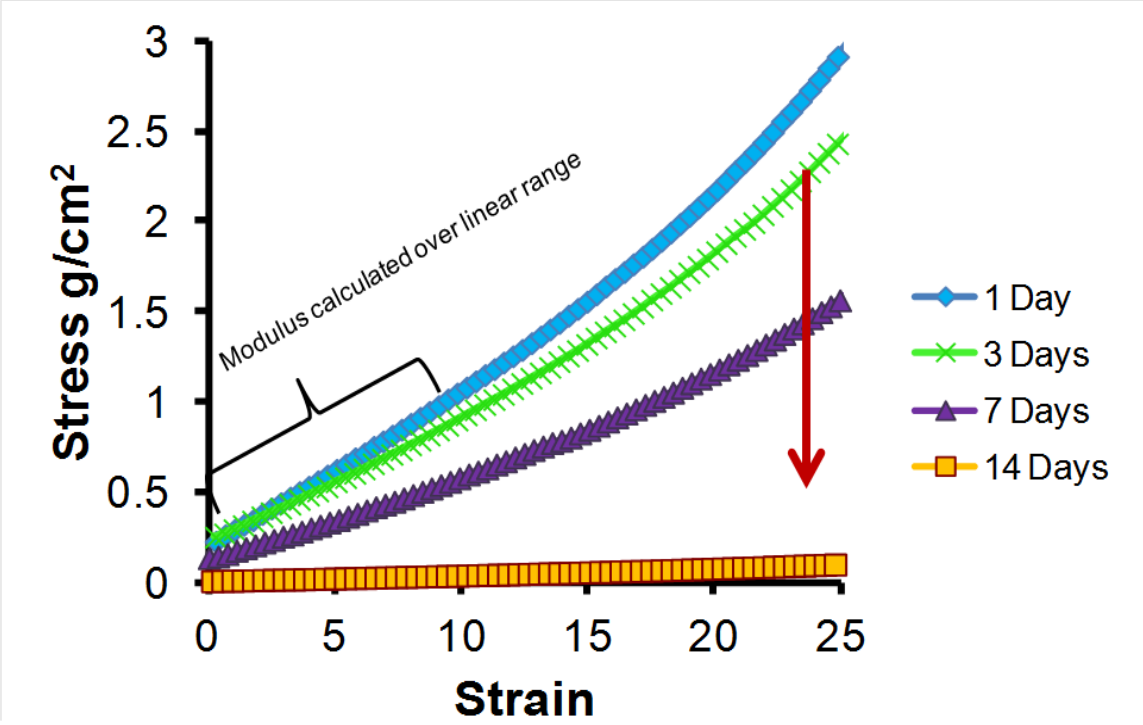

Figure 4.7 Representative data HA compression. Compression testing of stress-strain behavior of HA gel samples during a 14 day time period of degradation

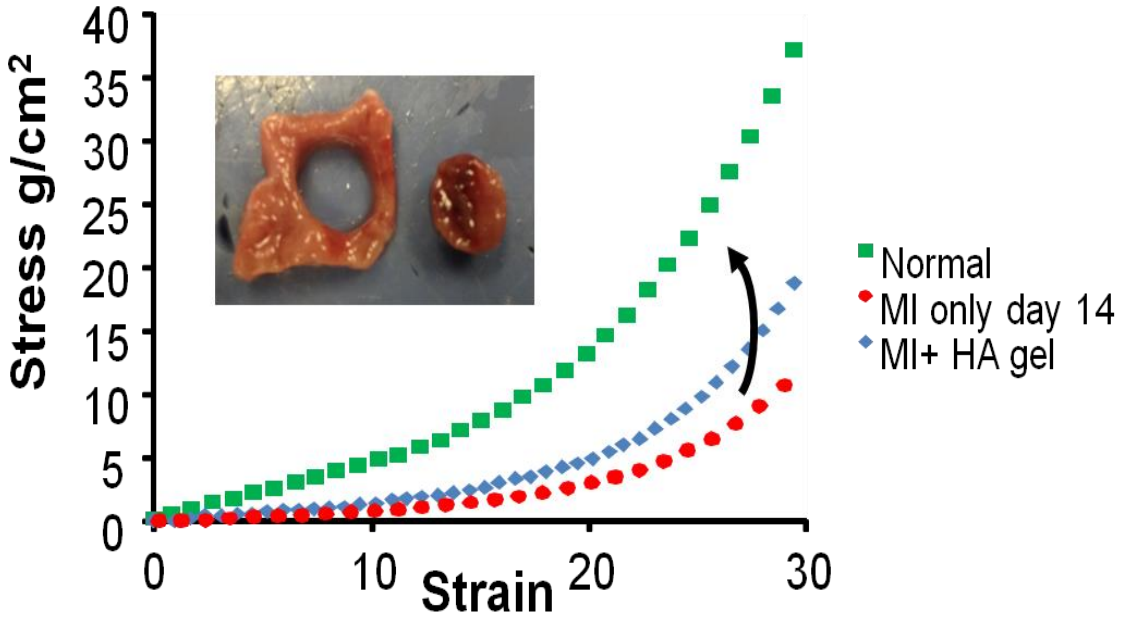

Figure 4.8 Representative tissue compression. Data from compression testing of stress-strain behavior of myocardial tissue from control and MI groups

CHAPTER 5

HARP ANALYSIS OF CHANGES IN STRAIN POST-MI AS A RESULT OF A HYALURONIC ACID GEL INTERVENTION [4]

[4] Romito E, Thorn S, Peters D, Doviak H, Logdon C B, Schuman J, Shazly T, Spinale FG, Sinusas A. To be submitted to *American Heart Association Scientific Sessions.*

5.1 Introduction

Immediately following the occurrence of a myocardial infarction (MI) a series of biochemical and mechanical changes begin in the left ventricle (LV) that ultimately result in what is known as post-MI remodeling. This remodeling is characterized by structural changes in both geometry and composition of the infarct region that serve to impair LV function increasing, a pathway that increases the chances of a patient's deterioration into heart failure (HF). Therapeutic strategies of increasing popularity have looked towards the modulation of post-MI remodeling with some success found in material injectates. Understanding classical mechanical variables such as strain are imperative in the creation of a successful strategy focused on the mechanical impact and outcomes that affect post-MI remodeling. Expanding upon a previous study done with hyaluronic acid hydrogel injections into the MI region, this continuing study is an analysis of the effects of the material intervention on strain formed the purpose of this study.

5.2 Materials and Methods

MI Model and MRI

MI was induced in male Yorkshire pigs (25 kg) by coronary ligation of OM1 and OM2, with the same protocol as the study in the previous section. Two distinct groups were created and randomized to targeted injections immediately post-MI of a hyaluronic acid (HA) based hydrogel (n=3) or saline injections (control, n=3) in a grid pattern identical to the previously described study. A control group of (n=3) was used as referent values for both of the experimental groups. The HA has been modified with the addition of hydroxyethyl methacrylate groups to allow for hydrolytic degradation of its backbone

to a degree of 15% methylation of groups along the HA backbone. The formulation utilized for the study was of a 4 wt % polymer content and was crosslinked through a redox reaction utilizing TEMED and APS as activators as previously described by Tous *et al* [22,77,92]. The endpoint of the study was 14-days post-MI at which point the animals underwent an MRI study. Images were acquired during breath holds on a 1.5 T whole body magnet (Sonata, Siemens system). The MRI study utilized a spatial modulation of magnetization (SPAMM) technique where horizontal and vertical tags with 7 mm of separation between the tag lines were created across the short-axis view of the heart (Figure 5.1). The slices from the base to the apex of the heart were of 6mm thickness with approximately 14-20 frames within each breath hold. The blood in the LV cavity has been made to appear black as a result of the application of a band saturation filter.

Harmonic phase imaging and strain analysis

Harmonic phase imaging uses the regularly distributed spectral peaks in k-space contained within SPAMM images. These spectral peaks provide a means by which to track the motion of the tags in a given direction during throughout the images captured during breath holds. The inverse Fourier transform of a spectral peak (one chosen for each direction in tagged image series) provides a complex image with a phase linearly related to a directional component of motion. Using software provided by the research group of Dr. Albert Sinusas, the strain computations are carried out with user input. A user-created mesh consisting of four segments and three distinct layers (endocardial, mid-wall, and epicardial) defines the LV (Figure 5.2). The points within the mesh (45 points per slice) are tracked throughout the frames of the breath hold with the first frame of the series serving as a reference point for the calculation of strain. The measures of strain

calculated were: Eulerian circumferential and radial strains, which represent circumferential shortening and radial thickening, and the Lagrangian circumferential strain.

5.3 Results

HARP Analysis

The analysis of the groups has been done on slices representative of three anatomical locations of the LV. As previously noted the strain analysis divides the LV into 4 equal segments, the primary segment analyzed has been that which contains the MI. This segment demonstrated values that were expected to have the largest deviation from those of the control group. In the basal, mid ventricular and basal slices analyzed, both treatment groups displayed values that deviated from the referent control composite value, but are not statistically significant between treatment groups at this time ($p>.05$). The percent change from the control values in radial thickening and circumferential shortening yielding statistical significance ($p<.05$) in the mid-ventricular level slice (Figures 5,1 and 5.2). The apical level slice showed a significance in Lagrangian circumferential strain values (Figure 5.3, .$p<.05$ compared to referent control).

5.4 Limitations

The limitations in this particular study primarily point towards the existence of through plane motion that is not completely captured in the 2D analysis of each slice. The spatial resolution combined with the HARP analysis allows for regional tracking of myocardial deformation. However, the out of plane motion in the SPAMM tagged images

contributes to tag-fading, creating a loss of the motion that translated through the volume of the heart.

5.5 Conclusions

The data gathered at this point shows a clear difference of the MI and MI-HA groups from the referent control values. The mid-ventricular level of the LV appears to be most affected at the endo- and epicardial layers with p values for circumferential shortening (endocardial layer) and radial thickening (epicardial layer) nearly approaching significance, $p<.06$ and $p<.057$ respectively. This is in line with expectations of the most affected levels in the, since the MI created by our experimental model is located in the mid to apical regions of the LV. Another interesting finding is that the MI-HA group displays a trend towards homogeneity across the various layers that is similar to the homogeneity found in the control group, which will be confirmed statistically with the addition of more control animals. The MI-HA group also demonstrated a larger reduction in Lagrangian circumferential strain than the MI group, which here we interpret as an increase in stiffness and will confirm with functional indices from further analysis of the MRI data gathered.

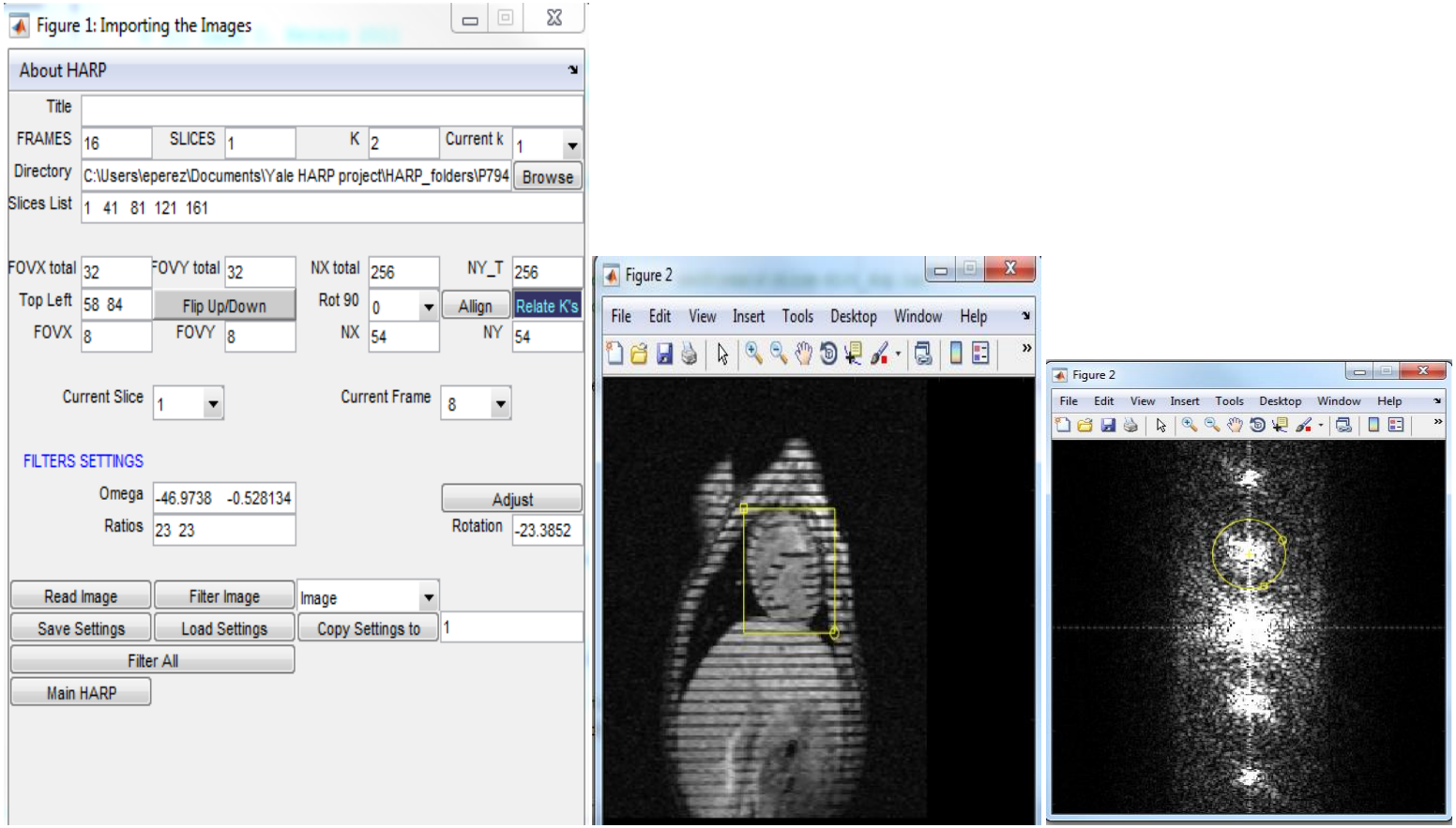

Figure 5.1 SPAMM Image filtering for HARP. The MRI images are processed to find spectral peaks in k-space to create complex images for harmonic phase analysis.

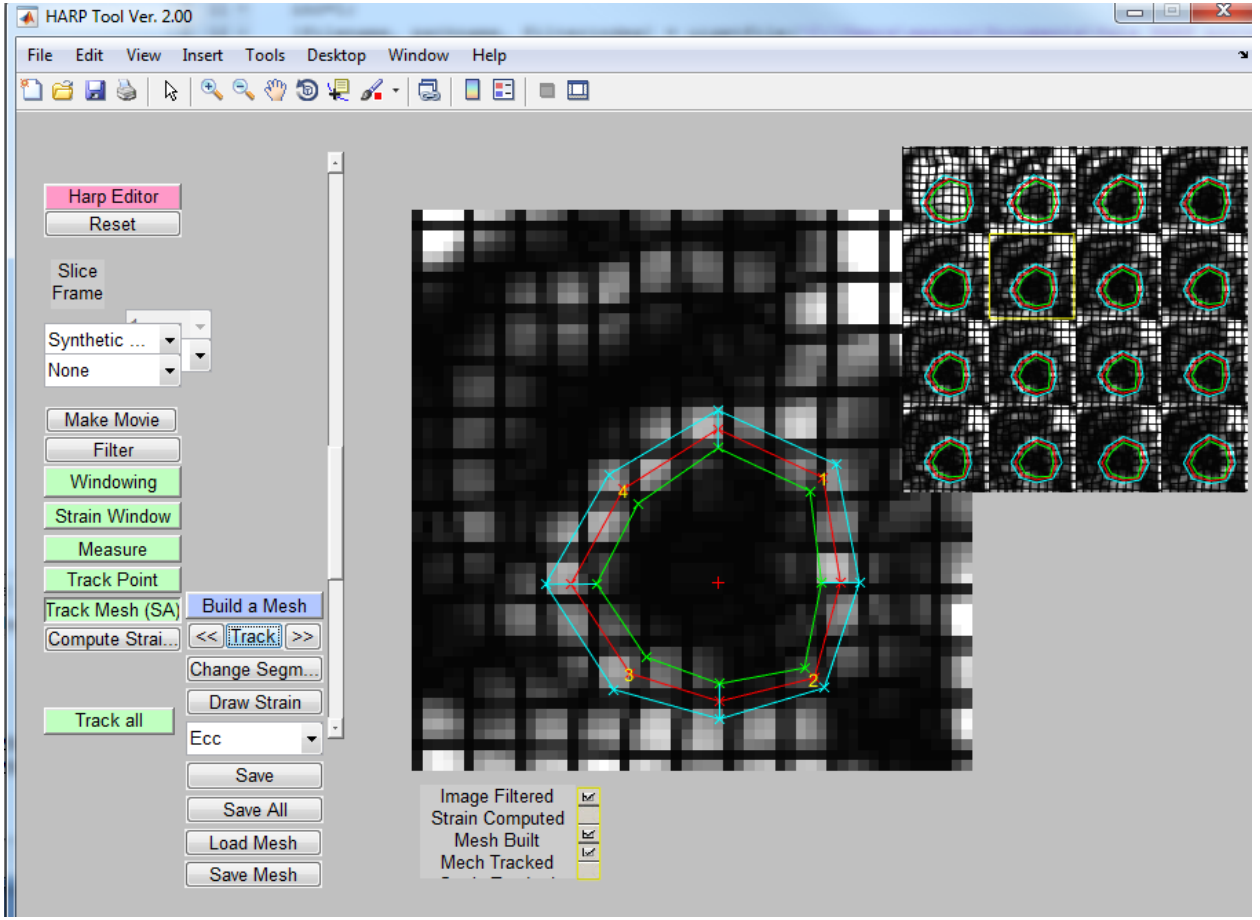

Figure 5.2 HARP analysis toolbox. The user created mesh of the LV is divided into four segments and three layers across the myocardial wall. The points within the mesh are tracked through the frames obtained during breath holds.

Table 5.1 Strain analysis of MI segment by layer of control, MI, and MI-HA groups at the basal level. †

	Control (n=1)	MI (n=3)	MI-HA (n=3)
Endocardial Layer			
Radial Thickening	4.27	-0.687 ± 3.75	7.67± 12.11
Circumferential Shortening	-8.04	-2.60 ± 2.69	-1.12 ± 7.13
Lagrangian Circumferential Strain (L_{Ecc})	-9.61	-5.64 ± 3.18	-5.10 ± 4.43
Mid-wall Layer			
Radial Thickening	4.36	2.03 ± 0.985	6.94 ± 9.89
Circumferential Shortening	-4.14	-2.16± 2.75	-1.95 ± 6.21
Lagrangian Circumferential Strain (L_{Ecc})	-6.32	-4.12 ± 3.99	-4.21 ± 1.65
Epicardial Layer			
Radial Thickening	4.34	1.46 ± 2.52	5.72 ± 9.42
Circumferential Shortening	-6.85	-3.18± 1.50	-3.33± 1.98
Lagrangian Circumferential Strain (L_{Ecc})	-7.82	-2.19± 1.97	-3.04± 2.29

Data is presented as the mean ± SD; Control values represent a composite value of all (4) segments.
†Post-MI time point of 14 days.

Table 5.2 Strain analysis of MI segment by layer of control, MI, and MI-HA groups at the mid-ventricular level. †

	Control (n=1)	MI (n=3)	MI-HA (n=3)
Endocardial Layer			
Radial Thickening	8.30	8.32 ± 1.99	11.89± 1.46
Circumferential Shortening	-7.47	-2.23 ± 4.75	-4.52 ± 2.37
Lagrangian Circumferential Strain (L_{Ecc})	-11.8	-9.48 ± 10.44	-6.47 ± 1.16
Mid-wall Layer			
Radial Thickening	6.54	6.83 ± 1.75	8.37 ± 2.67
Circumferential Shortening	-8.49	-2.261 ± 1.05	-4.72 ± 1.57
Lagrangian Circumferential Strain (L_{Ecc})	-9.39	-8.29 ± 10.48	-4.29 ± 1.51
Epicardial Layer			
Radial Thickening	7.43	8.42 ± 2.58	6.41 ± 5.41
Circumferential Shortening	-7.38	-.819 ± 1.37	-3.731 ± 1.32
Lagrangian Circumferential Strain (L_{Ecc})	-7.19	-6.70± 8.79	-3.01 ± 2.98

Data is presented as the mean ± SD;

† Post-MI time point of 14 days.

Table 5.3 Strain analysis of MI segment by layer of control, MI, and MI-HA groups at the apical level. †

	Control (n=1)	MI (n=3)	MI-HA (n=3)
Endocardial Layer			
Radial Thickening	12.04	.238 ± 1.53	1.57± 1.42
Circumferential Shortening	-8.17	-7.06 ± 4.47	-3.99 ± 4.31
Lagrangian Circumferential Strain (L_{Ecc})	-16.35	-6.84± 3.50	-5.87 ± .63
Mid-wall Layer			
Radial Thickening	10.03	.331± 1.10	1.87 ± 1.25
Circumferential Shortening	-8.94	-5.83 ± 5.47	-3.94 ± 4.21
Lagrangian Circumferential Strain (L_{Ecc})	-13.22	-4.65 ± 2.25	-5.57 ± .94
Epicardial Layer			
Radial Thickening	9.26	.314 ± 1.13	1.57 ± 1.75
Circumferential Shortening	8.28	-5.38± 4.49	-2.87 ± 4.15
Lagrangian Circumferential Strain (L_{Ecc})	-13.52	-3.26 ± 1.66	-4.47 ± 2.07

Data is presented as the mean ± SD;

† Post-MI time point of 14 days.

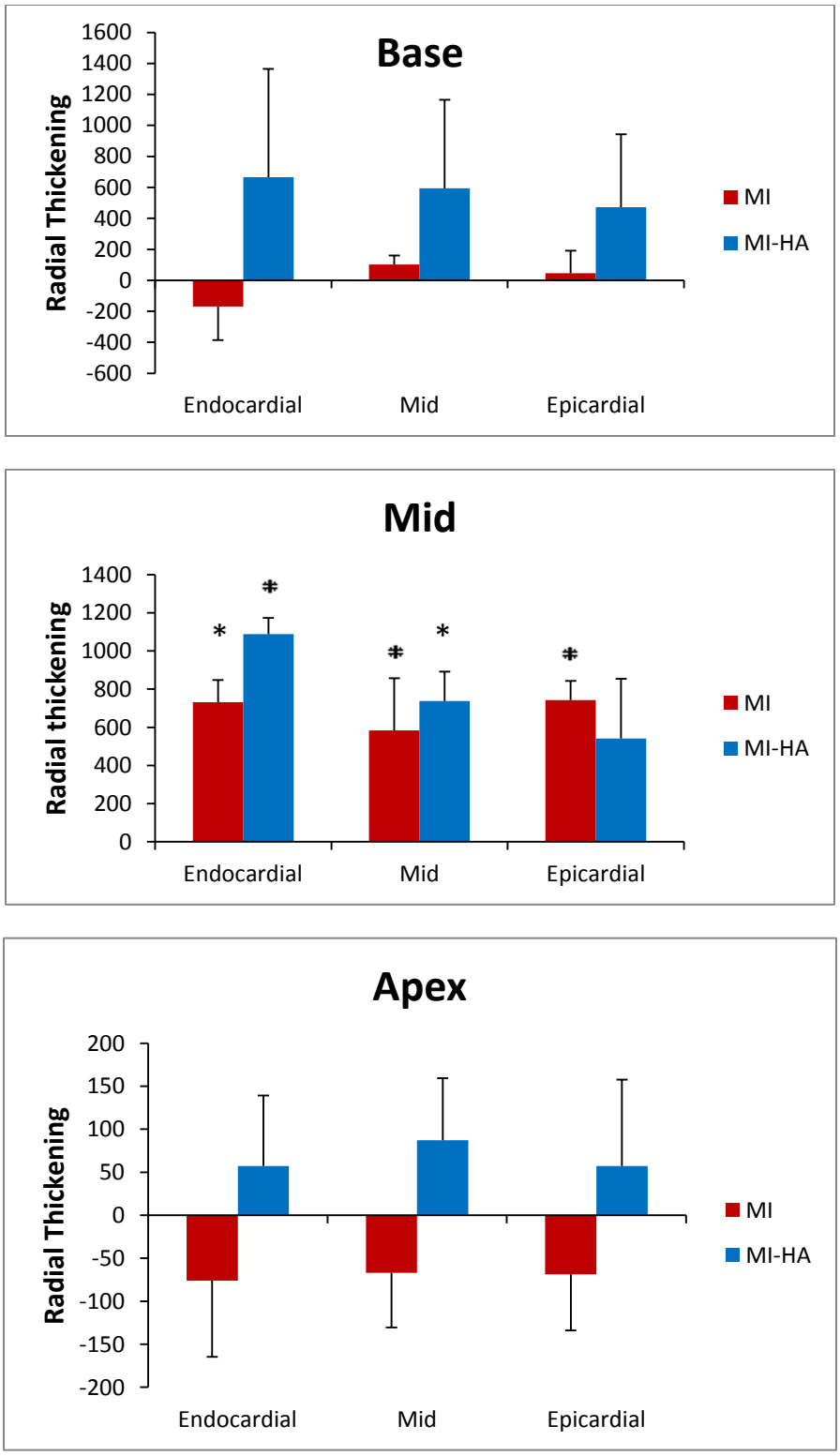

Figure 5.3 Radial thickening. Presented as a percent change from control compostive values by layer, and location in the LV

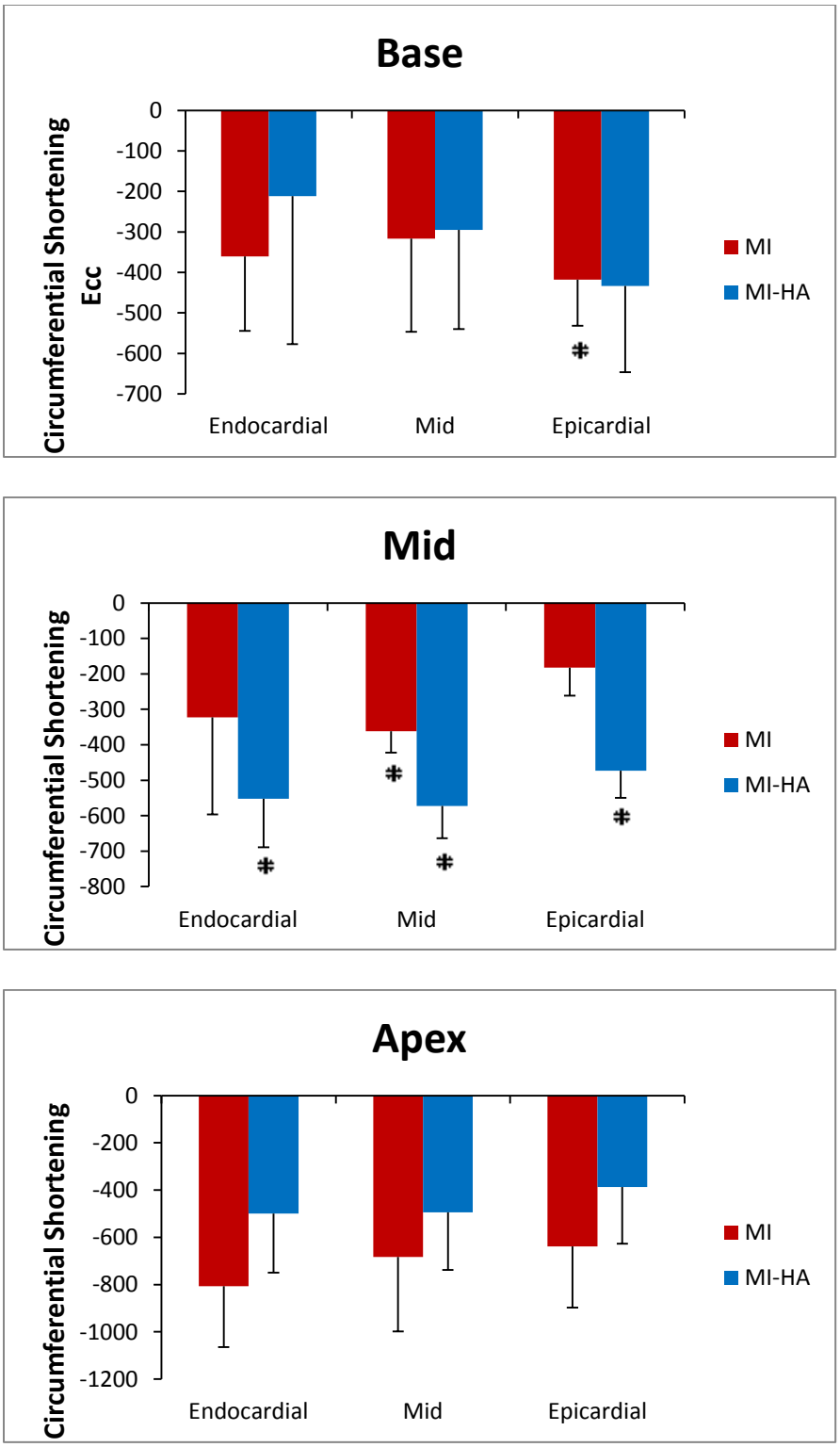

Figure 5.4 Circumferential Shortening. Presented as a percent change from control compostive values by layer, and location in the LV

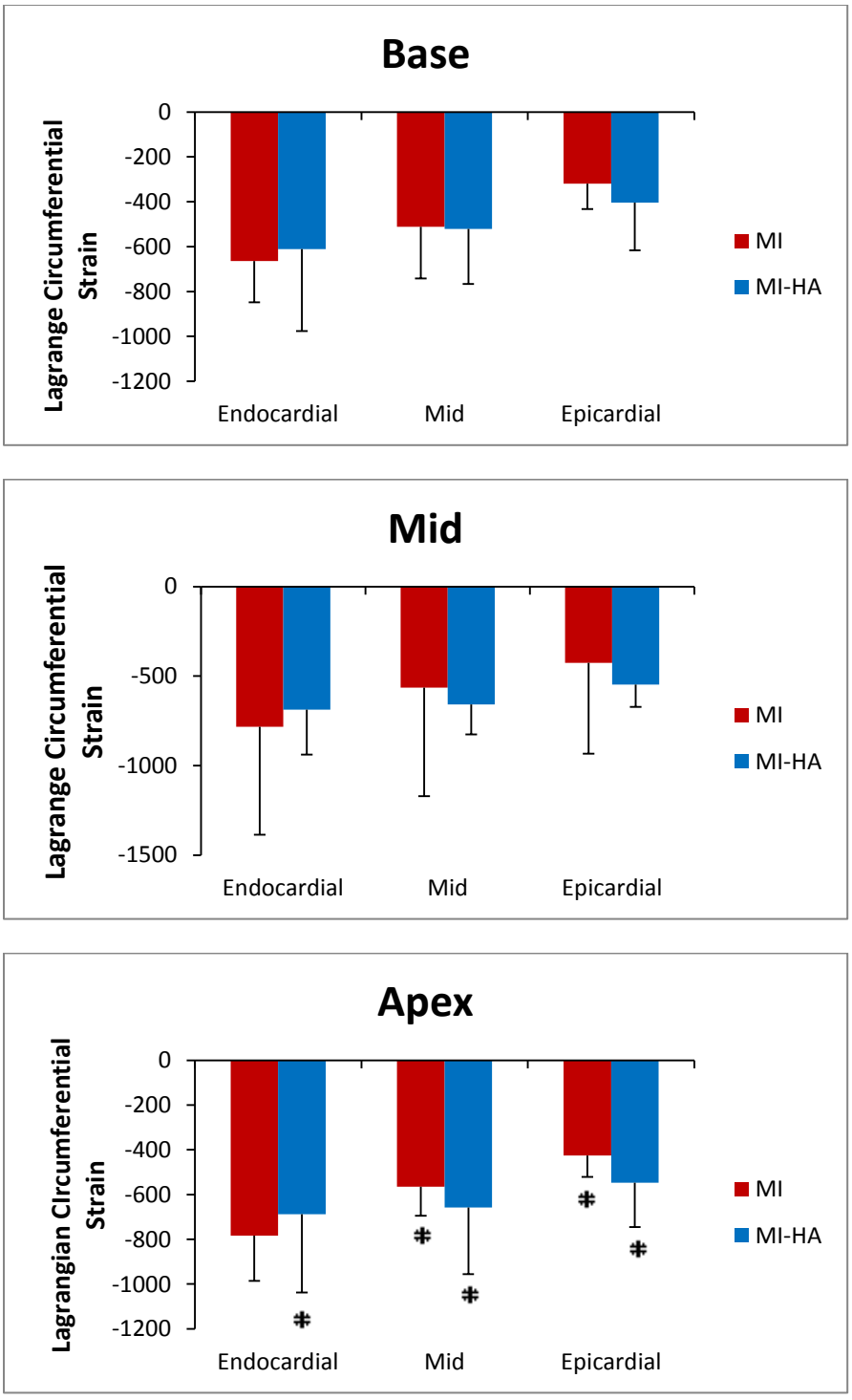

Figure 5.5 Lagrange Circumferential Strain. Presented as a percent change from control compostive values by layer, and location in the LV

CHAPTER 6

FUTURE WORK AND THESIS CONCLUSION

6.1 Future work

A completion of our control group allow for a complete analysis of the impact of the HA injections on the strain behavior post-MI. The expected completion of the control group will occur on March 8th, with the final set of MRI studies and analysis. The experimental design and data from the studies presented herein provides guidance for the development and testing of similar material strategies. The experimental difficulties and limitations are readily extendable to the testing of other forms of hydrogels with the intent to mechanically alter the material of the MI during the remodeling process.

We successfully established initial parameters for the injection sites and volumes that imparted an effect on the functional outcomes post-MI (Studies 3 & 4). However we did not propose any variations in pattern of injections or volumetric differences in injections within the patter. Furthermore we did not use sonomicrometry in a study that had a group composed of animals with the hydrogel injections. This experimentation entails a more advanced crystal layout (with a grid pattern for ease in analysis) and more importantly a chronically implanted set of crystals. In using a chronic model rather than acute implantation to record data, the changing mechanics of the MI region could be tracked

through remodeling and the effects of the hydrogel could potentially be optimized with respect to time post-MI in a more efficient manner.

6.2 Thesis Conclusion

An increased comprehension of the dynamic and complex changes that occur post-MI during the remodeling process has enabled the creation of therapeutic materials and techniques. The growing knowledge base of the functional effects of biomaterial injectates and the relationship to post-MI remodeling outcomes clearly motivates the need to better understand the affected mechanical environment. Through analysis of mechanical changes in the MI and the study of a hyaluronic acid based hydrogel as biomaterial injectate therapy we have extracted multiple mechanical descriptors and techniques with are applicable to the study of other therapeutics (not restricted to hydrogels). The findings of this work provide insight and metrics of value to be put forth in material design applications as well as computational simulations to eventually yield a predictive framework upon which therapeutics could be elegantly refined.

REFERENCES

.1. Abd-Elmoniem, K. Z., M. S. Tomas, T. Sasano, S. Soleimanifard, E.-J. P. Vonken, A. Youssef, H. Agarwal, V. L. Dimaano, H. Calkins, M. Stuber, J. L. Prince, T. P. Abraham, and M. R. Abraham. Assessment of distribution and evolution of mechanical dyssynchrony in a porcine model of myocardial infarction by cardiovascular magnetic resonance. *J. Cardiovasc. Magn. Reson.* 14:1, 2012.

2. Al-Mallah, M. H., and M. N. Shareef. The role of cardiac magnetic resonance imaging in the assessment of non-ischemic cardiomyopathy. *Heart Fail. Rev.* 16:369–80, 2011.

3. Amini, A. A., Y. Chen, M. Elayyadi, and P. Radeva. Tag Surface Reconstruction and Tracking of Myocardial Beads from SPAMM-MRI with. *IEEE Trans. Med. Imaging* 20:94–103, 2001.

4. Amirhamzeh, M. M., D. T. Hsu, S. E. Cabreriza, C. X. Jia, and H. M. Spotnitz. Myocardial edema: comparison of effects on filling volume and stiffness of the left ventricle in rats and pigs. *Ann. Thorac. Surg.* 63:1293–7, 1997.

5. Amundsen, B. H., T. Helle-Valle, T. Edvardsen, H. Torp, J. Crosby, E. Lyseggen, A. Støylen, H. Ihlen, J. a C. Lima, O. a Smiseth, and S. a Slørdahl. Noninvasive myocardial strain measurement by speckle tracking echocardiography: validation against sonomicrometry and tagged magnetic resonance imaging. *J. Am. Coll. Cardiol.* 47:789–93, 2006.

6. Ananthasubramaniam, K., R. Dhar, and J. L. Cavalcante. Role of multimodality imaging in ischemic and non-ischemic cardiomyopathy. *Heart Fail. Rev.* 16:351–67, 2011.

7. Andreu, I., T. Luque, A. Sancho, B. Pelacho, O. Iglesias-García, E. Melo, R. Farré, F. Prósper, M. R. Elizalde, and D. Navajas. Heterogeneous micromechanical properties of the extracellular matrix in healthy and infarcted hearts. *Acta Biomater.* 10:3235–42, 2014.

8. Artis, N. J., D. L. Oxborough, G. Williams, C. B. Pepper, and L. B. Tan. Two-dimensional strain imaging: a new echocardiographic advance with research and clinical applications. *Int. J. Cardiol.* 123:240–8, 2008.

9. Avenue, G. Instantaneous Pressure-Volume Relationships and Their Ratio in the Excised , Supported Canine Left Ventricle. 117–126, 1974.doi:10.1161/01.RES.35.1.117

10. Bachner-Hinenzon, N., O. Ertracht, A. Malka, M. Leitman, Z. Vered, O. Binah, and D. Adam. Layer-specific strain analysis: investigation of regional deformations in a rat model of acute versus chronic myocardial infarction. *Am. J. Physiol. Heart Circ. Physiol.* 303:H549–58, 2012.

11. Baxter, S. C., M. O. Morales, and E. C. Goldsmith. Adaptive changes in cardiac fibroblast morphology and collagen organization as a result of mechanical environment. *Cell Biochem. Biophys.* 51:33–44, 2008.

12. Becker, M., R. Hoffmann, H. P. Kühl, H. Grawe, M. Katoh, R. Kramann, A. Bücker, P. Hanrath, and N. Heussen. Analysis of myocardial deformation based on ultrasonic pixel tracking to determine transmurality in chronic myocardial infarction. *Eur. Heart J.* 27:2560–6, 2006.

13. Benejam, C., J. Bian, N. Mal, J. Drinko, K. Lee, F. Forudi, R. Reeg, N. L. Greenberg, J. D. Thomas, and M. S. Penn. Speckle-tracking echocardiography correctly identifies segmental left ventricular dysfunction induced by scarring in a rat model of myocardial infarction. 44195:2809–2816, 2007.

14. Bhan, A., A. Sirker, J. Zhang, A. Protti, N. Catibog, W. Driver, R. Botnar, M. J. Monaghan, and A. M. Shah. High-frequency speckle tracking echocardiography in the assessment of left ventricular function and remodeling after murine myocardial infarction. *Am. J. Physiol. Heart Circ. Physiol.* 306:H1371–83, 2014.

15. Blom, A. S., J. J. Pilla, J. Arkles, L. Dougherty, L. P. Ryan, J. H. Gorman, M. a Acker, and R. C. Gorman. Ventricular restraint prevents infarct expansion and improves borderzone function after myocardial infarction: a study using magnetic resonance imaging, three-dimensional surface modeling, and myocardial tagging. *Ann. Thorac. Surg.* 84:2004–10, 2007.

16. Bogaert, J., H. Bosmans, a Maes, P. Suetens, G. Marchal, and F. E. Rademakers. Remote myocardial dysfunction after acute anterior myocardial infarction: impact of left ventricular shape on regional function: a magnetic resonance myocardial tagging study. *J. Am. Coll. Cardiol.* 35:1525–34, 2000.

17. Bogen, D. K., and T. a McMahon. Do cardiac aneurysms blow out? *Biophys. J.* 27:301–16, 1979.

18. Braunwald, E. Biomarkers in heart failure. *N. Engl. J. Med.* 358:2148–59, 2008.

19. Braunwald, E., and R. a. Kloner. The stunned myocardium: prolonged, postischemic ventricular dysfunction. *Circulation* 66:1146–1149, 1982.

20. Braunwald, E., and R. a. Kloner. Myocardial Reperfusion: A Double-edged Sword? *J. Clin. Invest.* 76:1713–1719, 1985.

21. Bujak, M., and N. G. Frangogiannis. The role of TGF-beta signaling in myocardial infarction and cardiac remodeling. *Cardiovasc. Res.* 74:184–95, 2007.

22. Burdick, J. A., and G. D. Prestwich. Hyaluronic Acid Hydrogels for Biomedical Applications. 41–56, 2011.doi:10.1002/adma.201003963

23. Butt, R. P., and J. E. Bishop. Mechanical Load Enhances the Stimulatory Effect of Serum Growth Factors on Cardiac Fibroblast Procollagen Synthesis. *J. Mol. Cell Cardiol.* 1151:1141–1151, 1997.

24. Capasso, J. M., P. Li, X. Zhang, and P. Anversa. Heterogeneity of ventricular remodeling myocardial infarction in rats after acute. *Am. Physiol. Soc.* , 1992.

25. Carver, W., M. L. Nagpal, M. Nachtigal, T. K. Borg, and L. Terracio. Collagen expression in mechanically stimulated cardiac fibroblasts. *Circ. Res.* 69:116–122, 1991.

26. Cavasin, M. a, S. S. Sankey, A.-L. Yu, S. Menon, and X.-P. Yang. Estrogen and testosterone have opposing effects on chronic cardiac remodeling and function in mice with myocardial infarction. *Am. J. Physiol. Heart Circ. Physiol.* 284:H1560–9, 2003.

27. Chan, J., L. Hanekom, C. Wong, R. Leano, G.-Y. Cho, and T. H. Marwick. Differentiation of subendocardial and transmural infarction using two-dimensional strain rate imaging to assess short-axis and long-axis myocardial function. *J. Am. Coll. Cardiol.* 48:2026–33, 2006.

28. Christman, K. L., H. H. Fok, R. E. Sievers, Q. Fang, R. J. Lee, and D. Ph. Fibrin Glue Alone and Skeletal Myoblasts in a Fibrin Scaffold Preserve Cardiac Function after Myocardial Infarction. 10:, 2004.

29. Christman, K. L., and R. J. Lee. Biomaterials for the Treatment of Myocardial Infarction. *J. Am. Coll. Cardiol.* 48:, 2006.

30. Clark, N. R., N. Reichek, P. Bergey, E. A. Hoffman, D. Brownson, L. Palmon, and L. Axel. Circumferential myocardial shortening in the normal human left ventricle. Assessment by magnetic resonance imaging using spatial modulation of magnetization. *Circulation* 84:67–74, 1991.

31. Cleutjens, J., J. Kandala, E. Guarda, R. Guntaka, and K. Weber. Regulation of collagen degradation in the rat myocardium after infarction. *J. Mol. Cell. Cardiol.* 27:1281–1292, 1995.

32. Cleutjens, J. P., M. J. Verluyten, J. F. Smiths, and M. J. Daemen. Collagen remodeling after myocardial infarction in the rat heart. *Am. J. Pathol.* 147:325–38, 1995.

33. Cohn, J. N., R. Ferrari, N. Sharpe, and I. Forum. Cardiac Remodeling — Concepts and Clinical Implications : A Consensus Paper From an International Forum on Cardiac Remodeling. *J. Am. Coll. Cardiol.* 35:, 2000.

34. Costa, K. D., J. W. Holmes, and A. D. Mcculloch. Modelling cardiac mechanical properties in three dimensions. *Philos. Trans. R. Soc. A Math. Phys. Eng. Sci.* 359:1233–1250, 2001.

35. D, J., A. Heimdal, F. Jamal, T. Kukulski, B. Bijnens, F. Rademakers, L. Hatle, P. Suetens, and G. R. Sutherland. Regional Strain and Strain Rate Measurements by Cardiac Ultrasound : Principles , Implementation and Limitations. *Eur. J. Echocardiogr.* 1:154–170, 2000.

36. Demer, B. Y. L. L., and F. C. P. Yin. Passive biaxial mechanical properties of isolated canine myocardium. *J. Physiol.* 339:615–630, 1983.

37. Desmoulibre, A. Transforming Growth Factor-βl Induces alpha-Smooth Muscle Actin Expression in Granulation Tissue Myofibroblasts and in Quiescent and Growing Cultured Fibroblasts. *J. Cell Biol.* 122:103–111, 1993.

38. Dione, D., P. Shi, W. Smith, P. Deman, J. Soares, J. Duncan, and A. Sinusas. Three-Dimensional Regional Left Ventricular Deformation from Digital Sonomicrometry. 848–851, 1999.

39. Dobaczewski, M., M. Bujak, P. Zymek, G. Ren, M. L. Entman, and N. G. Frangogiannis. Extracellular matrix remodeling in canine and mouse myocardial infarcts. *Cell Tissue Res.* 324:475–88, 2006.

40. Dobaczewski, M., C. Gonzalez-Quesada, and N. G. Frangogiannis. The extracellular matrix as a modulator of the inflammatory and reparative response following myocardial infarction. *J. Mol. Cell. Cardiol.* 48:504–11, 2010.

41. Eaton, L. W., J. L. Weiss, B. H. BUlkley, J. B. Garrison, and M. L. Weisfeldt. Regional Cardiac Dilatation after Acute Myocardial Infarction — NEJM. , 1979.at <http://www.nejm.org/doi/pdf/10.1056/NEJM197901113000202>

42. Eckhouse, S. R., B. P. Purcell, J. R. McGarvey, D. Lobb, C. B. Logdon, H. Doviak, J. W. O'Neill, J. A. Shuman, C. P. Novack, K. N. Zellars, S. Pettaway, R. A. Black, A. Khakoo, T. Lee, R. Mukherjee, J. H. Gorman, R. C. Gorman, J. A. Burdick, and F. G. Spinale. Local hydrogel release of recombinant TIMP-3 attenuates adverse left ventricular remodeling after experimental myocardial infarction. *Sci. Transl. Med.* 6:223ra21, 2014.

43. Edvardsen, T., B. L. Gerber, J. Garot, D. A. Bluemke, J. A. C. Lima, and O. a Smiseth. Quantitative Assessment of Intrinsic Regional Myocardial Deformation by Doppler Strain Rate Echocardiography in Humans: Validation Against Three-Dimensional Tagged Magnetic Resonance Imaging. *Circulation* 106:50–56, 2002.

44. Eghbali, M., R. Tomek, V. P. Sukhatme, C. Woods, and B. Bhambi. Differential effects of transforming growth factor-beta 1 and phorbol myristate acetate on cardiac fibroblasts. Regulation of fibrillar collagen mRNAs and expression of early transcription factors. *Circ. Res.* 69:483–490, 1991.

45. Enomoto, Y., J. H. G. Iii, S. L. Moainie, B. M. Jackson, L. M. Parish, T. Plappert, A. Zeeshan, M. G. S. John-sutton, and R. C. Gorman. Infarction : Extent of the Wrap Determines the Outcome of Remodeling. , 2005.doi:10.1016/j.athoracsur.2004.05.072

46. Ertl, G., and S. Frantz. Healing after myocardial infarction. *Cardiovasc. Res.* 66:22–32, 2005.

47. Espe, E. K. S., J. M. Aronsen, K. Skårdal, J. E. Schneider, L. Zhang, and I. Sjaastad. Novel insight into the detailed myocardial motion and deformation of the rodent heart using high-resolution phase contrast cardiovascular magnetic resonance. *J. Cardiovasc. Magn. Reson.* 15:82, 2013.

48. Fishbein, M. C., D. Maclean, and P. R. Maroko. Experimental myocardial infarction in the rat: qualitative and quantitative changes during pathologic evolution. *Am. J. Pathol.* 90:57–70, 1978.

49. Fomovsky, G. M., and J. W. Holmes. Evolution of scar structure, mechanics, and ventricular function after myocardial infarction in the rat. *Am. J. Physiol. Heart Circ. Physiol.* 298:H221–8, 2010.

50. Fomovsky, G. M., S. Thomopoulos, and J. W. Holmes. Contribution of extracellular matrix to the mechanical properties of the heart. *J. Mol. Cell. Cardiol.* 48:490–6, 2010.

51. Fomovsky, Gregory M, Andrew D. Rouillard, J. W. H. Regional Mechanics Determine Collagen Fiber Structure in Healing Myocardial Infarcts. *J. Mol. Cell Cardiol.* 52:1083–1090, 2012.

52. Frangogiannis, N. G., C. W. Smith, and M. L. Entman. The inflammatory response in myocardial infarction. *Cardiovasc. Res.* 53:31–47, 2002.

53. Frantz, S., J. Bauersachs, G. Ertl, M. Klinik, and U. Würzburg. Post-infarct remodelling: Contribution of wound healing and inflammation. *Eur. Soc. Cardiol.* 1–26, 2008.

54. Fujimoto, K. L., Z. Ma, D. M. Nelson, R. Hashizume, J. Guan, K. Tobita, and W. R. Wagner. Biomaterials Synthesis , characterization and therapeutic efficacy of a biodegradable , thermoresponsive hydrogel designed for application in chronic infarcted myocardium. *Biomaterials* 30:4357–4368, 2009.

55. Gaasch, W. H., O. H. L. Bing, and I. Mirsky. Chamber compliance and myocardial stiffness in left ventricular hypertrophy. *Eur. Heart J.* 3:139–145, 1982.

56. Gaharwar, A. K., N. a Peppas, and A. Khademhosseini. Nanocomposite hydrogels for biomedical applications. *Biotechnol. Bioeng.* 111:441–53, 2014.

57. Garot, J., D. a. Bluemke, N. F. Osman, C. E. Rochitte, E. R. McVeigh, E. a. Zerhouni, J. L. Prince, and J. a. C. Lima. Fast Determination of Regional Myocardial Strain Fields From Tagged Cardiac Images Using Harmonic Phase MRI. *Circulation* 101:981–988, 2000.

58. Gerber, B. L., J. Garot, D. A. Bluemke, K. C. Wu, and J. A. C. Lima. Accuracy of Contrast-Enhanced Magnetic Resonance Imaging in Predicting Improvement of Regional Myocardial Function in Patients After Acute Myocardial Infarction. *Circulation* 106:1083–1089, 2002.

59. Geyer, H., G. Caracciolo, H. Abe, S. Wilansky, S. Carerj, F. Gentile, H.-J. Nesser, B. Khandheria, J. Narula, and P. P. Sengupta. Assessment of myocardial mechanics using speckle tracking echocardiography: fundamentals and clinical applications. *J. Am. Soc. Echocardiogr.* 23:351–69; quiz 453–5, 2010.

60. Gjesdal, O., T. Helle-Valle, E. Hopp, K. Lunde, T. Vartdal, S. Aakhus, H.-J. Smith, H. Ihlen, and T. Edvardsen. Noninvasive separation of large, medium, and small myocardial infarcts in survivors of reperfused ST-elevation myocardial infarction: a comprehensive tissue Doppler and speckle-tracking echocardiography study. *Circ. Cardiovasc. Imaging* 1:189–96, 2 p following 196, 2008.

61. Go, A. S. *et al.* Heart disease and stroke statistics--2013 update: a report from the American Heart Association. *Circulation* 127:e6–e245, 2013.

62. Go, A. S. *et al.* Heart disease and stroke statistics--2014 update: a report from the American Heart Association. *Circulation* 129:e28–e292, 2014.

63. Göktepe, S., S. N. S. Acharya, J. Wong, and E. Kuhl. Computational modeling of passive myocardium. *Int. j. numer. method. biomed. eng.* 27:1–12, 2011.

64. Gorcsan, J., and H. Tanaka. Echocardiographic assessment of myocardial strain. *J. Am. Coll. Cardiol.* 58:1401–13, 2011.

65. Gorman, J. H., K. B. Gupta, J. T. Streicher, R. C. Gorman, B. M. Jackson, M. B. Ratcliffe, D. K. Bogen, and L. H. Edmunds. Dynamic three-dimensional imaging

of the mitral valve and left ventricle by rapid sonomicrometry array localization. *J. Thorac. Cardiovasc. Surg.* 112:712–26, 1996.

66. Gupta, K. B., M. B. Ratcliffe, M. a. Fallert, L. H. Edmunds, and D. K. Bogen. Changes in passive mechanical stiffness of myocardial tissue with aneurysm formation. *Circulation* 89:2315–2326, 1994.

67. Hayashida, W., C. V. A. N. Eyll, M. F. Rousseau, and H. Pouleur. Regional Remodeling and Nonuniform Changes in Diastolic Function in Patients With Left Ventricular Dysfunction : Modification by Long-Term Enalapril Treatment. *JACC* 22:1403–1410, 1993.

68. Helle-valle, T., E. W. Remme, E. Lyseggen, E. Pettersen, T. Vartdal, A. Opdahl, H. Smith, N. F. Osman, H. Ihlen, T. Edvardsen, and O. A. Smiseth. Clinical assessment of left ventricular rotation and strain : a novel approach for quantification of function in infarcted myocardium and its border zones. 257–267, 2009.doi:10.1152/ajpheart.01116.2008.

69. Hochman, J. S., and B. H. Bulkley. Expansion of acute myocardial infarction: an experimental study. *Circulation* 65:1446–1450, 1982.

70. Hoffman, A. S. Hydrogels for biomedical applications. , 2012.

71. Holmes, J. W., T. K. Borg, and J. W. Covell. Structure and mechanics of healing myocardial infarcts. *Annu. Rev. Biomed. Eng.* 7:223–253, 2005.

72. Holmes, J. W., T. K. Borg, and J. W. Covell. Structure and mechanics of healing myocardial infarcts. *Annu. Rev. Biomed. Eng.* 7:223–53, 2005.

73. Holmes, J. W., J. A. Nunez, and J. W. Covell. Functional implications of myocardial scar structure. *Am J Physiol Hear. Circ Physiol* 272:H2123–2130, 1997.

74. Holmes, J. W., H. Yamashita, L. K. Waldman, and J. W. Covell. Scar remodeling and transmural deformation after infarction in the pig. *Circulation* 90:411–420, 1994.

75. Holzapfel, G. a, and R. W. Ogden. Constitutive modelling of passive myocardium: a structurally based framework for material characterization. *Philos. Trans. A. Math. Phys. Eng. Sci.* 367:3445–75, 2009.

76. Hunter, P. J., a D. McCulloch, and H. E. ter Keurs. Modelling the mechanical properties of cardiac muscle. *Prog. Biophys. Mol. Biol.* 69:289–331, 1998.

77. Ifkovits, J. L., E. Tous, M. Minakawa, M. Morita, J. D. Robb, and K. J. Koomalsingh. Injectable hydrogel properties in fl uence infarct expansion and

extent of postinfarction left ventricular remodeling in an ovine model. 1–6, 2010.doi:10.1073/pnas.1004097107

78. Jackson, B. M., J. H. Gorman III, S. L. Moainie, T. S. Guy, N. Narula, J. Narula, M. G. S. John-sutton, L. H. Edmunds, and R. C. Gorman. Extension of Borderzone Myocardium in Postinfarction Dilated Cardiomyopathy. *J. Am. Coll. Cardiol.* 40:, 2002.

79. Jaeschke, H., and W. C. Smith. Mechanisms of neutrophil-induced parenchymal cell injury. *J. Leukoc. Biol.* 61:647–653, 1997.

80. Jugdutt, B. I. Prevention of ventricular remodelling post myocardial infarction: timing and duration of therapy. *Can. J. Cardiol.* 9:103–14, 1993.

81. Jugdutt, B. I. Prevention of ventricular remodeling after myocardial infarction and in congestive heart failure. *Heart Fail. Rev.* 1:115–129, 1996.

82. Jugdutt, B. I. Remodeling of the Myocardium and Potential Targets in the Collagen Degradation and Synthesis Pathways. 1–30, 2003.

83. Jugdutt, B. I. Cyclooxygenase inhibition and adverse remodeling during healing after myocardial infarction. *Circulation* 115:288–91, 2007.

84. Jugdutt, B. I. Cyclooxygenase inhibition and adverse remodeling during healing after myocardial infarction. *Circulation* 115:288–91, 2007.

85. Jugdutt, B. I., and R. W. M. Amy. Healing after myocardial infarction in the dog: Changes in infarct hydroxyproline and topography. *J. Am. Coll. Cardiol.* 7:91–102, 1986.

86. Jugdutt, B. I., M. J. Joljart, and M. I. Khan. Rate of Collagen Deposition During Healing and Ventricular Remodeling After Myocardial Infarction in Rat and Dog Models. *Circulation* 94:94–101, 1996.

87. Julias, M., T. Riede, and D. Cook. Visualizing collagen network within human and rhesus monkey vocal folds using polarized light microscopy. *Ann. Otol. Rhinol. Laryngol.* 122:135–44, 2013.

88. Kang, T., J. D. Humphrey, F. C. Yin, F. C. P. Yin, and Y. Comparison. Comparison of biaxial mechanical properties of excised endocardium and epicardium Comparison of biaxial mechanical properties of excised endocardium and epicardium. *Am. J. Physiol. Heart Circ. Physiol.* 270:H2169–H2176, 1996.

89. Kellar, R. S., D. Ph, B. R. Shepherd, D. F. Larson, G. K. Naughton, and S. K. W. P. D. Cardiac Patch Constructed from Human Fibroblasts Attenuates Reduction in Cardiac Function after Acute Infarct. *Tissue Eng.* 11:1678–1687, 2005.

90. Kelley, S. T., R. Malekan, J. H. G. Iii, B. M. Jackson, C. Robert, Y. Suzuki, T. Plappert, D. K. Bogen, M. G. St, J. Sutton, and L. H. Edmunds. Restraining Infarct Expansion Preserves Left Ventricular Geometry and Function After Acute Anteroapical Infarction. *Circulation* 99:135–142, 1999.

91. Kenneth Mallory, G., P. D. White, and J. Salcedo-Salgar. The speed of healing of myocardial infarction. *Am. Heart J.* 18:647–671, 1939.

92. Kichula, E. T., H. Wang, S. M. Dorsey, S. E. Szczesny, D. M. Elliott, J. A. Burdick, and J. F. Wenk. Experimental and Computational Investigation of Altered Mechanical Properties in Myocardium after Hydrogel Injection. *Ann. Biomed. Eng.* , 2013.doi:10.1007/s10439-013-0937-9

93. Kilic, A., T. Li, T. D. C. Nolan, J. R. Nash, S. Li, D. J. Prastein, G. Schwartzbauer, S. L. Moainie, G. K. Yankey, C. DeFilippi, Z. Wu, and B. P. Griffith. Strain-related regional alterations of calcium-handling proteins in myocardial remodeling. *J. Thorac. Cardiovasc. Surg.* 132:900–8, 2006.

94. Klepach, D., L. C. Lee, J. F. Wenk, M. B. Ratcliffe, T. I. Zohdi, J. a Navia, G. S. Kassab, E. Kuhl, and J. M. Guccione. Growth and remodeling of the left ventricle: A case study of myocardial infarction and surgical ventricular restoration. *Mech. Res. Commun.* 42:134–141, 2012.

95. Korinek, J., J. Vitek, P. P. Sengupta, A. Romero-Corral, V. K. Krishnamoorthy, E. M. McMahon, B. K. Khandheria, and M. Belohlavek. Does implantation of sonomicrometry crystals alter regional cardiac muscle function? *J. Am. Soc. Echocardiogr.* 20:1407–12, 2007.

96. Korinek, J., J. Wang, P. P. Sengupta, C. Miyazaki, J. Kjaergaard, E. McMahon, T. P. Abraham, and M. Belohlavek. Two-dimensional strain--a Doppler-independent ultrasound method for quantitation of regional deformation: validation in vitro and in vivo. *J. Am. Soc. Echocardiogr.* 18:1247–53, 2005.

97. Kraitchman, D. L., a a Young, D. C. Bloomgarden, Z. a Fayad, L. Dougherty, V. a Ferrari, R. C. Boston, and L. Axel. Integrated MRI assessment of regional function and perfusion in canine myocardial infarction. *Magn. Reson. Med.* 40:311–26, 1998.

98. Kukielka, G. L., C. W. Smith, G. J. Larosa, A. M. Manning, L. H. Mendoza, T. J. Daly, I. B. J. Hughes, K. A. Youker, H. K. Hawkins, L. H. Michael, A. Rot, and M. L. Entman. Interleukin-8 Gene Induction in the Myocardium after Ischemia and Reperfusion In Vivo. *Am. Soc. Clin. Inverstigation* 95:89–103, 1995.

99. Leask, A. TGFbeta, cardiac fibroblasts, and the fibrotic response. *Cardiovasc. Res.* 74:207–12, 2007.

100. Lee, A. A., T. Delhaas, A. D. Mcculloch, and F. J. Villarreal. Differential Responses of Adult Cardiac Fibroblasts to in vitro Biaxial Strain Patterns. *J. Mol. Cell Cardiol.* 1843:1833–1843, 1999.

101. Leor, J., S. Aboulafia-etzion, A. Dar, L. Shapiro, I. M. Barbash, A. Battler, Y. Granot, and S. Cohen. Bioengineering Cardiac grafts: A new approach to repair the infarcted myocardium? , 2000.doi:10.1161/01.CIR.102.suppl

102. Leor, J., S. Tuvia, V. Guetta, F. Manczur, D. Castel, U. Willenz, Ö. Petneha, N. Landa, M. S. Feinberg, E. Konen, O. Goitein, O. Tsur-gang, M. Shaul, L. Klapper, and S. Cohen. Intracoronary Injection of In Situ Forming Alginate Hydrogel Reverses Left Ventricular Remodeling After Myocardial Infarction in Swine. 54:, 2009.

103. Leor, Jonathan, S. C. Myocardial Tissue Engineering: Creating a Muscle Patch for a Wounded Heart. *Ann. NY Acad. Sci.* 312–319, 2004.

104. Lerman, R. H., C. S. Apstein, H. M. Kagan, E. L. Osmers, C. O. Chichester, W. M. Vogel, C. M. Connelly, and W. P. Steffee. Myocardial healing and repair after experimental infarction in the rabbit. *Circ. Res.* 53:378–388, 1983.

105. Liao, S., Q. Ruan, M. Lin, and L. Yan. Value of segmental myocardial strain by 2-dimensional strain echocardiography for assessment of scar area induced in a rat model of myocardial infarction. *Cardiovasc. Ultrasound* 10:17, 2012.

106. Lijnen, P. J., V. V Petrov, and R. H. Fagard. Induction of cardiac fibrosis by transforming growth factor-beta(1). *Mol. Genet. Metab.* 71:418–35, 2000.

107. Liu, W., J. Chen, S. Ji, J. S. Allen, P. V Bayly, S. a Wickline, and X. Yu. Harmonic phase MR tagging for direct quantification of Lagrangian strain in rat hearts after myocardial infarction. *Magn. Reson. Med.* 52:1282–90, 2004.

108. Lo, L., J. Botas, R. Rubio, M. Moreno, and M. A. Garcı. Frequency of Left Ventricular Free-Wall Rupture in Patients with Acute Myocardial Infarction Treated with Primary Angioplasty. *Am. J. Cardiol.* 9149:757–760, 2000.

109. López, B., A. González, N. Hermida, F. Valencia, E. de Teresa, and J. Díez. Role of lysyl oxidase in myocardial fibrosis: from basic science to clinical aspects. *Am. J. Physiol. Heart Circ. Physiol.* 299:H1–9, 2010.

110. MacKenna, D., S. R. Summerour, and F. J. Villarreal. Role of mechanical factors in modulating cardiac fibroblast function and extracellular matrix synthesis. *Cardiovasc. Res.* 46:257–63, 2000.

111. Mann, D. L., and M. R. Bristow. Basic Science for Clinicians Mechanisms and Models in Heart Failure The Biomechanical Model and Beyond. 2837–2849, 2005.doi:10.1161/CIRCULATIONAHA.104.500546

112. Marinkovid, J., J. Lee, M. Tan, and J. D. Thomas. Serial Assessment of left Ventricular Chamber Stiffness After Acute Myocardial Infarction. *Am. J. Cardiol.* 77:361–364, 1995.

113. McKay, R. G., M. a. Pfeffer, R. C. Pasternak, J. E. Markis, P. C. Come, S. Nakao, J. D. Alderman, J. J. Ferguson, R. D. Safian, and W. Grossman. Left ventricular remodeling after myocardial infarction: a corollary to infarct expansion. *Circulation* 74:693–702, 1986.

114. Miller, R., N. H. Davies, J. Kortsmit, and P. Zilla. Outcomes of myocardial infarction hydrogel injection therapy in the human left ventricle dependent on injectate distribution. 870–884, 2013.doi:10.1002/cnm

115. Mirsky, I. Assessment of Passive Elastic Stiffness of Cardiac Muscle-Mathematical Concepts, Physiologic and Clinical Considerations Directions of Future Research. , 1976.

116. Mirsky, I., and J. S. Rankin. The effects of geometry, elasticity, and external pressures on the diastolic pressure-volume and stiffness-stress relations. How important is the pericardium? *Circ. Res.* 44:601–611, 1979.

117. Mirsky, I., T. Tajimi, and K. L. Peterson. The development of the entire end-systolic pressure-volume and ejection fraction-afterload relations : a new concept of systolic myocardial stiffness. *Circ. Res.* 76:343–356, 1987.

118. Mitchell, G. F., G. a Lamas, D. E. Vaughan, and M. a Pfeffer. Left ventricular remodeling in the year after first anterior myocardial infarction: a quantitative analysis of contractile segment lengths and ventricular shape. *J. Am. Coll. Cardiol.* 19:1136–44, 1992.

119. Moreno, R., J. López-Sendón, E. García, L. Pérez de Isla, E. López de Sá, A. Ortega, M. Moreno, R. Rubio, J. Soriano, M. Abeytua, and M.-A. García-Fernández. Primary angioplasty reduces the risk of left ventricular free wall rupture compared with thrombolysis in patients with acute myocardial infarction. *J. Am. Coll. Cardiol.* 39:598–603, 2002.

120. Morita, M., C. E. Eckert, K. Matsuzaki, M. Noma, L. P. Ryan, J. a Burdick, B. M. Jackson, J. H. Gorman, M. S. Sacks, and R. C. Gorman. Modification of infarct material properties limits adverse ventricular remodeling. *Ann. Thorac. Surg.* 92:617–24, 2011.

121. Morita, M., C. E. Eckert, K. Matsuzaki, M. Noma, L. P. Ryan, J. A. Burdick, B. M. Jackson, J. H. G. Iii, M. S. Sacks, and R. C. Gorman. Modification of Infarct Material Properties Limits. *ATS* 92:617–624, 2011.

122. Mukherjee, R., T. a. Brinsa, K. B. Dowdy, A. a. Scott, J. M. Baskin, A. M. Deschamps, A. S. Lowry, G. P. Escobar, D. G. Lucas, W. M. Yarbrough, M. R. Zile, and F. G. Spinale. Myocardial infarct expansion and matrix metalloproteinase inhibition. *Circulation* 107:618–625, 2003.

123. Okamoto, R. J., M. J. Moulton, S. J. Peterson, D. Li, M. K. Pasque, and J. M. Guccione. Epicardial suction: a new approach to mechanical testing of the passive ventricular wall. *J. Biomech. Eng.* 122:479–87, 2000.

124. Olivetti, G., J. M. Capasso, L. G. Meggs, E. H. Sonnenblick, and P. Anversa. Cellular basis of chronic ventricular remodeling after myocardial infarction in rats. *Circ. Res.* 68:856–869, 1991.

125. Omens, J. H., T. R. Miller, and J. W. Covell. Relationship between passive tissue strain and collagen uncoiling during healing of infarcted myocardium. *Cardiovasc. Res.* 33:351–8, 1997.

126. Osman, N. F., W. S. Kerwin, E. R. Mcveigh, and J. L. Prince. Cardiac Motion Tracking Using CINE harmonic phase (HARP). *Magn Reson Med.* 42:1048–1060, 2008.

127. Park, T., S. F. Nagueh, D. S. Khoury, H. A. Kopelen, S. Akrivakis, K. Nasser, G. Ren, N. G. Frangogiannis, and A. Helen. Impact of myocardial structure and function postinfarction on diastolic strain measurements : implications for assessment of myocardial viability. *Am. J. Physiol. Heart Circ. Physiol.* 77030:724–731, 2006.

128. Partington, S. L., R. Y. Kwong, and S. Dorbala. Multimodality imaging in the assessment of myocardial viability. *Heart Fail. Rev.* 16:381–95, 2011.

129. Patel, S. R., and I. L. Piña. From Acute Decompensated To Chronic Heart Failure. *Am. J. Cardiol.* , 2014.doi:10.1016/j.amjcard.2014.09.033

130. Pauschinger, M., D. Knopf, S. Petschauer, a. Doerner, W. Poller, P. L. Schwimmbeck, U. Kuhl, and H.-P. Schultheiss. Dilated Cardiomyopathy Is Associated With Significant Changes in Collagen Type I/III ratio. *Circulation* 99:2750–2756, 1999.

131. Périé, D., N. Dahdah, A. Foudis, and D. Curnier. Multi-parametric MRI as an indirect evaluation tool of the mechanical properties of in-vitro cardiac tissues. *BMC Cardiovasc. Disord.* 13:24, 2013.

132. Pfeffer, J. M., E. Braunwald, M. A. Pfeffer, P. J. Fletcher, and P. Finn. Progressive ventricular remodeling in rat with myocardial infarction. *Am. Physiol. Soc.* 91:H1406–H1414, 1990.

133. Pfeffer, M. A., and E. Braunwald. Ventricular Remodeling After Myocardial Infarction. Experimental observations and clinical implications. *Circulation* 81:1161–1172, 1990.

134. Pfeffer, M. A., E. Braunwald, L. A. Moye, L. Basta, E. J. Brown Jr., T. E. Cuddy, B. R. Davis, and E. M. Geltman. Effect of captopril on mortality and morbidity in patients with left ventricular dysfunction after myocardial infarction. *N. Engl. J. Med.* , 1992.

135. Pfeffer, M. a., J. M. Pfeffer, M. C. Fishbein, P. J. Fletcher, J. Spadaro, R. a. Kloner, and E. Braunwald. Myocardial infarct size and ventricular function in rats. *Circ. Res.* 44:503–512, 1979.

136. Pilla, J. J., J. H. Gorman, and R. C. Gorman. Theoretic impact of infarct compliance on left ventricular function. *Ann. Thorac. Surg.* 87:803–10, 2009.

137. Purcell, B. P., D. Lobb, M. B. Charati, S. M. Dorsey, R. J. Wade, K. N. Zellars, H. Doviak, S. Pettaway, C. B. Logdon, J. A. Shuman, P. D. Freels, J. H. Gorman, R. C. Gorman, F. G. Spinale, and J. A. Burdick. Injectable and bioresponsive hydrogels for on-demand matrix metalloproteinase inhibition. *Nat. Mater.* 13:653–61, 2014.

138. Raghupathy, R., C. Witzenburg, S. P. Lake, E. a Sander, and V. H. Barocas. Identification of regional mechanical anisotropy in soft tissue analogs. *J. Biomech. Eng.* 133:091011, 2011.

139. Raya, T. E., R. G. Gay, L. Lancaster, M. Aguirre, C. Moffett, and S. Goldman. Serial changes in left ventricular relaxation and chamber stiffness after large myocardial infarction in rats. *Circulation* 77:1424–1431, 1988.

140. Reimer, K. a., J. E. Lowe, M. M. Rasmussen, and R. B. Jennings. The wavefront phenomenon of ischemic cell death. 1. Myocardial infarct size vs duration of coronary occlusion in dogs. *Circulation* 56:786–794, 1977.

141. Roberts, C. S., D. Maclean, P. Maroko, and R. A. Kloner. Early and Late Remodeling of the Left Ventricle After Acute Myocardial Infarction. *Am. J. Cardiol.* 54:407–410, 1984.

142. Romson, J. L., B. G. Hook, S. L. Kunkel, G. D. Abrams, M. a. Schork, and B. R. Lucchesi. Reduction of the extent of ischemic myocardial injury by neutrophil depletion in the dog. *Circulation* 67:1016–1023, 1983.

143. Ross, A. J., Z. Yang, S. S. Berr, W. D. Gilson, W. C. Petersen, J. N. Oshinski, and B. a French. Serial MRI evaluation of cardiac structure and function in mice after reperfused myocardial infarction. *Magn. Reson. Med.* 47:1158–68, 2002.

144. Ross, A. J., Z. Yang, S. S. Berr, W. D. Gilson, W. C. Petersen, J. N. Oshinski, and B. a French. Serial MRI evaluation of cardiac structure and function in mice after reperfused myocardial infarction. *Magn. Reson. Med.* 47:1158–68, 2002.

145. Rouillard, A. D., and J. W. Holmes. Mechanical regulation of fibroblast migration and collagen remodelling in healing myocardial infarcts. *J. Physiol.* 590:4585–602, 2012.

146. Rouillard, A. D., and J. W. Holmes. Coupled agent-based and finite-element models for predicting scar structure following myocardial infarction. *Prog. Biophys. Mol. Biol.* 115:235–243, 2014.

147. Ryan, L. P., K. Matsuzaki, M. Noma, B. M. Jackson, T. J. Eperjesi, T. J. Plappert, M. G. S. John-sutton, J. H. G. Iii, and R. C. Gorman. Dermal Filler Injection : A Novel Approach for Limiting Infarct Expansion. *ATS* 87:148–155, 2009.

148. Sacks, M. S., and W. Sun. Multiaxial mechanical behavior of biological materials. *Annu. Rev. Biomed. Eng.* 5:251–84, 2003.

149. Saeed, M., A. J. Martin, D. Saloner, L. Do, and M. Wilson. Noninvasive MR characterization of structural and functional components of reperfused infarct. *Acta Radiol.* 51:1093–102, 2010.

150. Sakamoto, H., L. M. Parish, H. Hamamoto, L. P. Ryan, T. J. Eperjesi, T. J. Plappert, B. M. Jackson, M. G. St John-Sutton, J. H. Gorman, and R. C. Gorman. Effect of reperfusion on left ventricular regional remodeling strains after myocardial infarction. *Ann. Thorac. Surg.* 84:1528–36, 2007.

151. Schmidt, A., C. F. Azevedo, A. Cheng, S. N. Gupta, D. a Bluemke, T. K. Foo, G. Gerstenblith, R. G. Weiss, E. Marbán, G. F. Tomaselli, J. a C. Lima, and K. C. Wu. Infarct tissue heterogeneity by magnetic resonance imaging identifies enhanced cardiac arrhythmia susceptibility in patients with left ventricular dysfunction. *Circulation* 115:2006–14, 2007.

152. Schuleri, K. H., M. Centola, K. S. Evers, A. Zviman, R. Evers, J. a C. Lima, and A. C. Lardo. Cardiovascular magnetic resonance characterization of peri-infarct zone remodeling following myocardial infarction. *J. Cardiovasc. Magn. Reson.* 14:24, 2012.

153. Selvaraj, S., F. G. Aguilar, E. E. Martinez, L. Beussink, K.-Y. a Kim, J. Peng, D. C. Lee, A. Patel, J. Sha, M. R. Irvin, D. K. Arnett, and S. J. Shah. Diastolic wall

strain: a simple marker of abnormal cardiac mechanics. *Cardiovasc. Ultrasound* 12:40, 2014.

154. Sideman, S. Relating left ventricular dimension to maximum elastance by fiber mechanics. , 1986.

155. Singelyn, J. M., and K. L. Christman. Injectable Materials for the Treatment of Myocardial Infarction and Heart Failure : The Promise of Decellularized Matrices. 478–486, 2010.doi:10.1007/s12265-010-9202-x

156. Singelyn, J. M., P. Sundaramurthy, T. D. Johnson, P. J. Schup-Magoffin, D. P. Hu, D. M. Faulk, J. Wang, K. M. Mayle, K. Bartels, M. Salvatore, A. M. Kinsey, A. N. Demaria, N. Dib, and K. L. Christman. Catheter-deliverable hydrogel derived from decellularized ventricular extracellular matrix increases endogenous cardiomyocytes and preserves cardiac function post-myocardial infarction. *J. Am. Coll. Cardiol.* 59:751–63, 2012.

157. Singelyn, J. M., P. Sundaramurthy, T. D. Johnson, P. J. Schup-Magoffin, D. P. Hu, D. M. Faulk, J. Wang, K. M. Mayle, K. Bartels, M. Salvatore, A. M. Kinsey, A. N. Demaria, N. Dib, and K. L. Christman. Catheter-deliverable hydrogel derived from decellularized ventricular extracellular matrix increases endogenous cardiomyocytes and preserves cardiac function post-myocardial infarction. *J. Am. Coll. Cardiol.* 59:751–63, 2012.

158. Smith, W. B., L. Noack, Y. Khew-goodall, S. Isenmann, M. A. Vadasr, and J. R. Gamblep. Transforming Growth Factor-pl Inhibits the Production of 11-8 and the Transmigration of Neutrophils Through Activated Endothelium'. , 1996.

159. Soleimanifard, S., K. Z. Abd-Elmoniem, T. Sasano, H. K. Agarwal, M. R. Abraham, T. P. Abraham, and J. L. Prince. Three-dimensional regional strain analysis in porcine myocardial infarction: a 3T magnetic resonance tagging study. *J. Cardiovasc. Magn. Reson.* 14:85, 2012.

160. Spinale, F. G., M. L. Coker, S. R. Krombach, R. Mukherjee, H. Hallak, W. V Houck, M. J. Clair, S. B. Kribbs, L. L. Johnson, J. T. Peterson, and M. R. Zile. Matrix metalloproteinase inhibition during the development of congestive heart failure : effects on left ventricular dimensions and function. *Circ. Res.* 85:364–376, 1999.

161. Stewart, S., K. MacIntyre, D. J. Hole, S. Capewell, and J. J. V. McMurray. More "malignant" than cancer? Five-year survival following a first admission for heart failure. *Eur. J. Heart Fail.* 3:315–322, 2001.

162. Sun, M., F. Dawood, W.-H. Wen, M. Chen, I. Dixon, L. a Kirshenbaum, and P. P. Liu. Excessive tumor necrosis factor activation after infarction contributes to

susceptibility of myocardial rupture and left ventricular dysfunction. *Circulation* 110:3221–8, 2004.

163. Sun, Y., and K. T. Weber. Infarct scar: a dynamic tissue. *Cardiovasc. Res.* 46:250–6, 2000.

164. Sutton, M. G. S. J., and N. Sharpe. Left Ventricular Remodeling After Myocardial Infarction : Pathophysiology and Therapy. *Circulation* 101:2981–2988, 2000.

165. Takahashi, T., M. J. Levine, and W. Grossman. Regional diastolic mechanics of ischemic and nonischemic myocardium in the pig heart. *J. Am. Coll. Cardiol.* 17:1203–1212, 1991.

166. Tao, Z.-Y., M. A. Cavasin, F. Yang, Y.-H. Liu, and X.-P. Yang. Temporal changes in matrix metalloproteinase expression and inflammatory response associated with cardiac rupture after myocardial infarction in mice. *Life Sci.* 74:1561–1572, 2004.

167. Theroux, P., J. Ross, D. Franklin, J. W. Covell, C. M. Bloor, and S. Sasayama. Regional myocardial function and dimensions early and late after myocardial infarction in the unanesthetized dog. *Circ. Res.* 40:158–165, 1977.

168. Thorstensen, A., B. H. Amundsen, H. Dalen, P. Hala, G. Kiss, S. A. Aase, H. Torp, and A. Støylen. Strain rate imaging combined with wall motion analysis gives incremental value in direct quantification of myocardial infarct size. *Eur. Heart J. Cardiovasc. Imaging* 13:914–21, 2012.

169. Thorstensen, A., H. Dalen, P. Hala, G. Kiss, J. D'hooge, H. Torp, A. Støylen, and B. Amundsen. Three-dimensional echocardiography in the evaluation of global and regional function in patients with recent myocardial infarction: a comparison with magnetic resonance imaging. *Echocardiography* 30:682–92, 2013.

170. Thygesen, K. *et al.* Third universal definition of myocardial infarction. *J. Am. Coll. Cardiol.* 60:1581–98, 2012.

171. Tous, E., J. L. Ifkovits, K. J. Koomalsingh, T. Shuto, T. Soeda, N. Kondo, J. H. Gorman, R. C. Gorman, and J. A. Burdick. Influence of Injectable Hyaluronic Acid Hydrogel Degradation Behavior on Infarction-Induced Ventricular Remodeling. *Biomacromolecules* , 2011.

172. Urheim, S., T. Edvardsen, H. Torp, B. Angelsen, and O. a. Smiseth. Myocardial Strain by Doppler Echocardiography : Validation of a New Method to Quantify Regional Myocardial Function. *Circulation* 102:1158–1164, 2000.

173. Villarreal, F. J., and W. Y. Lew. Finite strains in anterior and posterior wall of canine left ventricle. *Am. J. Physiol.* 259:H1409–H1418, 1990.

174. Walker, J. C., M. B. Ratcliffe, P. Zhang, A. W. Wallace, B. Fata, E. W. Hsu, D. Saloner, and J. M. Guccione. MRI-based finite-element analysis of left ventricular aneurysm. *Am. J. Physiol. Heart Circ. Physiol.* 289:H692–700, 2005.

175. Wall, S. T., J. C. Walker, K. E. Healy, M. B. Ratcliffe, and J. M. Guccione. Theoretical Impact of the Injection of Material A Finite Element Model Simulation. *Circulation* 114:2627–2635, 2006.

176. Wang, V. Y., H. I. Lam, D. B. Ennis, B. R. Cowan, A. a Young, and M. P. Nash. Modelling passive diastolic mechanics with quantitative MRI of cardiac structure and function. *Med. Image Anal.* 13:773–84, 2009.

177. Weber, K. T., Y. Sun, and L. C. Katwa. Wound healing following myocardial infarction. *Clin. Cardiol.* 19:447–55, 1996.

178. Weisman, H. F., D. E. Bush, J. a. Mannisi, and B. H. Bulkley. Global cardiac remodeling after acute myocardial infarction: A study in the rat model. *J. Am. Coll. Cardiol.* 5:1355–1362, 1985.

179. Weisman, H. F., D. E. Bush, J. a. Mannisi, M. L. Weisfeldt, and B. Healy. Cellular mechanisms of myocardial infarct expansion. *Circulation* 78:186–201, 1988.

180. Whittaker, P., D. R. Boughner, and R. a. Kloner. Role of collagen in acute myocardial infarct expansion. *Circulation* 84:2123–2134, 1991.

181. Wilson, E. M., S. L. Moainie, J. M. Baskin, A. S. Lowry, M. Anne, R. Mukherjee, T. S. Guy, M. G. S. John-sutton, H. Joseph, G. Iii, L. H. Edmunds, R. C. Gorman, and F. G. Spinale. Region and Type-Specific Induction of Matrix Metalloproteinases in Post-Myocardial Infarction Remodeling. *Circ. Res.* 107:2857–2863, 2003.

182. Wong, E. Y., M. O'Donnell, K. Thiele, C. B. Compas, X. Huang, S. Sampath, B. a. Lin, P. Pal, X. Papademetris, D. Dione, L. Staib, A. J. Sinusas, and J. S. Duncan. 4-D echocardiography assessment of local myocardial strain using 3-D speckle tracking combined with shape tracking. *2013 IEEE Int. Ultrason. Symp.* 100–103, 2013.doi:10.1109/ULTSYM.2013.0026

183. Yang, Z., B. Zingarelli, and C. Szabo. Crucial role of endogenous interleukin-10 production in myocardial ischemia/reperfusion injury. *Circulation* 10:, 2000.

184. Yankey, G. K., T. Li, A. Kilic, G. Cheng, A. Satpute, K. Savai, S. Li, S. L. Moainie, D. Prastein, C. DeFillipi, Z. J. Wu, and B. P. Griffith. Regional remodeling strain and its association with myocardial apoptosis after myocardial infarction in an ovine model. *J. Thorac. Cardiovasc. Surg.* 135:991–8, 998.e1–2, 2008.

185. Yarbrough, W. M., R. Mukherjee, T. a Brinsa, K. B. Dowdy, A. a Scott, G. P. Escobar, C. Joffs, D. G. Lucas, F. a Crawford, and F. G. Spinale. Matrix metalloproteinase inhibition modifies left ventricular remodeling after myocardial infarction in pigs. *J. Thorac. Cardiovasc. Surg.* 125:602–610, 2003.

186. Yeon, S. B., N. Reichek, B. A. Tallant, J. A. . Lima, L. P. Calhoun, N. R. Clark, E. A. Hoffman, K. K. . Ho, and L. Axel. Validation of in vivo myocardial strain measurement by magnetic resonance tagging with sonomicrometry. *J. Am. Coll. Cardiol.* 38:555–561, 2001.

187. Yin, F. C., R. K. Strumpf, P. H. Chew, and S. L. Zeger. Quantification of the mechanical properties of noncontracting canine myocardium under simultaneous biaxial loading. , 1987.

188. Young, A. a, B. a French, Z. Yang, B. R. Cowan, W. D. Gilson, S. S. Berr, C. M. Kramer, and F. H. Epstein. Reperfused myocardial infarction in mice: 3D mapping of late gadolinium enhancement and strain. *J. Cardiovasc. Magn. Reson.* 8:685–92, 2006.

189. Zhang, Y., A. K. Y. Chan, C.-M. Yu, G. W. K. Yip, J. W. H. Fung, W. W. M. Lam, N. M. C. So, M. Wang, E. B. Wu, J. T. Wong, and J. E. Sanderson. Strain rate imaging differentiates transmural from non-transmural myocardial infarction: a validation study using delayed-enhancement magnetic resonance imaging. *J. Am. Coll. Cardiol.* 46:864–71, 2005.

190. Zhang, Z., D. Dione, B. a Lin, J. S. Duncan, A. J. Sinusas, and S. Sampath. Early diastolic function observed in canine model of reperfused transmural myocardial infarction using high temporal resolution MR imaging. *J. Cardiovasc. Magn. Reson.* 14:W65, 2012.

191. Zimmerman, S. D., J. Criscione, and J. W. Covell. Remodeling in myocardium adjacent to an infarction in the pig left ventricle. *Am. J. Physiol. Heart Circ. Physiol.* 287:H2697–704, 2004.

192. Zimmerman, S. D., W. J. Karlon, J. W. Holmes, J. H. Omens, and J. W. Covell. Structural and mechanical factors influencing infarct scar collagen organization Structural and mechanical factors influencing infarct scar collagen organization. *Am. J. Physiol. Hear. Circ. Physiol.* 278:H194–H200, 2000.

193. Zimmerman, S. D., W. J. Karlon, J. W. Holmes, J. H. Omens, and W. Covell. Structural and mechanical factors influencing infarct scar collagen organization Structural and mechanical factors influencing infarct scar collagen organization. *Am. J. Physiol. Heart Circ. Physiol.* 278:H194–H200, 2013.

194. estimating passive mechanical properties in a myocardial infarction using MRI and finite element simulations.pdf

APPENDIX A

PERMISSION TO REPRINT

Jamie Page
to me

Mar 31 (2 days ago)

Dear Dr. Romito,

Thank you for this additional information. Yes, you can use your own work. If you have any other questions please feel free to contact us.

Sincerely,
Jamie

Link to AHA copyright permission request form:
http://copyright.heart.org

-

Ms. Jamie Page
Copyright Permissions Specialist/CEO-Legal Dept.
7272 Greenville Avenue, Dallas TX 75231-4596
Phone: 214.706.1131 - Fax: 214.373.9818
www.heart.org Toll Free: 800.242.8721

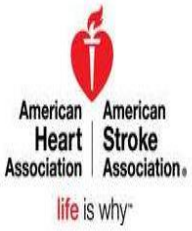

From: Eva Juarez [mailto:evajrz24@gmail.com]
Sent: Thursday, March 31, 2016 9:45 AM
To: Jamie Page <jamie.page@heart.org>
Subject: Re: AHA Copyright Permission Request: 11684-University of South Carolina - Student - Dr Eva Romito - Use of Sessions material - 03.31.2016